UNIVERSITÀ DEGLI STUDI DI SALERNO

UNIVERSITÀ DEGLI STUDI DI SALERNO

Dipartimento di Farmacia

PhD Program

in **Drug Discovery and Development**

XXXIV Cycle — Academic Year 2021/2022

PhD Thesis in

Annexin A1 in pancreatic cancer progression

Candidate

Nunzia Novizio

Supervisor

Prof. *Antonello Petrella*

PhD Program Coordinator: Prof. Dr. *Gianluca Sbardella*

Firmato digitalmente da: GIANLUCA SBARDELLA
Luogo: Fisciano
Data: 20/01/2022 16:21:10

Table of contents

Abstract pag. 4
Preface pag. 6
Introduction pag. 8
1. Pancreas pag. 8
1.1 Pancreatic anatomy pag. 8
1.2 The exocrine portion pag. 9
1.3 The endocrine portion pag. 13
1.4 Pancreatic carcinoma pag. 16
1.4.1 Introduction: etiology, epidemiology and symptoms pag. 16
1.4.2 Phathophisiology pag. 18
1.4.3 Tumor microenvironment pag. 20
1.4.4 Biomarkers and staging pag. 21
1.4.5 Treatment pag. 23
2. Extracellular vesicles pag. 25
2.1 Introduction pag. 25
2.2 Biogenesis pag. 27
2.2.1 ESCRT-dependent mechanisms pag. 28
2.2.2 ESCRT-independent mechanisms pag. 28
2.3 Vesicles release pag. 29
2.4 EVs composition pag. 30
2.5 EVs interactions with cells pag. 32
2.5.1 Protein interaction pag. 33
2.5.2 Cell surface membrane fusion pag. 34
2.5.3 Endocytosis pag. 34
2.6 Roles of tumor EVs pag. 37
2.6.1 EVs role in Pancreatic cancer pag. 37
3. Annexin A1 pag. 39
3.1 Introduction pag. 39
3.2 ANXA1 structure pag. 39
3.3 Intracellular ANXA1 pag. 41
3.4 Extracellular ANXA1 pag. 43
3.5 Externalized ANXA1 pag. 45
3.6 ANXA1 in cancer pag. 47
3.6.1 ANXA1 in brest cancer pag. 48
3.6.2 ANXA1 in prostate cancer pag. 49
3.6.3 ANXA1 in colon rectal cancer pag. 50
3.6.4 ANXA1 in lung cancer pag. 50
3.6.5 ANXA1 in melanoma pag. 50

3.6.6 ANXA1 in pancreatic cancer pag. 51
4. Heparan sulfate pag. 52
4.1 Structure, role, functions pag. 52
5. Three-dimensional (3D) cell model pag. 56
5.1 3D culture tecniques pag. 58
6. Aim of the work pag. 61
7. Material and methods pag. 62
7.1 Cell cultures pag. 62
7.2 Exosome enrichment pag. 62
7.3 Western blotting pag. 63
7.4 Wound-healing assay pag. 64
7.5 Invasion assay pag. 65
7.6 Tube formation assay pag. 65
7.7 Gelatin gel zymography pag. 66
7.8 Measurement of intracellular Ca^{2+} signaling pag. 66
7.9 Confocal microscopy pag. 67
7.10 RNA isolation and quantitative Real Time-Polymerase Chain Reaction (RT-PCR) pag. 68
7.11 Clonogenic assay pag. 69
7.12 MTT assay pag. 69
7.13 Macrophages generation pag. 69
7.14 Flow cytometry pag. 69
7.15 hrANXA1 purification pag. 70
7.16 Differential scanning fluorimetry (DSF) pag. 71
7.17 Surface plasmon resonance (SPR) pag. 71
7.18 Co-Culture system pag. 72
7.19 ELISA for VEGF-A pag. 73
7.20 H&E tissue staining and tissue immunofluorescence pag. 75
7.21 Monocytes isolation pag. 75
7.22 3D model generation and area analysis pag. 75
7.23 Counting live cells in 3D model pag. 76
7.24 Cell viability for 3D model pag. 76
7.25 Statistical Analysis pag. 76
8. Results pag. 77
8.1 Effects of extracellular vesicles (EVs) from wild type (WT) and ANXA1 Knock-Out (KO) MIA PaCa-2 cells on fibroblast migration and invasion pag. 77
8.2 Ac2-26 peptide promoted fibroblasts and endothelial cells motility through FPRs pag. 79
8.3 PC cells-EVs interact with FPRs on human fibroblasts pag. 81
8.4 ANXA1-containing EVs interact with FPRs on endothelial Cells pag. 83
8.5 WT EVs promoted the fibroblasts switch more than ANXA1 KO EVs pag. 84
8.6 WT EVs are able to induce the EndMT through FPRs pag. 86
8.7 The PC cell-derived EVs influence the macrophage polarization pag. 88

8.8 The Effects of EVs from WT and ANXA1 KO MIA PaCa-2 cells on macrophage migration and invasion pag. 90
8.9 ANXA1 affects the tumor microenvironment pag. 92
8.10 WT MIA PaCa-2 EVs influence the endothelial cell activation pag. 94
8.11 TAMs support the fibroblast activation pag. 96
8.12 Characterization of macrophage infiltration in WT and ANXA1 KO tumor and metastases pag. 98
8.13 The ability of ANXA1 to affect tumor 3D model pag. 100
8.14 HS directly interacts with ANXA1 N-terminal peptide pag. 102
8.15 HS inhibits the migration and invasion rate of WT MIA PaCa-2 cells and not of ANXA1 KO clone pag. 104
8.16 HS reduces the pro-migratory and invasive effects of ANXA1 pag. 105
8.17 The effects of Ac2-26 on WT MIA PaCa-2 cells are inhibited by HS pag. 106
8.18 The mesenchymal phenotype of WT MIA PaCa-2 cells is reverted by HS pag. 108
8.19 The Ac2-26-enhanced aggressive behavior of PANC-1 cells is reduced by HS pag. 110
8.20 The activation of HUVEC cells, enhanced in presence of Ac2-26, is notably inhibited when the ANXA1 peptide is administered together with HS pag. 112
8.21 HS blocks the interaction of ANXA1 with FPRs pag. 114
9. Discussion pag. 116
Bibliography pag. 126

Abstract

Pancreatic cancer (PC) is one of the most aggressive cancers in the world and it correlates to poor prognosis and high mortality due to late diagnosis, even if early diagnosed. Resectable PC patients have unfavorable outcome due to several factors like chemoresistance by tumor microenvironment (TME) and by tumor cells per se. Recent studies have focused on TME that plays a critical role in PC progression, highlighting the strong relationship between the microenvironment and metastasis. Several extracellular factors are involved in its development and metastasis. In PC, the protein Annexin A1 (ANXA1) appears overexpressed and may be identified as an oncogenic factor, also as component in tumor-deriving extracellular vesicles (EVs). Indeed, these microvesicles are known to nourish the TME. Our published data have highlighted that autocrine/paracrine activities of extracellular ANXA1 depend on its presence in EVs. The aim of the first and second year of my PhD project has been to investigate the paracrine effect of ANXA1 on cellular components of TME, mainly stromal cells like fibroblasts, endothelial ones to demonstrate how the ANXA1-EVs complex can stimulate this mechanism. EVs from Wild Type (WT) and ANXA1- Knock-Out (KO) MIA PaCa-2 cells, obtained by CRISPR/Cas9 genome editing system, have been purified from cell conditioned medium by differential centrifugation and then administrated on stromal cells.

Moreover, as oncogenic factor, ANXA1 needs to be inhibited, mainly by blocking its extracellular form, as a new model of cancer adjuvant therapy. Heparan sulfate (HS) is a glycosaminoglycan of the extracellular matrix known to bind growth factors and cytokines, generating a kind of reservoir in the extracellular environment. One of these molecules is represented by ANXA1 and previous study has shown that ANXA1 notably binds to sulfate glycans, mainly HS and heparin. In this regard, the second annual aim has been to investigate the interaction between HS and ANXA1 and how this glycosaminoglycan could influence ANXA1

oncogenic action. In this way, it would be possible to confirm the relevance of ANXA1 in PC progression as actor of the cross-talk among tumor cells and the microenvironment.

In order to amplify the knowledge about the role of ANXA1 on PC stroma, the aim of my third year has been to demonstrate that the complex ANXA1/EVs modulates the macrophage polarization further contributing to cancer progression. The WT and ANXA1 KO EVs have been administrated to THP-1 macrophages finding that ANXA1 is crucial for the acquisition of a pro-tumor M2 phenotype. The M2 macrophages activate endothelial cells and fibroblasts to induce angiogenesis and matrix degradation, respectively. Once shown *in vitro* the multifaceted role of ANXA1 in the intensification of PC-stroma cells cross-talk, we have also found a significantly increased presence of M2 macrophage in mice tumor and liver metastasis sections previously obtained by orthotopic xenografts with WT cells. Finally during the third year of the PhD program, I had the opportunity to work at "Institut national de la santé et de la recherche médicale" (INSERM), Marseille (FR), where I deepened the role of ANXA1 in TME using tumor 3D model, both in monoculture and co-culture with cancer associated fibroblasts (CAFs) and monocytes.

Taken together, our data interestingly suggest the relevance of ANXA1 as potential diagnostic/prognostic and/or therapeutic PC marker. In this way, it would be possible to confirm the relevance of ANXA1 in PC progression as actor of the cross-talk among tumor cells and the microenvironment.

Preface

My PhD three years course in Drug Discovery and Development at the Department of Pharmacy, University of Salerno, started in November 2018 under the supervision of Professor Antonello Petrella.

My research project has focused on studying the role of Annexin 1 (ANXA1) in Pancreatic Cancer (PC) progression. My research activity is based on achieving three main objectives:

1. Study of effects of extracellular vesicles (EVs) from wild type (WT) and ANXA1-Knockout (KO) MIA PaCa-2 cells on PC microenvironment, like stromal cells;
2. Study of the role of HS as an inhibitor of ANXA1 and as a potential chemotherapeutic adjuvant;
3. Deepen the role of ANXA1 in tumor microenvironment (TME) by tumor 3D model.

In particular, I have achieved the last aim during the three months spent at the “Institut national de la santé et de la recherche médicale” (INSERM), Marseille (FR), under the supervision of Professor Richard Tomasini.

List of publications related to the scientific activity performed during the three years Ph.D. course in Drug Discovery and Development.

- D'Arrigo P, Tufano M, Rea A, Vigorito V, **Novizio N**, Russo S, Romano MF, Romano S. Manipulation of the Immune System for Cancer Defeat: A Focus on the T Cell Inhibitory Checkpoint Molecules. *Curr Med Chem*. 2020, 27(15):2402-2448. doi: 10.2174/0929867325666181106114421
- Belvedere R, **Novizio N**, Pessolano E, Tosco A, Eletto D, Porta A, Campiglia P, Perretti M, Filippelli A, Petrella A. Heparan sulfate binds the extracellular Annexin A1 and blocks its effects on pancreatic cancer cells. *Biochem Pharmacol*. 2020, 182:114252. doi: 10.1016/j.bcp.2020.114252.
- **Novizio N**, Belvedere R, Pessolano E, Tosco A, Porta A, Perretti M, Campiglia P, Filippelli A, Petrella A. Annexin A1 Released in Extracellular Vesicles by Pancreatic Cancer Cells Activates Components of the Tumor Microenvironment, through Interaction with the Formyl-Peptide Receptors. *Cells*. 2020, 9(12):2719. doi: 10.3390/cells9122719.
- Belvedere R, Morretta E, Pessolano E, **Novizio N**, Tosco A, Porta A, Whiteford J, Perretti M, Filippelli A, Monti MC, Petrella A. Mesoglycan exerts its fibrinolytic effect through the activation of annexin A2. *Journal of Cellular Physiology*. 2021, 236(7):4926-4943. doi: 10.1002/jcp.30207.
- Pessolano E, Belvedere R**, Novizio N**, Filippelli A, Perretti M, Whiteford J, Petrella A. Mesoglycan connects Syndecan-4 and VEGFR2 through Annexin A1 and formyl peptide receptors to promote angiogenesis. *FEBS J*. 2021, 288(22):6428-6446. doi: 10.1111/febs.16043.
- Belvedere R, Pessolano E, **Novizio N**, Tosco A, Eletto D, Porta A, Filippelli A, Petrella F, Petrella A. The promising pro-healing role of the association of mesoglycan and lactoferrin on skin lesions. *Eur J Pharm Sci*. 2021, 163:105886. doi: 10.1016/j.ejps.2021.105886.
- Belvedere R, **Novizio N**, Eletto D, Porta A, Bagnuolo A, Cerciello A, Di Maio U and Petrella A. The Procoagulant Activity of Emoxilane: a New Appealing Therapeutic Use in Epistaxis of the Combination of Sodium Hyalurate, Silver Salt, α-tocopherol and D-panthenol. *Life (Basel).* 2021, 11(9):992. doi: 10.3390/life11090992.
- **Novizio N**, Belvedere R, Pessolano E, Morello S, Tosco A, Campiglia P, Filippelli A and Petrella A. ANXA1 Contained in EVs Regulates Macrophage Polarization in Tumor Microenvironment and Promotes Pancreatic Cancer Progression and Metastatis. *Int J Mol Sci*. 2021, 22(20):11018. doi: 10.3390/ijms222011018.
- Belvedere R, Morretta E, **Novizio N**, Morello S, Bruno O, Brullo C, Petrella A. The Pyrazolyl-Urea Gege3 Inhibits the Activity of ANXA1 in the Angiogenesis Induced by the Pancreatic Cancer Derived EVs. *Biomolecules*. 2021, 11(12):1758. doi: 10.3390/biom11121758.

1 Pancreas

1.1 Pancreatic anatomy

The pancreas is an organ of the digestive and endocrine systems of vertebrates. It has an elongated, uneven and paramedian shape, of 12-20 cm in length and a weight of about 100 grams and placed in the abdominal cavity in a retroperitoneal position. The name pancreas derives from the Greek roots ‘pan’ meaning ‘all’ and ‘creas’ meaning ‘flesh’ [1]. It is composed by four parts as head, neck, body and tail in a manner represented in figure 1.1.

In humans it is found posterior to the stomach, and functions as an anphrine (i.e., endocrine and exocrine secretion) gland. The pancreas is kept stable in its position by the duodenum, which houses its head, by the posterior parietal peritoneum, which covers it, and by the pancreaticolienal ligament, which fixes its tail to the hilum of the spleen.

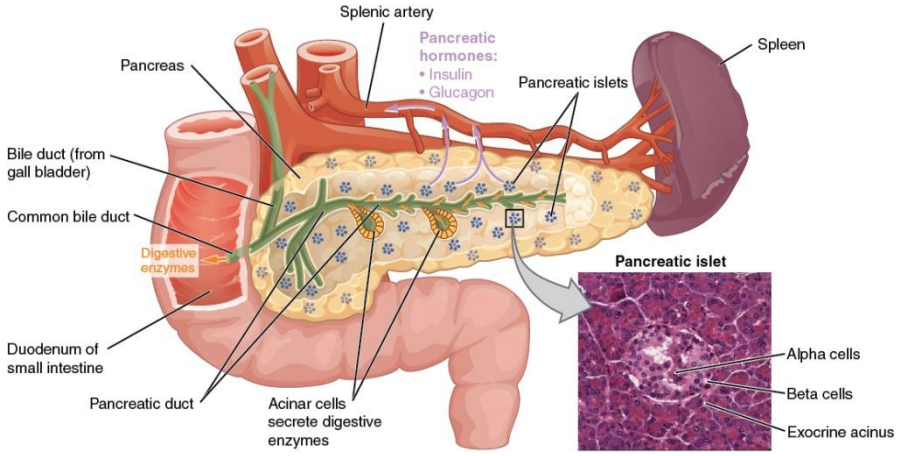

Figure 1.1 Anatomic relationships of the pancreas with surrounding organs and structures; (Micrograph provided by the Regents of University of Michigan Medical School © 2012)

The tail of the pancreas and the spleen are in the left upper quadrant of the abdomen, instead the head of the pancreas is in the right upper quadrant just to the right of the midline (Fig. 1.1) [2]:

- the head of the pancreas lies in the loop of the duodenum;

- the tail of the pancreas lies near the hilum of the spleen;
- the body of the pancreas lies posterior to the distal portion of the stomach between the tail and the neck;
- the portion of the pancreas that lies anterior to the aorta is thinner than the adjacent portions of the head and body of the pancreas. This region is sometimes designated as the neck of the pancreas and marks the junction of the head and body;
- the neck of the pancreas is really close to major blood vessels posteriorly including the superior mesenteric artery, superior mesenteric-portal vein, inferior vena cava, and aorta;
- the common bile duct passes through the head of the pancreas to join the main duct of the gland near the duodenum. The portion nearest the liver lies in a groove on the dorsal aspect of the head;
- the minor papilla where the accessory pancreatic duct drains into the duodenum and the major papilla (ampulla of Vater) where the main pancreatic duct enters the duodenum are depicted.[3; 4].

The celiac trunk and the superior mesenteric artery both arise from the abdominal aorta and have multiple branches that supply several organs including the pancreas. The anastomosis of their branches around the pancreas provides collateral circulation that generally assures a secure arterial supply to the organ. Most of the arteries are accompanied by veins that drain into the portal and splenic veins as they pass behind the pancreas. The superior mesenteric vein becomes the portal vein when it joins the splenic vein [3].

1.2 The exocrine portion

The exocrine pancreas is a compound acinar gland, divided into two lobules by loose connective sepiments that branch off from its capsule and into which blood vessels, lymphatic vessels and

nerves run. Each pancreatic lobule is divided into hundreds of acini, spherical cell clusters and secreting units of the gland. From each acinus, a preterminal duct starts flowing into an intralobular duct and many of these ducts converge to form an intercalary duct which in turn flows into ducts of increasing caliber until it flows into the main or accessory pancreatic duct. Pancreatic acinar cells have a pyramidal shape with the base often in contact with thin capillaries, from which it is separated from the endothelium and a basal lamina, and with apexes facing the intralobular duct. They have a rounded nucleus, surrounded on the sides and at the base by a wrinkled endoplasmic reticulum particularly developed due to their secretory function, a smooth endoplasmic reticulum, many mitochondria, especially in the basal region, numerous ribosomes; furthermore, in the central position we find the Golgi apparatus, while in the apical portion of the cell there are large granules containing electrondensic substances, and zymogen granules. Chemical composition studies of the zymogen granules, that appear as spherical, have shown that they contain about 12 to 15 different digestive enzymes, in an inactive form called proenzymes, which make up about 90% of the granule protein. [5; 6]. The proteins are synthesized in the rough endoplasmic reticulum, processed in the Golgi and excreted in the lumen of the intralobular duct at the apex of the cell. Each acinar cell is connected to the adjacent cells by numerous specialized junctions located on the lateral plasma membrane, while on its basal portion there are often cholinergic nerve endings (excitosecretory and parasympathetic). The apical portion of the membrane is provided with numerous protrusions. Stained with hematoxylin-eosin acinar cells are strongly basophilic due to their rough endoplasmic reticulum, nucleus and ribosomes. Hormonal stimulation of these cells occurs with the release of duodenal cholecystokinin (CKK) from the duodenum. The centroacinous cells, located in the center of the berry, are adjacent to the intralobular ducts and are involved in the production of bicarbonate ions and in the transport of water. These aspects are regulated both neurally by the posterior vagus nerve through cholinergic endings and hormonally by secretin from the duodenum and jejunum. The cells that delimit the intralobular ducts are initially flattened, as the caliber of the duct increases they become first cubic and finally cylindrical. Neuroendocrine cells can be found scattered among

the cells of the acini and pancreatic ducts. While the stellate cells, having a central body and long cytoplasmic processes, embrace a portion or an entire acinus, even if they are also found in the ductal system. Their function, not fully understood, would seem to facilitate the emptying of the secretion in the ducts. They are regulated by hormonal stimulation. The integrity of the duct system is of key importance in preventing entry of the exocrine enzymes into the interstitial space where they may be activated and cause tissue damage manifest as pancreatitis. The main and interlobular ducts have thick dense collagenous walls. The connective tissue component of the duct wall becomes progressively thinner as the ducts branch and become narrower. Intercellular tight junctions, also called zonula occludens, between duct cells, centroacinar cells and acinar cells play a major role in preventing leakage of the duct system [5]. Ductal cells express markers such as cytokeratin 19 (K19), cystic fibrosis transmembrane receptor (CFTR), carbonic anhydrase II (CAII), DBA lectin and transcriptional factors as HNF1β (Hepatocyte Nuclear Factor 1 β), HNF6 (Hepatocyte Nuclear Factor) and Sox9 [7]. The pancreas is primarily an exocrine gland, secreting pancreatic juice, made up of a variety of digestive enzymes, involved into digestion of food. The stomach slowly releases partially digested food into the duodenum, the first part of the small intestine, as a thick and acidic liquid called chyme. The acini, the major functional units of the pancreas, secrete pancreatic juice, to complete the digestion of chyme in the duodenum. These secretions collect in the acinus center and then go into the intralobular ducts draining into the main pancreatic duct which in turn conveys it into the duodenum. In this way, about 1.5 - 3 liters of pancreatic juice is secreted every day [8]. The cells of each acinus are filled with granules containing digestive enzymes capable of breaking down carbohydrates, proteins and lipids. These are secreted in an inactive form called a zymogen or proenzyme. The latters, when released into the duodenum, are activated by the enzyme enterokinase present in the duodenum. Once activated, the enzymes are divided into [8]:

- The enzymes that break down proteins: Trypsin (from zymogen trypsinogen), chymotrypsin (endopeptidases, from zymogen chymotrypsinogen) and carboxypeptidase (exopeptidase). They are

protein-digesting enzymes that break proteins down into their aminoacid subunits. These aminoacids can then be absorbed by the intestines;

- Enzymes involved in fat digestion include lipase, phospholipase A2, lysophospholipase and cholesterol esterase. Pancreatic lipase is a lipid-digesting enzyme that breaks large triglyceride molecules into fatty acids and monoglycerides. Bile released by the gallbladder emulsifies fats to increase the surface area of triglycerides that pancreatic lipase can react with. The fatty acids and monoglycerides produced by pancreatic lipase can be absorbed by the intestines;
- Enzymes that break down starch and other carbohydrates include amylase. Pancreatic amylase: it breaks large polysaccharides like starches and glycogen into smaller sugars such as maltose, maltotriose and glucose. Maltase, secreted by the small intestine, then breaks maltose into the monosaccharide glucose, which the intestines can directly absorb.
- Enzymes that digest nucleic acid like ribonuclease and deoxyribonuclease. Ribonuclease breaks down molecules of RNA into the sugar ribose and the nitrogenous bases adenine, cytosine, guanine and uracil. Deoxyribonuclease digests DNA molecules into the sugar deoxyribose and the nitrogenous bases adenine, cytosine, guanine, and thymine.

These enzymes are secreted into a bicarbonate-rich fluid that maintains an alkaline pH where the enzymes work most efficiently and also help neutralize stomach acids entering the duodenum. [8] Secretion is affected by hormones, including secretin, cholecystokinin and vasoactive intestinal peptide (VIP), as well as stimulation with acetylcholine from the vagus nerve. Secretin, released by duodenal S cells in response to stimulation of stomach acid, with VIP increase the secretion of enzymes and bicarbonate. Cholecystokinin is released by duodenal Ito cells and jejunum primarily in response to long-chain fatty acids, increasing the effects of secretin. [8] Duct cells secrete a bicarbonate-rich fluid at a considerable variable flow rate of 0.4 ml/min depending of the state of pancreas stimulation. This secretion is through a sodium and bicarbonate transporter which acts following the depolarization of the membrane and is regulated by cAMP-dependent protein kinase or CFTR protein, which is defective just in cystic fibrosis. Secretin and VIP act to increase the

opening of this protein resulting in greater membrane depolarization and increased secretion of bicarbonate. [8] Several mechanisms act to ensure that the digestive action of the pancreas does not act to digest the pancreatic tissue itself. For this reason the enzymes are produced like proenzymes and are packaged in the zymogen granules. They remain inactive until their reach to the duodenal lumen. For example, once in the duodenum, trypsinogen, the major proteolytic enzyme is converted to active trypsin by an enzyme called enterokinase, a brush border enzyme expressed in the duodenal mucosa. The same active trypsin is essential for the activation of other proteolytic and lipolytic pancreatic enzymes. Finally, acinar cells product also the trypsin inhibitor, which is packaged in zymogen granules together with trypsinogen and activates small amounts of trypsin that may form inside the cells or the body of pancreas [9; 10].

1.3 The endocrine portion

The endocrine pancreas is made up of about 1 million *islets of Langerhans*, cell clusters (diameter: 100 micrometers) with a rounded shape made up of cords, distributed in particular in the tail and body of the gland. They are the endocrine cells of the pancreas and secrete insulin, glucagon and several other hormones. In hematoxylin-eosin staining they appear as poorly colored cell aggregates in the middle of the strongly basophilic exocrine parenchyma. They do not have lymphatic vessels but are crossed by a dense plexus of fenestrated capillaries into which they pour their hormones and have a rich innervation so that almost all cells are in contact with a capillary and many with nerve endings. Five cell types have been identified within each Langerhans island [11]:

- the α cells are located on the periphery of the island, are quite numerous (15-20% of the total) and secrete glucagon;
- the β cells are the most numerous (65-80%), mostly located centrally in the islets and secrete insulin and amylin;
- the γ cells are very rare (1-2%) often they are almost all grouped in a single peripheral area of the island and secrete the pancreatic polypeptide (PP);

- the δ cells are rare (3-10%), uniformly distributed and secrete somatostatin;
- the ε cells are very rare (<1%) and secrete ghrelin.

In humans, the islets are subdivided into units, each of which exhibits a central aggregation of β cells surrounded by varying numbers of peripherally located cells that secrete the other hormones.

The nerve endings present at the base of the plasma membrane of Langerhans islet cells can be cholinergic, adrenergic, or noradrenergic. The adrenergic endings stimulate the secretion of glucagon and insulin, the noradrenergic endings inhibit the release of insulin, while they can act in coordination to regulate the release of somatostatin and PP. These fibers are almost all parasympathetic.

The endocrine portion of the pancreas controls the homeostasis of glucose in the bloodstream through insulin and glucagon production. Insulin works to reduce blood glucose levels by facilitating its absorption by cells (especially skeletal muscles) and promoting its use in the synthesis of proteins, fats and carbohydrates; it is therefore considered an anabolic hormone. Insulin is initially synthesized as a precursor called preproinsulin. This is converted into proinsulin and then cleaved by the C peptide into insulin which is then stored in beta cell granules. Glucose is taken up in beta cells and broken down. The ultimate effect of this is to cause depolarization of the cell membrane which stimulates insulin release. By contrast, glucagon, acting typically in an antagonistic fashion to insulin, functions as a catabolic hormone. It works to increase glucose levels by promoting its synthesis and the breakdown of glycogen into glucose in the liver. Moreover it reduces the absorption of glucose into lipids and muscles. Glucagon release is stimulated by low blood glucose levels or during physical activity [12].

The main factor affecting the insulin and glucagon secretion is the level of glucose in the blood plasma. Low level stimulates the release of glucagon while high level stimulates the release of insulin. There are others additional factors that influence the secretion of these hormones: somatostatin functions in the inhibition of insulin and glucagon secretion, whereas the significance

of pancreatic polypeptide and ghrelin are unclear [13; 14]. Moreover Some amino acids, by-products of protein digestion, stimulate the release of insulin and glucagon. Moreover nutrients in the form of glucose, aminoacids and long chain-free fatty acids (LC-FFAs), absorbed from the gastrointestinal tract and then detected by β cells, can involve in insulin production and release into the blood stream. the autonomic nervous system is also involved in maintaining this glycemic balance. The activation of the beta-2 receptors of the sympathetic nervous system by the catecholamines, secreted by the sympathetic nerves, stimulates the secretion of insulin and glucagon; while the activation of the alpha-1 receptors inhibits this secretion. [12] The M3 muscarinic receptors of the parasympathetic nervous system act when stimulated by the right vagus nerve to stimulate the release of insulin from beta cells. [12]

Studies have shown that the autocrine/paracrine response of insulin is via its receptor signaling.Although the insulin receptor is present in organs (for example, liver, muscle, fat and brain) and cells (α cells and β cells of the pancreatic islet) its actions in each of these differ:

- in the liver, insulin promotes glycolysis, inhibits gluconeogenesis, promotes synthesis of glycogen (glycogenesis) and inhibits the breakdown of glycogen (glycogenolysis);
- in adipose tissue, insulin promotes glucose uptake and glycolysis, the synthesis and storage of triglycerides (TGs) and the inhibition of lipid breakdown;
- in skeletal muscle, insulin promotes glucose uptake and glycolysis, the synthesis and storage protein and the inhibition of protein breakdown;
- in bone, insulin acts primarily on osteoblasts to promote osteoclast activity and enhance production and release of osteocalcin (OCN), a hormone that supports insulin release by the β cell.
- in the brain, insulin is involved into regulation of female fertility, appetite, and overall glucose homeostasis.

Regarding its affects in β cell, it sustains cellular growth, survival and function. Finally the actions of insulin in these tissues support anabolic pathways that lead to the generation of ATP and

the conversion of ingested nutrients into the major storage forms of energy (glycogen, protein and fat) [14]. In contrast glucagon, secreted by α cells, serves to counterbalance the actions of insulin. It promotes:

- in liver and skeletal muscle, glucagone induces glycogenolysis and inhibits glycogenesis;
- in adipose tissue, the hormone enhances lipolysis and inhibits triglyceride synthesis.

α cells also express cell surface insulin receptor and respond locally to secreted insulin by suppressing glucagon release.

The gut thanks to incretin hormones (glucagon-like peptide-1 or GLP-1 and glucose-dependent insulinotropic peptide or GIP), support glucose-dependent insulin secretion and β cell replication. Both GLP-1 and GIP are proteolytic products of the larger proglucagon peptide, which is also produced by α cells.

In addition, a healthy gut microbiota profile is thought to be essential to maintain normal β cell function. Finally, the cells of the central nervous system are known to secrete multiple peptides (melanin concentrating hormone –MCH-, serotonin and prolactin -PRL- and others) that have been shown both in vitro and in vivo to support β cell function and proliferation. Likewise, bone-derived OCN has been shown to support β cell replication and insulin secretion [15; 16].

1.4 Pancreatic carcinoma

1.4.1 Introduction: etiology, epidemiology and symptoms

Pancreatic cancer (PC) is still a highly lethal gastrointestinal cancer with a low 5-year survival rate and difficulty in early detection. At present, the incidence and mortality of pancreatic cancer are increasing year by year worldwide, in particular in the United States, Europe, Japan, and China. Globally, the incidence of PC is projected to increase of 1.1% meaning that pancreatic cancer will become the second leading cause of cancer death [17; 18] with a 5-year survival rate of only 3% and a median survival of less than 6 months. An early diagnosis of PC represents now the really problem of this tumor due to a lack of specific symptoms and limitations in diagnostic methods. To

date pancreaticoduodenectomy, the first one was in 1935, offers the only possibility of cure, although surgical intervention alone rarely achieves a curative end point but, for the surgically resected patients, the 5-year survival increased to 17.5% [19; 20]. The etiology of PC remains poorly defined, therefore, in order to prevent its insurgence, it is really important have a thorough and comprehensive understanding of pancreatic cancer risk factors. The exact cause of pancreatic cancer is unknown, but we can distinguish into non-modifiable and modifiable risk factors, associated with its development. Non-modifiable risk factors include age, gender, ethnicity, ABO blood group, microbiota, diabetes mellitus (DM), and family history and genetic susceptibility, while modifiable risk factors include smoking, alcohol drinking, dietary factors, pancreatitis, obesity, infection, and socioeconomic status. Some studies have shown that PC is generally associated with advancing age, from the age of 40, rarely before, and gradually to the age of 80, with 40-fold increased risk. Its incidence is declining slowly in white men, but it is increasing in other groups, possibly due to the risk factor of smoking. Women account for 57% of new cases and smoking, diabetes and obesity increase risk. Instead a link between alcohol or coffee consumption and PC has not been verified [21-24]. Physical activity, high fruit and vegetable intake and, possibly, nonsteroidal anti-inflammatory drugs reduce the risk [25]. On the familiary susceptibility, numerous studies have hilighted an increased risk (approximately threefold) in relatives of PC patients, it is estimated that 10% of PCs are due to an inherited predisposition [26-29]. Hereditary PC includes inherited cancer syndromes with a known germline mutation associated with an increased cancer risk [30]. The PC insorgence is also correlated with Genetic mutations wich increased the risk. These mutations include: STK11/LKB1, CDKN2A (p16), BRCA1/2, PRSS1/SPINK1/CFTR, mismatch repair genes (MLH1/MSH6/MSH2/PMS2), ATM, and PALB2 (a new pancreatic cancer susceptibility gene)[31]. This cancer often develops without clear early signs or symptoms and the eventual manifestations depends on the tumor location within the gland. Among the signs and symptoms found and known we have:

- jaundice, into 50% of patients, which is more common with patients whose cancers are located in the head of the pancreas where tumors can cause obstruction of the adjacent biliary system [32];
- vague abdominal discomfort, nausea and weight loss;
- duodenal obstruction or gastrointestinal bleeding due to large tumors that advance beyond the pancreas;
- steatorrhea which can also result from obstruction of the pancreatic duct;
- hyperglycemia and diabetes have been associated with early manifestation of disease;
- abdominal and back pains, anorexia, dyspepsia, gallbladder enlargement, migratory thrombosis (Trousseaux syndrome), subcutaneous fat necrosis (panniculitis), hyperglycemia, ascites and depression have been associated in patients with advanced disease[29; 33; 34].

Based on the physiologic development of pancreas, it has been found that metaplasia can be associated with the increased risk of cancer; in particular pancreatic acinar cells have the capacity to undergo metaplasia to a ductal cell phenotype, through acute or chronic inflammation, representing an direct link to pancreatic ductal adenocarcinoma (PDAC). Acinar-ductal metaplasia (ADM) might represent reprogramming pathway of a progenitor population [35]. Metaplastic acinar structures are highly proliferative, express Notch target genes, and exhibit mosaic expression patterns for EGFR, ErbB2, and pErk, reminiscent of the PDAC precursors [36-38].

1.4.2 Pathophysiology

PDAC evolve through noninvasive precursor lesions, most typically pancreatic intraepithelial neoplasias, acquiring clonally selected genetic and epigenetic alterations along the way. Pancreatic cancers can also evolve from intraductal papillary mucinous neoplasms or mucinous cystic neoplasms. Thanks to a global genomic analysis reported in [39], the exomes of 24 PDAC were sequenced to characterize more fully the genes mutated in PC. The most frequent genetic mutations

in invasive PDAC are abnormal activation of the KRAS oncogene, inactivation of tumour-suppressor genes including CDKN2A, TP53, SMAD4, and BRCA2, [40] widespread chromosomal losses, gene amplifications [39], and telomere shortening [41]. The latter and KRAS mutations are the earliest known genetic abnormalities highlighted, even in low-grade pancreatic intraepithelial neoplasias [41; 42] and telomere shortening is believed to contribute to chromosomal instability. Instead the inactivation of TP53, SMAD4, and BRCA2 is found in advanced pancreatic intraepithelial neoplasias and invasive carcinomas [43; 44].

Moreover, in <20% of PC, the genes mutated are oncogenes such as BRAF, MYB, AKT2, and EGFR, and tumor-suppressor genes such as MAP2K4, STK11, TGFBR1, TGFBR2, ACVR1B, ACVR2A, FBXW7, and EP300 [45]. Finally, the frequency of mutated genes like PIK3CG, DGKA, STK33, TTK, and PRKCG is low in this kind of cancer [46]. Intraductal papillary mucinous neoplasms share some of the mutations found in pancreatic intraepithelial neoplasias but with notable differences like the intraductal papillary mucinous neoplasms rarely inactivate SMAD4. Some studies, using in vivo models like genetically engineered mouse targeting some of the genes most commonly altered in human PC, have investigated the underlying mechanisms and the possible therapeutic agents [47]. In addition to the gene alterations, even epigenetic changes like alterations in DNA methylation and histone modifications and non-coding RNAs can alter gene function in PC [48]. One of the first studies on PC reported the promoter methylation and gene silencing for the tumor-suppressor gene CDKN2A in neoplasms without genetic inactivation [49]. Only a few classic tumor-suppressor and DNA-repair genes undergo epigenetic silencing in this cancer like MLH1 and CDH1 which are methylated in a small proportion of tumors. Furthermore other genes, including CDKN1C, RELN, SPARC, TFPI2,SFN, MSLN, and S100A4 and mucin genes are frequent targets of these kind of epigenetic alterations in PC [48; 50-57]. Some of these alterations have been evaluated for their diagnostic or biological relevance [48; 55; 58]. Mutations involved in microRNA expression seem also to contribute to cancer development and progression. Overexpression of several microRNAs in PC, including miR-21, miR-34, miR-155, miR-196a and

miR-200, is thought to play a major role in neoplastic progression [59-62]. Furthermore, these microRNAs, easily detectable in human plasma, could be useful diagnostic markers [60].

1.4.3 Tumor microenvironment

In the last 10 years, the scientific community began to consider the tumor microenvironment (TME) role in PC development and evolution rather than just a supportive or structural tissue to the tumor. Previously, the first vision on TME led to the substantial development of therapeutic tools focused on cancer cell targeting, excluding the impact of the stromal compartment, which could be involved in limited improvement in patients survival. To date, despite the recent knowledge on the impact of TME, some clinical trials targeting this cellular compartment, have not yet led to better patient management. This suggests that much more is needed to be discovered on the functional relationship between the various cell types composing this kind of cancer. It is well established that PC is made of up to 90% of stromal cells, mainly cancer-associated fibroblasts (CAFs), endothelial, nerve and immune cells and several studies revealed their key roles in PC development [63; 64].
CAFs have a key role in PC development, progression and chemoresistance. They secrete multiple extracellular matrix (ECM) components, forming a dense fibrous matrix characteristic of PC. CAFs are a mixed population of cells originating from resident fibroblasts, bone marrow-derived cells and pancreatic stellate cells (PSCs) that ,once activated, switch into myofibroblast-like phenotype and modify their star-like shape into a spindle shape. Activated fibroblats consequently start expressing alpha-smooth muscle actin (α-SMA), type-I collagen, transforming growth factor-β1 (TGF-β) and other proteins involved in cell proliferation, migration, ECM remodeling, epithelial to mesenchymal transition (EMT) and inflammation [65]. The endothelial cells in PC TME are also found [66]. Generally, PC is an extremely hypoxic tumor and is poor vascularized [67]. Under hypoxia, hypoxia-inducible factor (HIF-1α) drives VEGF upregulation which promotes tumor angiogenesis, proliferation and metastasis [67]. Finally in TME, macrophages, indicated in this case as tumor-associated macrophages (TAMs), represent the major immune component and are crucial for cancer

progression. Most macrophages originate from circulating monocytes and form a heterogeneous population. A network of molecules, factors and post-transcriptional regulators participate in directing macrophage polarization, discernible in classically activated macrophages M1 and alternatively activated macrophages M2 [68]. M1 macrophages are characterized by a pro-inflammatory phenotype, develop in response to lipopolysaccharides (LPS) or interferon-γ (INF-γ) and release interleukin (IL)-1β, tumor necrosis factor-α (TNF-α), IL-6 or IL-12 to induce immune responses [69]. Instead, the M2 macrophages present an anti-inflammatory phenotype with an elevated expression of the mannose (CD-206) and scavenger receptor (CD-163) as well as a secretion of TGF-β1 and IL-10 to promote the remodeling of extracellular matrix and angiogenesis [70]. Macrophages polarize in M2 group in response to IL-4 and IL-13 and, particularly as TAMs, they acquire an M2-like pro-tumor phenotype. M2 effects are balanced by the M1 anti-tumor group [71]. A marked expression of M2-markers in tumor tissues is correlated with a worse diagnosis and prognosis of cancer patients [72; 73]. In several preclinical studies, TAM depletion has been shown to reduce metastatic burden, improve response to the chemotherapy drug gemcitabine [74] and alter gene programmes that define the basal-like/squamous subtype [75].

All these cells, tumoral and stromal cells, with the ECM and extracellular components such as extracellular vesicles (EVs) form the TME, as like a dense stroma. Their interaction influence, in a pro- or anti-tumoral manner, cancer development, evolution and resistance to treatments, with a consequent impact on patients care and survival. Some studies highlighted the implication of extracellular vesicles in this crosstalk and its consequent impact on PC progression. Therefore the stroma is not only a mechanical barrier but also constitutes a dynamic compartment critically involved in the process of tumor formation, progression, invasion and metastasis.

1.4.4 Biomarkers and staging

In recent years, thanks to our knowledge acquired on PC molecular changes, it was possible identify new serum tumor markers. Currently, there are 6 common tumor biomarkers in PC [76]:

- CA19-9;
- CA242;
- carcinoembryonic antigen [CEA];
- CA125;
- microRNAs;
- gene mutations (K-RAS, TP53, CDKN2A, Smad4, PDAC1 and BRCA2 [77; 78].

The combination of tumor markers and imaging methods may be the first choice for early screening for PC [79], incresing the sensitivity and the specificity [80]. In last years, advances in cytology and genomics in combination with serum tumor markers have also improved its early diagnosis. CA19-9 is the most commonly used indicator for postoperative detection in PC recurrence and prognosis [81; 82]. B7-H4, IL-6, IL-8, and IL-10 are indicators for assessing poor prognosis in PC [83; 84]. In recent years, circulating cell-free DNA (CfDNA) and mutation-specific circulating cell-free tumor DNA (CftDNA) have been identified as new potential biomarkers. The current studies show that there is a statistically significant correlation between changes in cfDNA and cftDNA concentrations and treatment response. Therefore, cfDNA and cftDNA may become new biomarkers for evaluating the efficacy of cancer after treatment, and because of their correlation with the tumor volume of metastases, they can also be used as tools to estimate tumor volume [85]. Clinical staging classifies patients into:

- resectable;
- borderline;
- resectable;
- locally advanced;
- metastatic disease.

This classification is necessary for initial treatment. Chest imaging is recommended to detect metastases.

1.4.5 Treatment

Traditional PC treatment includes surgery, chemotherapy, radiotherapy, and palliative care. In recent years, research on targeted therapy, immunotherapy, and microbial therapy has become more and more in-depth, and may be combined with traditional methods for the treatment of PC in the future. Similarly, the stage of PC determines its treatment. In many clinical trials it has been demonstrated that surgical resection is more likely if chemotherapy/radiation is given prior to surgery, in order to obtain a better local tumor control, eliminate potential metastatic lesions and ultimately improve/increase patient survival and quality of life [86] Chemotherapy alone is sometimes used for patients too frail to tolerate radiation.

To date, chemotherapy is an important part of the comprehensive treatment of PC. After radical resection, modified leucovorin, 5-fluorouracil, irinotecan, and oxaliplatin (MFOLFIRINOX) are often used for 6 months of adjuvant chemotherapy, or 6 months of gemcitabine and capecitabine. In patients with metastatic PC, the preferred option is the FOLFIRINOX (5-FU, irinotecan, and oxaliplatin) regimen, gemcitabine and NAB-paclitaxel in combination with chemotherapy. When patient is not suitable for combination chemotherapy, gemcitabine is the first choice. For patients with locally advanced PC, combination therapy with chemotherapy (gemcitabine with or without erlotinib) and radiation therapy is the first choice for this type of patient. Currently, researchers are investigating other forms of topical therapy such as radiofrequency ablation, high-intensity focused ultrasound, microwave ablation, irreversible electroporation, and topical anti-KRAS therapy (using siG12D-Loder). In patients with locally advanced unresectable cancer, neoadjuvant therapy combined with chemotherapy and surgical treatment is the only opportunity for secondary surgery in such patients [87]

Immune checkpoint blockade (ICB) therapy, approved for various types of cancer, in PC is not much considered because this cancer is less immunogenic. The PC microenvironment is thought to create an immunosuppressive environment. Therefore, there is not a currently immunotherapy

approved for patients with PC. Monotherapy of CTLA-4 or PD1 inhibitors is essentially ineffective in PC patients, and many clinical studies have tested immunotherapy in combination with chemotherapy, chemoradiotherapy, vaccines, and cytokine antagonism in order to improve this treatment.

There is now strong evidence that the human microbiota plays a key role in regulating PC development and response to treatment. To date, some studies have confirmed that the intestinal microflora is able to form a systemic immunity and tumor-specific immunity in PC, but the mechanism remains to be studied [88; 89].

Finally PC patients need palliative care. They are important like than other treatment in order to improve the life of patients. Mainly there are 3 approaches form management of patients with gastric outlet obstruction: percutaneous bile duct drainage, surgical gastrojejunostomy, and endoscopic duodenal stents [90].

2. Extracellular vesicles

2.1 Introduction

Intercellular communication is a key characteristic of both for unicellular organisms and for multicellular organisms. Communication between cells can occur through direct contact, as in the case of gap junctions, whose permeability is strictly regulated and incurs the passage of molecules involved in various cellular processes such as proliferation, differentiation, apoptosis and carcinogenesis [91]

Furthermore, cellular communication can also occur through the binding of released molecules with receptors present on the surface of target cells, or also thanks to the release of soluble factors (chemokines, cytokines, growth and hormones). The latters can act in an autocrine way on the same cell that has them released, in a paracrine way on adjacent cells, or in an endocrine way on distant cells through biological fluids [92-95]. In last decades, a new mechanism for intercellular communication has emerged, involving the intercellular transfer of extracellular vesicles. The EVs serve a variety of purposes, in addition to their functions in communication, they are involved in transfer of genetic information, removal of dangerous substances and unnecessary metabolites such as chemotherapeutics or oxidised lipids from cells [96]. It is not sure if the process of vesicle secretion belongs to all the eukaryotic cells, but for those that do, it seems to be maintained throughout the evolution timeline. Different types of cells can release distinct types of vesicle. Moreover, from a single cell may be released EVs of varying size, biogenesis, and cargo, which can change with the physiological state of the cell. Several number of EVs subtypes have been identified, and common distinction of EVs rely on size. The smallest diameter of the phospholipid vesicles can be between 10 and 20 nm, while the upper limit of the EVs is not known. It is known that the size of apoptotic bodies and "oncosomes" is in the order of microns (1-to 10-μm in diameter), while mammalian platelets are approximately 2 μm in diameter. For this reason, many

studies therefore concentrate on EVs with a diameter of 1 micron or less. Depending on the size and their biogenesis, the EVs are divided into three broad classes (Fig. 2.1.1).

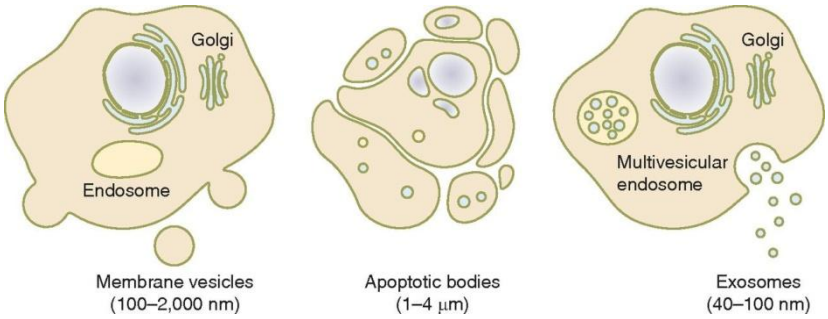

Figure 2.1.1 EVs classification [97].

The vesicles with the largest diameter are included in the apoptotic bodies group. They are heterogeneous diameter vesicles, which vary from 200 nm to 5 μm in diameter and are released from the plasma membrane of cells during programmed cell death. Instead, microvesicles or ectosomes have a diameter of 100-800 nm and are known to be released from the plasma membrane of viable cells. Finally, the exosomes represent the smallest group of vesicles, they have a size of 30-150 nm. They are formed when MVBs merge with the plasma membrane and expel their intraluminal vesicles which are released into extracellular space [98].

These three big groups of EVs, comprise subgroups further divided according to the size of the particles, biogenesis and biomarkers. They are:

- Oncosomes or large oncosomes are large EVs released by highly aggressive cancer cells (1000–10,000 nm) [99].
- Migrasomes (up to 3000 nm) are oval-shaped microvesicles containing small vesicles. the cells that secrete migrasomes from tips of their retraction fibers. These vesicles are formed and released in migration-dependent manner [100].

- Microvesicles or MVs (100–1000 nm) are released from the surface of cells. MVs share some biomarkers with exosomes, such as CD63, and both the vesicles transport bioactive cargos between cells [101].
- Exosomes are vesicles (30–100 nm), this group includes three subpopulations of exosomes: large exosomes (Exo-L, 90–120 nm) and small exosomes (Exo-S, 60–80 nm) and non-membranous smaller nanoparticle named “exomeres” (< 50 nm) [85]tion-dependent manner [100].

2.2 Biogenesis

Recent research efforts have highlited the importance of the secretion of MVs from cell plasma membrane during tumor stadiation. This biogenesis requires rearrangements of the plasma membrane, including changes in lipid components, protein composition and calcium levels. Calcium-dependent mechanism triggers with the increase in intracellular calcium, induced by an external signal, inducing aminophospholipid translocases (flippases and floppases). Calcium ions are also able to active enzymes, such as gelsolin and calpain, which modify the actin cytoskeleton allowing the disassembly of the cortical actin. This process determines the curvature and protrusion of the membrane plasmatic and the consequent release of the vesicle from the membrane [102; 103]. The calcium, however, is not the only second messenger involved in the EVs release mechanism; in this way it has been shown that the activation of protein kinase C (PKC) trigger the release of EVs [104-106]. Exosomes and MVs have different type of biogenesis, in distinct sites within the cells. However, the biogenesis of both entities involves common intracellular mechanisms and sorting machines. Exosomes are formed from late endosomes induced by the inward budding of the multivesicular body (MVB) membrane. Invagination of late endosomal membranes contributes to the formation of intraluminal vesicles (ILVs) in broad MVBs [107].

2.2.1 ESCRT-dependent mechanisms

One of the most approved mechanisms for the creation of MVBs and ILVs is the endosomal sorting complex needed for the transport (ESCRT) function. This protein machinery comprises four complexes (0 through III) and work with other associated proteins such as VPS4, VTA1, ALIX also called PDCD6IP [108]. More in detail, the subunit ESCRT-0 consists of HRS that can bind clathrin coats and create a protein network on endosomal membranes, collects ubiquitinated cargo proteins and starts their sorting through the MVB pathway. HRS recruits the tumour-susceptibility protein (TSG101) of ESCRT-I subunit and ubiquitinated cargo proteins and interacts with ESCRT-II [109]. ESCRT-I is then involved in the recruitment of ESCRT-III via ESCRT-II or ALIX. Indeed, this starting complex is important in initiating ESCRT-III recruitment and assembly. Unlike the other ESCRT complexes, ESCRT-III does not form a stable cytoplasmic complex, but consists of four core subunits: Vps20, Snf7, Vps24, and Vps2. Some of these subunits form linear polymers that have been implicated in cargo trapping, membrane deformation and vesicle abscission. At this step, intervene the AAA-ATPase VPS4 which is involved in the scission of the forming vesicle and also for the recycling of the ESCRT machinery for subsequent rounds of sorting [110]. It was demonstrated that ESCRT-III-associated protein ALIX facilitates intraluminal budding of vesicles in endosomes and thus exosome biogenesis, following association with syntenin, the cytoplasmic adaptor of heparan sulphate proteoglycan receptors. Syndecan (heparan sulphate proteoglycan receptors) cargo creates syndecan assemblies that can recruit syntenin–ALIX. Syntenin interacts directly with ALIX through LYPX(n)L motifs, supporting the intraluminal budding of endosomal membranes [111].

2.2.2 ESCRT-independent mechanisms

Moreover, concomitant inactivation of four proteins of the four separate ESCRT complexes does not preclude the development of MVBs, indicating that MVBs and ILVs that can develop in the

absence of ESCRT activity [112]. Indeed, recent research favours an alternative mechanism for sorting exosomal cargo into MVBs in an ESCRT-independent manner, which appears to rely on raft-based microdomains for lateral segregation of cargo inside the endosomal membrane. Such micro-domains that contain high concentrations of sphingolipids from which ceramides are produced. Ceramide may cause the agglomeration of small micro-domains into larger domains that facilitate domain-induced budding [113]. This ceramide-dependent mechanism highlights the main role of exosomal lipids as well as tetraspanins in exosomal biogenesis. Tetraspanin CD81, for example, plays a crucial role in sorting target receptors and intracellular components into exosomes. However, CD81 acts with tetraspanin-enriched microdomains (TEMs) as ubiquitous complex membrane sites for the compartmentalization of receptors and signalling proteins in the plasma membrane [114].

Over CD81, there are identified other tetraspanins such as CD82 and CD90 to play a role in the development of microdomains and exosome cargo sorting [115]. These proteins may aggregate and create rafts with other tetraspanins or other cytosolic proteins, resulting in cytoskeletal remodelling and micro-domain creation [116].

2.3 Vesicles release

Once the microvesicles are formed, EVs and the exosomes are released in different ways and times. Microvesicles come out of the plasma membrane faster and in a way dependent on the interaction between actin and myosin fibers with a subsequent ATP-dependent contraction [117]. Instead, exosome secretion is a longer process in which the transport and apposition of MVBs onto the plasma membrane is necessary to merge and release ILV into the extracellular environment. The formed MVBs can either fuse with lysosomes or after incorporation with the plasma membrane are released in an extracellular environment as exosomes. The transfer of these vesicles through the cells to cell membrane depends on the interaction with the cytoskeleton and it is regulated by several proteins. This machinery of the scission/release of MVs includes cytoskeleton (actin and

microtubules), related molecular motors (kinesins and myosins), molecular switches (small GTPases) and fusion machines (Soluble NSF Attachment Protein Receptor (SNAREs) and tethering factors). Among the GTPase proteins Rab family is particularly important, even if their involvement seems cells specific. Rab27a and Rab27b are involved in the release of exosomes from HeLa cells. In detail, Rab27b regulates the motility of MVBs towards the cell membrane, while Rab27a promotes their fusion [118]. Instead, other proteins of the Rab family are involved in the release of exosomes in other cell structures, as in the case of Rab35 in the Oli-neu cells (oligodendroglial cell lines) [119] and Rab11 in the K562 cells (chronic myeloid leukemic cells of the bone marrow) [120].

The proteins of the SNARE family play a key role in the final step of the membrane fusion process and release of exosomes. It is necessary that three or four elements of the SNARE family form a complex. The members of this protein family are known also as R- or Q-SNARE. The formation of this complex requires one R-SNARE (usually v-SNARE) and three Q-SNAREs (usually t-SNAREs) [121]. Their activity is determined partly by the state of phosphorylation of these proteins, which influences their localisation and their interaction with SNARE partners, thus leading to the release of regulated exosomes [122].

The release of EVs from the plasma membrane is induced by stimuli leading to an increment of intracellular calcium and cytoskeleton remodelling [123]. In comparison to plasma membrane derived EVs, the exosome secretion is typically studied in the absence of a signal established to cause this secretion, indeed the intracellular signals involved are not known.

2.4 EVs composition

During their biogenesis, the vesicles incorporate material belonging to the “mother cell”, including cell-specific proteins, lipids, RNA or even DNA as a "molecular signature". Indeed, by studying the pools of vesicles from samples composed of various types of cells (as in the case of blood) it is possible to discriminate the cell of origin of a vesicle on the basis of its content. Despite

the selective proteins, particularly in exosomes, there are omnipresent proteins that are most likely related to biogenesis or exosome functions. Among those always present, there are cytoskeletal proteins such as tubulin, actin and actin-binding proteins, proteins involved in intracellular membrane fusions and transport such as annexins and Rab, heat shock proteins, such as the constitutive isoforms of HSP70 and HSP90, tetraspanins such as CD9, CD63, CD81 and CD82 and metabolic enzymes.

Even on the basis of the origin of the vesicles their content can change, indeed exosomes derived via the endolysosomal compartment appear to be most enriched with histocompatibility complex class II (MHC class II) and CD37, CD53, CD63, CD81, and CD82 histocompatibility complexes [124]. As described before, the use of the ESCRT complex for biogenesis requires accessory proteins. Therefore, regardless of the cell of origin, the exosomes generated in an ESCRT dependent manner contain proteins ESCRT, Alix, TSG101 and chaperones, such as Hcs70 and Hsp90 [125]. Then, MHC II, tetraspanine, ESCRT, Alix, TSG101 and heat shock proteins that we find in all exosomes regardless of the type of parent cell, can be considered exosomal markers [125]. Instead, MVs compared to exosomes contain more proteins with post-translational modifications, such as glycoproteins or phosphoproteins [126]. By isolating EVs through a differential centrifuge, mitochondrial proteins such as Aconitase, Golgi apparatus such as GM130, endoplasmic reticulum such as Calreticulin and some cytoplasmic proteins such as α-tubulin have not been found. For this reason the purity of EVs can be confirmed by checking the absence of these proteins [127]. Through spectrometric analysis, the content of vesicles from ovarian cancer cells was analysed. These EVs are enriched in proteins that undergo acetylation and phosphorylation such as phosphatidylinositol-3-kinase, mitogen-activated protein kinase (MAPK). The presence of kinases which are key signalling molecules can probably explain the ability of these EVs to affect recipient cells [127]. Exosomes derived from tumour cells and oncosomes are characterized by MMP inside them. These enzymes are necessary to digest the ECM and improve

tumour invasiveness and therefore can carry signalling messages from the cells of origin to the receiving cells [128].

EVs, like cells, are covered with a double-layer phospholipid which, however, is enriched with sphingomyelin, gangliosides and unsaturated lipids, that suggest a more stable casing than cell membranes. Instead, their amount of phosphatidylcholine and diacylglycerol is decreased relative to the membranes in their cells of origin [129].

As with the previous EVs components, the RNA content also varies according to the cell of origin. The RNA carried by EV is generally less than 200 nucleotides, therefore shorter. In the vesicles there are both coding and non-coding RNA (miRNA, tRNA, rRNA, small nuclear (snRNA), small nucleolar (snoRNA) and interacting RNA with piwi (piRNA) [130]. The RNA transported by EVs can be released to the acceptor cells [131], and it is interesting to note that, for example, transported miRNAs can regulate the translation of the target mRNAs in the receiving cells. This process that can be crucial in tumour progression [132].

Finally, among the material contained in EVs there is also DNA in size from 100 base pairs (bp) to 2.5 kilobase pairs (kB). The information deriving from the analysis of the genetic material contained in the vesicles can be exploited as a circulating biomarker in the early diagnosis of tumours and in the monitoring of the response to treatment [133].

2.5 EVs interactions with cells

Once released, EVs can rapidly degrade, thus releasing their cargo in extracellular environment close to the cells that released them, or they can reach target sites far from the site of release, through the circulation in different biological fluids [134; 135]. The messages that these vesicles carry within them can influence the physiology of the receiving cells, promoting physiological or pathological changes. However, the process responsible for EVs cell internalisation has generated a lot of controversy in the literature, because various types of mechanism can be applied for this communication. Interaction with target cells can occur through different mechanisms (Fig. 2.5.1):

- protein interaction, binding specific receptors expressed on the surface of target cells, which can trigger a signaling mechanism and the consequent formation of extracellular complex;
- direct vesicles membrane fusion with target cell membrane and subsequent release of its contents inside the cell;
- endocytosis.

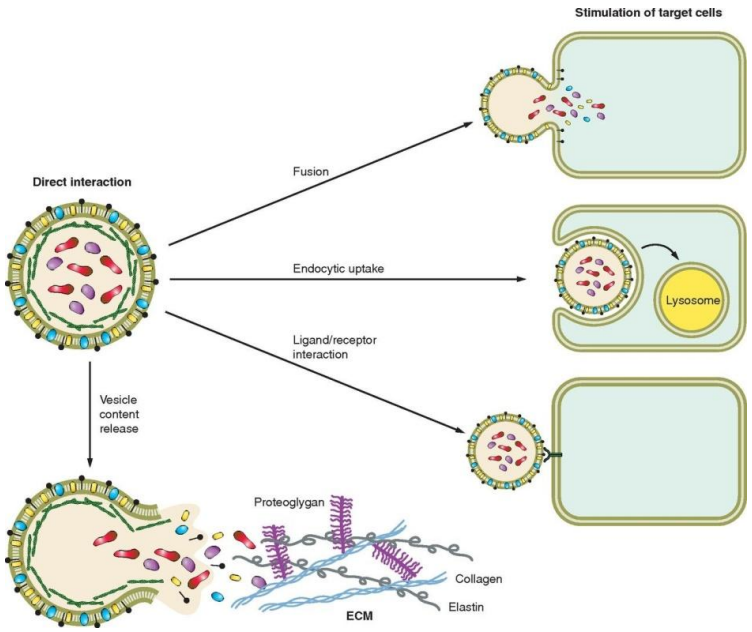

Figure 2.5.1 EVs interactions with cells [97].

2.5.1 Protein interaction

The uptake mechanisms of EVs involve protein interactions that facilitate subsequent endocytosis [136; 137]. The list of specific protein-protein interactions that mediate EVs attachment and absorption in cells is continuously updated in the literature.

Tetraspanins, as seen above, are very abundant in EVs and play a role in cell adhesion. Based on this evidence, they could also have a function in EVs uptake [138]. To support this, studies conducted using antibodies against tetraspanins CD81 or CD9 have reduced the internalization of

vesicles by dendritic cells. Another class of proteins involved in cell adhesion, and therefore potential promoters of uptake are integrins. Using antibodies that mask the binding sites of αv (CD51) and β3 (CD61) integrins on the cell surface, results a reduced absorption of EVs in dendritic cells [139].

Heparin sulfate proteoglycans (HSPG) are highly glycosylated proteins that act as co-receptors in cells. They are used by viral particles and lipoproteins to enter in the cells. To understand whether they are also able to promote the entry of EVs into cells, studies have been conducted by marking both the vesicles and the membrane proteoglycans (syndecan and glypican) of the receiving cells with fluorescent probes. From this studies a co-localization of both fluorescent signals was observed, suggesting that HSPG are needed on the cell surface for efficient internalization of EVs [136].

2.5.2 Cell surface membrane fusion

The fusion is the process whereby two distinct membranes (one of EVs and the other of the plasma membrane) merge. When the lipid bilayers are close together, they have the outer leaflets in direct contact. This leads to the formation of a hemi-fusion stalk in which the outer-leaflets are fused. Subsequently, the expansion of the stalk produces the double layer of the hemi-fusion diaphragm from which a fusion pore opens. It can be promoted by several factors, such as acid pH, wich in the extracellular environment has been shown to improve fusion [140].

2.5.3 Endocytosis

The most accredited method for uptake of EVs is endocytosis [141; 142], which can be rapid up to 15 minutes after exposure [143]. It is also a process that requires energy from cells, indeed the ability to internalise EVs at 4°C is drastically reduced [136; 142]. Besides requiring energy, EVs requires a functioning cytoskeleton. Treating cells with cytochalasin D (metabolite that

depolymerizes actin filaments with inhibition of endocytic pathways) there is a significant reduction of EVs internalization in a dose dependent manner [137; 142].

The term endocytosis encompasses several mechanisms including clathrin-mediated endocytosis (CME), phagocytosis, macropinocytosis and plasma or endosomal membrane fusion that are involved in the uptake of EVs.

- Clathrin-mediated endocytosis: it is also called receptor-mediated endocytosis. EVs have transmembrane molecules on their surface that interact with molecules on cell membranes. Following this ligand-receptor interaction, the cells internalize molecules by invagination of the plasma membrane which collapses into a vesicular bud, matures, and pinches. The resulting intracellular vesicle is covered with clathrin and then merges with the endosome where it deposits its contents. In ovarian cancer cells [142] and in phagocytic receptor cells [143] has been observed that the use of chlorpromazine prevents the formation of clathrin-coated pits on the plasma membrane, reducing the absorption of EVs by the receiving cells.
- Caveolin-dependent endocytosis: caveolae are tiny cave-like invaginations in the plasma membrane that may be internalised into the cell. Caveolin-1 is a protein necessary and sufficient for the formation of caveole. A specific knockdown of the CAV1 gene leads to a reduction of the caveolin-1 protein and to a reduced absorption of EVs, highlighting its importance [144]. At the same time, the precise role of this path can vary between cell types and EVs, as with CAV1 knockout in mouse embryonic fibroblast cells which instead leads to an increase in the absorption of EVs [137].
- Macropinocytosis: the EVs may be internalised through macropinocytosis, where the membrane protrusions stick out from the cell, wrapping up the EVs and enclosing them to the lumen of the macropinosome. Or, if EVs are stucked in membrane ruffles, are macropinocytosed. This mechanism requires Na +/H+ exchanger activity and it is also rac1-, actin- and cholesterol-dependent [145]. In microglial, the macropinocytosis of EVs

derived from oligodendrocytes has been abrogated through different approaches. Significant reduction in uptake occurred by inhibiting the Na + / H + exchanger. Even using the molecule NSC23766, small molecules used as inhibitor of rac1, the absorption of EVs by the microglia was reduced [146]. Instead, other studies using inhibitors did not reduced macropinocytosis in EVs uptake [136; 143; 144].

- Phagocytosis: this method is generally used by macrophages and is able to internalize both small molecules (such as exosomes) and larger molecules. Phosphoinositide 3-kinase (PI3K) plays a key role in phagocytic processes in facilitating membrane incorporation in phagosome creation. To study the involvement of PI3K in phagocytosis, PI3K inhibitor such as wortmannin and LY294002 were administered to macrophages. Both molecules blocked EV uptake in a dose-dependent manner [143].
- Involvement of lipid rafts: the composition of the plasma membrane is not the same in all its regions, there are regions morphologically represented by accumulations of particular proteins and lipids. For these lipid accumulations in some areas of the membrane, it appears thicker. To study the involvement of lipid drafts in EVs uptake, inhibitors of components belonging to these areas of the plasma membrane were used. Fumonisin B1 and N-butyldeoxynojirimycin hydrochloride, molecules that decrease the glycosphingolipidic composition in the plasma membrane were administered to dendrid cells by preventing its biosynthesis. Resulted the evidence that the internalization of EVs has been significantly reduced, suggesting that sphingolipids play an important role in endocytosis [147]. Protein from these areas of the membrane can also play a key role in the EVs uptake. Annexin II may have a role to play in the anchoring of EVs to the plasma membrane lipid raft domains, whereas Annexin-VI may lead to the trafficking of EVs to the late endosomal compartment [148].

2.6 Role of tumor EVs

EVs play an important and complex role in some pathologies, particularly in tumors. Cancer cells are able to release EVs, involved in intercellular communication, supporting the tumor progression. In this way they support tumor growth and expansion, ensuring the survival of the same cells [149]:

- promoting the angiogenesis, because they contain mRNAs or growth factors like VEGF and HGF involved in this process [150];
- promoting the tumor migration and invasion by degradation of the extracellular matrix through metalloproteases (MMP-2 and -9) and the urokinase activator of plasminogen (uPA). Once externalised, the MMPs can degrade the components of the extracellular matrix; while uPA converts the plasminogen into plasmin, also contributing in this case to extracellular matrix degradation and in addition activating the same MMPs [151-154];
- carrying oncogenes that induce the transformation in a more aggressive mesenchymal phenotype of target cells, favouring tumor progression and metastases;
- inducing apoptosis escape (thanks to the elimination of caspase-3 via vesicles) and acquisition of chemotherapy resistance [155; 156];
- participating in the escape from the immune system; on EVs surface is exposed Fas ligand which, by interacting with the Fas receptor, induce apoptosis of immune cells like T lymphocytes [157]. Moreover EVs are also capable of interfere with antigen presentation [158];
- influencing the formation of metastatic niches.

2.6.1 EVs role in Pancreatic Cancer

Several studies demonstrated EVs as playing important roles in PC. Migration and invasive properties are recurrent gain-of-functions for PC tumor cells following autocrine uptake of EVs.

Indeed, several studies reported that highly metastatic PC tumor cells-derived EVs are able to transfer metastatic potential to recipient cells, promoting migration and invasion, as shown in [159] through the transfer of EVs containing zinc finger protein 4 or by the transfer of EVs carrying the receptor tyrosine kinase Eph receptor A2 (EphA2) [160]. EVs, reported as key effectors of cell–cell communication in PC, from its development to evolution, affect cellular physiology in autocrine and paracrine manners [161-163]. These vesicles, containing biological messengers like microRNAs, long non-coding RNAs, specific cancer stem cell markers as well as proteins and lipids, can affect themself or cells of TME, as stromal cells, sustaining cell aggressiveness, [164] and chemoresistance. The prevalence of stromal cells in PC further reinforces the potential role of EVs and intercellular communication promoting tumor progression and invasion. Recent studies have showed that PDAC-derived exosomes play a critical role in pre-metastatic niche formation. As reported in [165] the exosomes from the pancreatic primary tumor can be taken up by Kupffer cells, upregulating TGFβ secretion and fibronectin production in order to form a fibrotic microenvironment in the liver, which can recruit macrophages for immunosuppression. Additionally, a greater number of exosomes are found in stage I PDAC patients who later develop liver metastasis, indicating that exosomes could promote liver metastasis and may be a diagnostic marker [165]. In another study of PDAC exosomes it is showed that they are involved in metastasis to the lung, liver, or both, and also in vehiculation and expression of integrins like α6β4 and α6β [166]. Moreover, exosome integrin uptake by resident cells (lung fibroblasts and epithelial cells, liver Kupffer cells) activates Src phosphorylation and pro-inflammatory S100 gene expression, which contributes to pre-metastatic niche formation [166].

3 Annexin A1

3.1 Introduction

Annexins, also known as lipocortins, are a family of structurally related proteins that bind in a calcium-dependent manner to anionic membrane phospholipids [166]. They have been discovered at the end of 70's and have been identified both in mammalian organisms and in mildews or plants. The name Annexin derives from the Latin "adnexio", meaning their main properties to bind and to keep themselves joined to plasma membranes. In order to identify an annexin protein two principal parameters are important: the capability to interact with the negative membrane phospholipids though the Calcium (Ca^{2+}) and the presence of a repeated segment of 70 amino acids defined as "annexin repetition". This repeated segment is particularly preserved in about all annexins, instead the NH2-terminal part is more variable. The role of these proteins appears quite important, both in cytosol and at the plasma membranes, as confirmed by over 100 annexins identified in in 65 animal species [167; 168].

3.2 ANXA1 structure

ANXA1 represents 2–4% of the total cytosolic protein in several cell types and is also located in the nucleus. The gene of Annexin A1 has been the first one to be cloned, it is localized on the human chromosome 9, particularly at 9q12-21.2 and codes for a protein of 38,71 kDa. The promoter is particularly preserved and presents consensus sequences for some molecules [169]. ANXA1 is the first characterised member of the annexin family, comprising twelve proteins, identified in humans, conventionally referred to as annexin A1-13. The first annexin described with its crystal structure was the Annexin A5, but the first longer annexin studied by high resolution crystallography has been just the ANXA1. Each annexin is made up of two main domains: the N-terminal tail, different in length and sequence, and the C-terminal. The latter includes four homologous segments (except for annexin A6 which contains eight), numbered from I to IV and

each consisting of five helices, called A, B, C, D, and E, which accommodates the sites binding Ca^{2+} cations. The four domains together form a disc with a slight curvature.

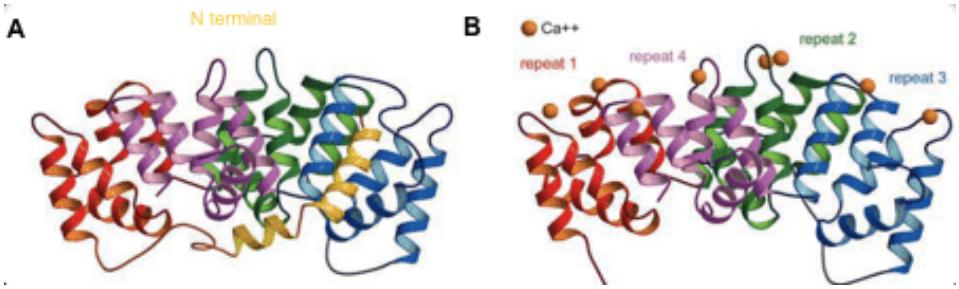

Figure 3.2.1 Molecular structure of Annexin A1

As shown in figure 3.2.1, the convex side is situated in front of plasma membrane, on the other hand, the concave one is accessible for the interactions with the N-term of the same protein or with other molecular partners [170]. The N-terminal domain of ANXA1 contains 41 residues and folds to form a unit structurally separate, probably on the concave side of the protein core. The first 26 amino acid residues of the N-terminal domain form two α-helices, which are inclined by 60 ° with respect to each other at the level of the amino acid Glu17. The α-helix between residues 26 and 18 interacts with the surface of segment IV of the central domain, while the other points towards the convex portion of the molecule. In absence of calcium, the latter partly occupies the position of the helix D of segment III within the protein, which extrudes from the surface. When the N-terminal domain is hidden within the core protein of ANXA1, it represents the inactive form of the molecule. Following calcium-mediated binding of annexin to the membrane, the segment III D helix acquires the appropriate conformation to bind calcium, forming a type II binding site. During this process, the N-terminal domain is expelled from the hydrophobic pocket and becomes accessible from the concave side of the molecule. It can interact with specific molecules causing aggregation of membranes through various mechanisms: the interaction of the N-terminal helix with a second bilayer, the dimerisation of two annexin molecules through the N-terminal helices, or the binding of

the concave sides of two annexins mediated by a dimer of the S100A11 protein, molecular partner of ANXA1. The N-terminal domain also contains the EGF phosphorylation site (Tyr21). It is located in the second α-helix and, when the protein is in the inactive state, this residue is hidden inside a hydrophobic pocket. In absence of calcium, therefore, annexin cannot be phosphorylated [171].

3.3 Intracellular ANXA1

ANXA1 show a different subcellular distribution, both at the nuclear, cytosolic level and in association with the membranes, depending of the calcium concentration, which justifies its participation in different processes, such as proliferation, apoptosis, survival, differentiation and migration [161; 162; 172; 173]. The N-terminal domain plays a fundamental role in the localization of ANXA1: its proteolytic cleavage causes a redistribution of this protein from multivesicular endosomes to late endosomes, as occurs in the internalization of the EGF receptor. ANXA1 together with S100A11 participates in the internal vesiculation process that generates multivesicular endosomes starting from early endosomes, as this complex is able to connect the membrane surfaces [171]. Once the forming vesicles evolve through the final fusion process, ANXA1 is phosphorylated by internalized EGF receptors intended for degradation. Phosphorylation makes this protein susceptible to proteolysis of the N-terminal domain: in this way not only the sequence required for the localization of annexin in early endosomes is eliminated, but also the binding site with S100A11. As a result, the S100A11 dimer is released, along with the N-terminal sequence of ANXA-1, in a process that accompanies actual membrane fission and internal vesicle release. This annexin involvement may not be essential for endosome maturation and transport, but it may facilitate kinetics by providing a support structure for membranes [174]. By acting as a substrate for the tyrosine kinase domain of the EGF receptor, ANXA1 inhibits EGF-mediated proliferation. It can bind the Grb2 protein, which is located upstream of the MAPK signal cascade [173]. ANXA1 exerts a negative regulation of proliferation in different cell types through sustained activation of

the ERK cascade. This involves an anomalous organization of the actin cytoskeleton which, together with the inhibition of cyclin D1 mediated by annexin, causes a block of proliferation [175]. ANXA1 is phosphorylated by various kinases, such as those associated with the PDGF receptor, the hepatocyte growth factor receptor and protein kinase C, thus contributing to its importance in proliferation [173]. Furthermore the annexins don't contains nuclear targeting sequences but different reports have indicated the nuclear location of ANXA1 [176; 177]. To date, the precise mechanism leading to ANXA1 translocation from the cytoplasm to the nucleus, and its functional relevance are not fully understood. However, some studies have showed the role of nuclear ANXA1 in cell transformation and cancer. ANXA1 translocates to the nucleus by mitogenic/proliferative and DNA-damaging stimuli such as EGF, heat, hydrogen peroxide, sodium arsenite and phorbol 12-myristate 13-acetate (PMA) [178; 179]. In another study have used inhibitors of different signalling kinases such as extracellular signal-related kinase (ERK), p38, phosphoinositide 3-kinase (PI3K) and protein kinase C (PKC), and they identified PKCδ as the kinase responsible for ANXA1-nuclear translocation [179]. PKCδ can phosphorylate ANXA1 at Thr24, Ser27 and/or Ser28 residues [180], suggesting that ANXA1 nuclear translocation depends on its phosphorylation by PKCδ. Once in the nucleus, ANXA1 is mostly modified by SUMO [181] in Lys257, known as a site located in a hot spot where several overlapping modulation sites, including a Ca^{2+}-binding site (Asp253, Leu256 and Glu261) and a nuclear export signal (NES), from Leu254 to Asp259, were co-located [182]. The overlap between NES region and the sumoylation site suggests that this modification could involve the ANXA1 detention in the nucleus. Two independent studies showed that ANXA1 phosphorylated in the cytoplasm at Tyr21 [183] then translocated to the nucleus [178]. Altogether, these data suggest that nuclear translocation of ANXA1 is associated with a phosphorylation process (tyrosine and possibly threonine and serine phosphorylations).

3.4 Extracellular ANXA1

In addition to its intracellular localization, ANXA1 can be released and act on specific cells in an autocrine or paracrine manner. Most times, the protein is externalised during cell activation or due to stimulation by glucocorticoids. Indeed, they lead to an increase in the synthesis of ANXA1 in different cell types: a treatment with glucocorticoids causes a rapid exocytosis of annexin both in peripheral and central tissues. They can also induce phosphorylation of this protein and translocation to the membrane. It is not always completely clear how ANXA1 is released from cells. In the case of polymorphonuclear cells, the extrusion of the granules leads to an enrichment of annexin on the cell surface, but in cells where this protein is not stored in granules, the secretion is mediated through a different mechanism. ANXA1 does not contain a sequence or other secretory signal, but the involvement of the ABC-A1 protein, a transmembrane transporter, has been shown. Furthermore, since it has amphipathic properties, another possibility could be in passing through pores or channels. In recent years, the importance of Ser27 residue phosphorylation as a secretion signal has become evident. This post-transcriptional modification is commonly observed prior to the appearance of ANXA1 outside the cells [184]. Since its discovery, in the late 1970s, ANXA1 has been shown to be capable of modulating the immune system to affect a number of anti- and pro-inflammatory events. Originally described as an inhibitor of phospholipase A2 (PLA2), ANXA1 can affect several components of the inflammatory response, limiting the supply of arachidonic acid needed for the synthesis of prostaglandins, thus suppressing inflammation. Initially, the inhibition of PLA2 activity was attributed to a binding of annexin to the substrate rather than to a direct interaction with the enzyme. This idea has been reconsidered as both a secreted form and a cytosolic form of this enzyme have been discovered. Cytosolic PLA2 is sensitive to calcium and shows a predilection for arachidonyl-containing phospholipids. This enzyme is mainly involved in the production of lipid mediators of inflammation, and the activation of arachidonic acid and PLA2 represents a limiting step in the synthesis of these molecules. ANXA1 has been shown to inhibit the

activity of this enzyme directly, rather than through substrate depletion. However, the interaction between PLA2 and ANXA1 is unclear and occurs in specific cells [173]. ANXA1 has also been found in plasma, particularly during inflammatory events such as myocardial infarction. It specifically inhibits the trans-endothelial migration of leukocytes, limiting inflammation by the interaction with receptors present on neutrophils and monocytes, which belong to the receptor family of the Met-Leu-Phe formylated peptide (FPR). FPRs are G-protein-coupled receptors initially identified as targets for bacterial peptides. The latter direct leukocytes as they migrate to the site of infection, activating a signal cascade mediated by FPR that leads to a reorganization of the cytoskeleton necessary for cell movement. ANXA1 also binds the FPR2 receptor, also defined ALXR or receptor of lipoxin A4; in any case, the interaction is mediated by the N-terminal portion (the first 25 residues), which is found in a free form at the infection sites. The receptor activation also induces the loss of L-selectin from the leukocyte surface and the detachment of the attached leukocytes from the activated endothelium. Therefore, through the activation of members of the FPR family, ANXA1 can act as a regulator of leukocyte migration and as an endogenous anti-inflammatory protein. Furthermore, since the presence of FPR is not limited to leukocytes only, the interaction between these receptors and ANXA1 can regulate the migratory activity of other cell types, such as dendritic cells, hepatocytes, astrocytes and type II alveolar cells [185]. In general, ANXA1 exerts a powerful suppressive effect on the innate immune system, acting on granulocytes (PMN), monocyte-macrophages and mast cells, along with other different cell types. Polymorphonuclear leukocytes contain an abundant amount of annexin stored in granules. When PMNs are activated, the protein is immediately mobilised to the plasma membrane, where it acts negatively on the FPR2. The action of the protein at this site is terminated in a few minutes by the action of a membrane-bound enzyme, which cuts the annexin between residues 29 and 33. ANXA1 is also involved in the apoptosis of neutrophils, limiting the inflammatory response [186]. As with granulocytes, ANXA1 is released by macrophages and binds to FPR2, reducing the activity of these cells, including the release of eicosanoids and superoxide radicals. Mast cells represent a site of

intense synthesis of ANXA1, which is on the granules, or within them, and in other compartments, including the cytoplasm and the nucleus. Through interaction with the FPR2 membrane receptors, annexin leads to the reduction of histamine secretion and the production of prostaglandin D2 [242184]. ANXA1 exhibits a different distribution and function in the cells of the adaptive immune system: lymphocytes contain a small amount of ANXA1 and do not bind this protein in the same way as monocytes / macrophages. In baseline conditions, both annexin and FPR2 are present on the membrane of T cells. Stimulation of T cells through TCRs leads to the externalisation of FPR2 and the release of ANXA1. The activation of this receptor by annexin modulates the strength of the signal mediated by TCR, increasing the levels of transcription factors such as AP-1, NF-κB and NFAT. An additional anti-inflammatory role of ANXA1 is in its ability to mediate the action of glucocorticoids, as it is involved in the antipyretic effect of these molecules and in blocking the hyperalgesic effect mediated by COX-2 [187]. Besides intervening in inflammatory processes, such as glucocorticoids, ANXA1 is involved in the regulation of hormonal secretion, suppressing the release of corticotropin and vasopressin, respectively, from the adenohypophysis and hypothalamus. It also contributes to the regulating action of glucocorticoids on other pituitary hormones, such as prolactin, thyroid stimulating hormone, luteinizing hormone and growth hormone. ANXA1 appears to mediate the in vitro glucocorticoid-induced reduction in testosterone production in the testis, and to exert positive effects on glucose-mediated insulin release from pancreatic cells [187]. In addition to the role of mediator of the action of glucocorticoids, ANXA1 is involved in the regulation of apoptosis: in some cases for its pro-aptotic effect, in others a link between ANXA1 and cell resistance to apoptosis has been observed. The reason for this difference could be due to the cell type or the state of differentiation [173].

3.5 Externalized ANXA1

The proteins secreted by eukaryotic use an N-terminal signal peptide to direct their co-translation to the ribosome of the rough endoplasmic reticulum. Subsequently, they progress to the Golgi

apparatus and, finally, through secretory vesicles, they are directed to the cell surface or to the extracellular environment [188]. Studies conducted on ANXA1 revealed that this protein lacks the N-terminal signal peptide necessary for the classic protein externalization; this suggests that ANXA1 could be externalised through different secretory pathways [189]. Furthermore, it has been observed that, after its externalization, ANXA1 undergoes a proteolytic cleavage on the N-terminal [190]. Thanks to various studies, it has been deduced that ANXA1 can be externalised through five mechanisms:

- ANXA1 externalisation may depend on a myristylation process. Indeed, the protein sequence has potential sites for this modification, and PKC can target its myristylated substrate to the plasma membrane. The passage of ANXA1 across the plasma membrane could be facilitated by lipidization [191];
- the ATP-Binding Cassette (ABC)-A1 transporter is involved in ANXA1 secretion, but its inibition can only partially suppress the protein's externalization, suggesting that other mechanisms may contribute to its release [192];
- it occur in PMNs, upon adhesion to endothelial cell, by degranulation where the granules fuse with the plasma membrane and release ANXA1 in the extracellular compartment [193];
- by the activation of flippase and scramblase, the lipid bilayer orients itself outward exposing the phosphatidylserine. Since ANXA1 has a great affinity for acid phospholipids (in particular phosphatidylserine), it has been hypothesised that this protein is exposed on the surface of microparticles, for example, released by PMNs [194].
- by the fusion of small vesicles, called exosomes, with the plasma membrane. All the proteins associated with these nano-vesicles could be externalised, including ANXA1 [195].

Studies conducted by [196] highlight the role of EVs containing ANXA1 in the intestinal inflammatory process and in intestinal epithelial lesions acting as a biomarker of inflammation.

Furthermore, EVs containing ANXA1 mediate tissue wound repair processes: their role in colonoscopy-induced lesions of the murine intestinal mucosa was studied by [196]. Our previous study showed the role of ANXA1 in promoting the secretion of EVs and their involvement in the processes of metastasis, in particular in the process of angiogenesis underlying the development of metastases. The exosomes can induce the formation of new vessels that guarantee an adequate supply of nutrients and oxygen to the tumour [197; 198].

3.6 ANXA1 in cancer

Besides its anti-inflammatory activities, ANXA1 role in cancer development and progression stands out [199]. ANXA1 was initially thought to be useful as a diagnostic or prognostic biomarker due to its differential expression between normal and tumor tissue samples.

In this context, it has been suggested that ANXA1 plays a role in malignant transformation, activation of oncogenes, inactivation of tumor suppressor genes, induction of proliferation, apoptosis, chemosensitivity or chemoresistance, cellular migration, invasion and metastasis, [200-204]

However, ANXA1 can act either as an anti-tumor or as a pro-tumoral factor, depending on localization and tumor type, and stage [205] and its expression can be upregulated or downregulated in different cancers, so its role may not be that simple. High ANXA1 expression levels have been found in breast cancer [206; 207], melanomas [208], hepatocellular carcinomas [209], pancreatic cancer [210], colorectal cancers [211], gastric cancer [212], gliomas [213], lung adenocarcinomas [214; 215] correlating with poor prognosis, lower disease-free survival rates, reduced metastasis-free survival and lower overall survival [209; 215; 215]. On the contrary, low expression levels of AnxA1 have been observed in squamous head and neck cancer [216], nasopharyngeal carcinoma [217], esophageal carcinoma [218], prostate carcinoma [219], thyroid cancer [220] and associate with a worse prognosis, poor differentiation, lower overall survival and higher relapse rates [216; 220; 221].

3.6.1 ANXA1 in breast cancer

The expression of ANXA1 in breast cancer (BC), however, is more complicated with contradictory reports. The protein is down-modulated in estrogen-resistant cells, compared with the nonmalignant ones and up-modulated in the triple-negative subtype [222] and lymph node metastasis, when compared to the corresponding primary tumors [207]. ANXA1 might act as a stress protein protecting cells from heat- and estrogen-induced growth arrest, DNA damage and proliferation in MCF-7 cells, possibly through enhanced ERK activation and inhibited JNK activation [223; 224]. ANXA1 knockdown by siRNA attenuates proliferations of MCF-7 and MDA-MB-231, suggesting a mitogen function through FPR activation [225; 226]. Moreover, it is demonstrated the crucial role of ANXA1 in supporting the epithelial–mesenchymal transition (EMT) event, promoting migration, invasion and metastasis formation in BC. RNAi-mediated ANXA1 knockdown induced EMT and metastasis in non-metastatic cells but the restored expression reversed EMT and abolished the tumor metastasis [227]. By using the triple-negative cell line, MDA-MB-231, it is showed that ANXA1 promotes the metastasis by enhancing the TGF-β signaling, resulting in increased phosphorylation of the small mothers against decapentaplegic homolog 2 (Smad2), with actin reorganization, which facilitates an EMT-like switch [228]. Another study also showed that ANXA1 displays pro-angiogenic functions in breast cancer by supporting the activation of the nuclear factor-kappa B (NF-kB) transcriptional factor [229]. All these information suggest that ANXA1 can perform a double role in BC development, functioning as oncogene and oncosuppressor. In addition, ANXA1 -/- mice showed a particular reduction of the known EMT markers like vimentin, as well as myosin light-chain kinase which has been reported to induce Rho-kinase mediated assembly to stress fibers known to be implicated in the EMT [230].

3.6.2 ANXA1 in prostate cancer

ANXA1 dysregulation in prostate cancer (PCa) has been reported by numerous studies with controversial results. It has been shown that overall ANXA1 expression is unaffected or downregulated in in situ PCa whereas cancer microarray databases (Oncomine) show an increase of the protein expression in the more metastatic PCa stages [219]. In human prostate adenocarcinoma, particularly in androgenstimulated prostate cancer, the protein is decreased if compared to benign prostate epithelium; the loss of protein expression is an useful indicator for cancer proliferation and progression and a potential parameter to evaluate the anticancer drug resistance. ANXA1 negatively mediates IL-6 expression and play a proapoptotic role by mediating p38 and JNK [231-233]. In vitro, ANXA1 expression reduced tumourigenicity and cell viability in prostate cancer cell lines by enhancing activation of pro-apoptotic signaling pathways [234]. The inverse expression of CK18 and ANXA1 has been well characterized also in prostate cancer cells: luminal cells, with epithelial phenotype present poor level of ANXA1, instead the basal cells (expressing CK5) has high level of this protein. Furthermore it has been reported that ANXA1 from prostate-derived cancer-associated fibroblasts (CAF) is capable of inducing EMT, promoting de novo generation of cancer stem cells (CSCs) and stimulating the CSC population from prostate cancer cells [235]. Another important event during the EMT and prostate tumor progression is the break in the dynamic dialog between ANXA1 and cytokeratin 18 (CK18), a cytoskeleton protein, considered as one the most important epithelial markers. In normal breast tissue but also in benign lesion or breast carcinoma, the difference in the expression between ANXA1 and CK18 is not significant. During the EMT, in luminal cells becoming mesenchymal ones, CK18 is lost, on the other hand, ANXA1 expression increases, in this way, ANXA1 cannot co-localize with CK18/CK8, a protein complex involved in the cytoskeleton organization. A very similar situation appears in the prostate cancer where the ANXA1 has been studied in the acquisition of a more aggressive phenotype: the more invasive prostate cancer cells show not only EMT but also CSCs markers and express an increased level of

ANXA1. When the ANXA1 expression decreases, the invasive and migratory capability of these cells falls down together with all the detected markers for EMT and CSCs (like NANOG, Oct-4, ALDH7A1, CD44 and CD133 as well as Snail and Sox2), beyond to other genes involved in the acquisition of chemoresistance as ABCG2 [219].

3.6.3 ANXA1 in colon rectal cancer

In colon rectal cancer (CRC) ANXA1 promotes progression, invasion and metastasis, as demonstrated by in vitro and in vivo systems and positively correlates with K-ras gene mutations in tumorigenesis. In CRC the protein through FPR binding elicits signaling pathways related to chronic inflammation that activate ERK, MAPK and the transcriptional factors, NF-kB and the signal transducer and activator of transcription 3 (STAT3). [236-240].

3.6.4 ANXA1 in lung cancer

ANXA1 is up-regulated in A549-LAC and H446-SCLC lung cancer cells and patients' tissues; ANXA1 is associated with progression, metastasis, drug resistance and differentiation of this cancer [241-243]. In a study about lung cancer, the authors reported that the expression of ANXA1, A2 and A3 closely related to cisplatin resistance and an up-regulation in cisplatin resistant patients' tissues appears both in mRNA and protein levels [244].

3.6.5 ANXA1 in melanoma

The ANXA1 expression has been well studied is melanoma. The protein is up-regulated in metastatic B16 mouse cells and subsequent syngeneic primary tumors when compared with non-metastatic B16F10 cells. Full-length and cleaved ANXA1 levels in human melanoma cell lines were found to positively correlate with cell invasion and metastasis capacity thanks to its interaction with the FPRs [245-247]. This effect occurred at least partially through ERK and STAT3

phosphorylation, which in turn induced the expression of MMP2 and its release to the extracellular compartment [248; 249]

3.6.6 ANXA1 in pancreatic cancer

Comparative analysis of protein profiles of pancreatic cancer and normal pancreatic cells had already highlighted a significant over-expression of ANXA1 [250-252].

The protein correlates with poor differentiation, prognosis and drug resistance of PC [250-252]. Previous studies have shown that the ANXA1 strongly affects migration and invasion of PC cells. Exosome proteomic analysis performed by Yu et al., identified ANXA1 as one of the proteins associated to PC metastasis in multiple organs, mostly in liver [253]. The autocrine loop created by ANXA1 on origin/recipient cells, triggering by the protein interaction with the FPRs, has been elucidated.

Moreover, thanks to the establishment of ANXA1 knock-out (KO) MIA PaCa-2 PC cells through the CRISPR/Cas9 genome editing system, it has been possible to show that the protein is able to trigger the EMT, leading to a more aggressive phenotype [161-163; 254]. Studies investigating the mechanisms of ANXA1 secretion have found that this protein is also involved in the biogenesis of extracellular vesicles (EVs); as a component of these microvesicles enriched in exosomes (40–100 nm diameter), the protein further contributes to the aggressiveness of PC [pessolano]. So the ANXA1, in PC, is able to act in autocrine and paracrine manner, essential for their diffusion in distant sites [161-163].

4 Heparan sulfate

4.1 Structure, role and function

Heparan sulfate (HS) belongs to the family of glycosaminoglycans (GAGs), macromolecules of the ECM and characterized by linear polyanionic polysaccharidic structures [255-261]. It is synthesized as long polysaccharidic chains covalently bound to a serine residue that is part of a GAG attachment sequence in a protein core, forming HS proteoglycans (HSPGs), or as unconjugated chains (Fig. 4.1.1).

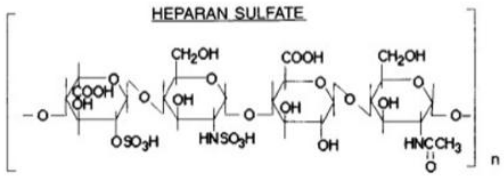

Figure 4.1.1 HS structure

In both of these two forms, HS is well described as able to bind a large number of proteins, including growth factors, cytokines and chemokines, enzymes and enzyme inhibitors, ECM proteins, and membrane receptors. These binding are usually dominated by charge–charge interactions between the anionic carboxylate and/or sulfate group of the polysaccharide and basic amino acids of the proteins [262-264], although other interactions also contribute. HS, synthesized by most cells is able to affect multiple biological processes, like development and homeostasis, as well as in many pathological conditions, including inflammation, neoplastic transformation, and cancer progression [261; 265-275]. Through binding to stromal components, such as laminin, collagen, and fibronectin, HS participate in the maintenance of ECM integrity. In addition, by sequestering growth factors, cytokines, and chemokines, HS protect them from protease degradation, acting as an extracellular reserve, modulating their bioavailability, and allow the formation of ligand gradients. Moreover, it directly participates in cell signaling as co-receptor for

high-affinity growth factor receptors and integrins [265; 269; 276; 277]. Anothers characterized examples are the interaction with the fibroblast growth factor (FGF), platelet-derived growth factor (PDGF) and vascular endothelial growth factor (VEGF) whose activities are strongly increased in carcinogenesis.[278] As reported in [279] HS and ANXA1 are able to interact each other and this interaction is mediated by calcium which is further responsible of a great part of ANXA1 functions [280]. However, there is a lack of information on the biological implication of this complex and on the HS ability to bind the extracellular form of ANXA1 which could mean blocking its autocrine/paracrine and juxtacrine effects, mediated by the interaction with FPRs involving in many cancers like PC [161-163; 219]. Alterations of HS chains are common in malignant transformation and progression [281]; in this regard it is being developed for a wide range of disorders, including cancer [282-286]. A major role in the post-translational modification of HS structure, and consequently, its bioactivity, is assumed by heparanase and the endosulfatases, Sulf-1 and Sulf-2. The functions of these enzyme activities during development, homeostasis, tissue repair, and other physiological processes appear to be positively involved in cancer. In fact, some studies indicate that the altered expression or activity of these enzymes determines a profound impact on tumor behavior [287-290]. Since from started a few analyses of clinical studies, as well as prospective trials, that support a beneficial effect of heparins on cancer patient survival [291-296], in this way studies have been also conducted on HS. Ongoing clinical trials are designed to test its effect in cancer progression, prevention of metastasis and chemoresistence in adjuvant, coadjuvant and preoperative settings [296].

An intensive synthetic effort led to the production of HS derivatives characterized by the ability to mimic its activities. Thanks to the evidence for a role of HS in essentially all aspects of tumor biology prompted the development of this class of compounds as anticancer therapeutics. The beneficial antitumor effects of HS mimetics are presumed mainly to be related to their direct and/or indirect interference on heparanase activity, adhesion molecules, the tissue factor pathway, and signaling triggered by chemokines/cytokines, growth factors, tissue-degrading enzymes, or

endosulfatases. Given the increasingly recognized clinical significance of heparanase, the HS-specific endo-β-d-glucuronidase implicated in multiple aspects of tumor growth and progression [297-302], extensive efforts were made to identify agents targeting the HS-degrading activity of this enzyme [303-307]. Accumulating evidence indicates, however, that HS mimetics can affect tumor biological behavior by exerting pleiotropic effects through a specific mechanism of action based not only on heparanase inhibition, but also on the HS functions. he phospho-sulfo-mannan PI-88 (muparfostat) (Fig. 4.1.2) was identified among sulfated oligosaccharides endowed with antiangiogenic and antiheparanase activity [308; 309]. As an HS structural mimetic non-cleavable by heparanase, it inhibited the endo-β-d-glucuronidase activity and prevented the release of proangiogenic growth factors (i.e., FGF1, FGF2, and VEGF) by competing with HS [310]. PI-88 appeared well tolerated in animal studies, and its ability to significantly inhibit tumor growth, angiogenesis, and metastasis in preclinical models prompted its clinical investigation.

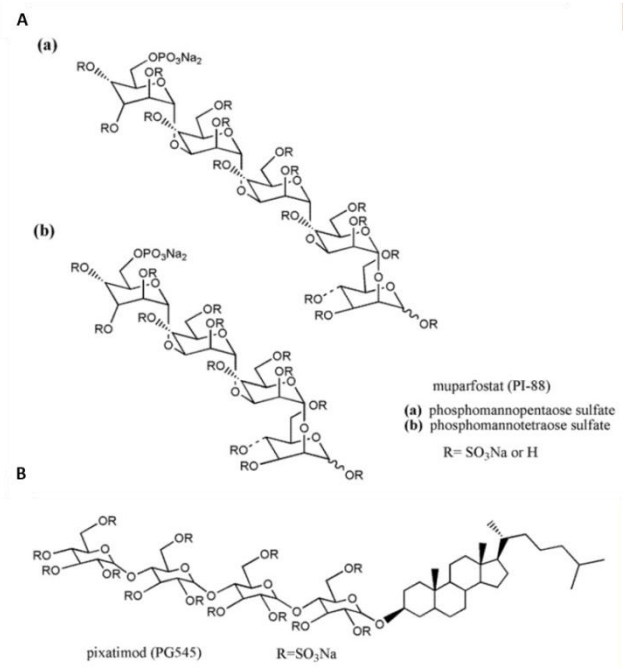

Figure 4.1.2 HS mimetics

Other mimetic is PG545 (pixatimod). It is a fully sulfated respected to PI-88 (Fig. 4.1.2), tetrasaccharide functionalized with a cholestanyl aglycone, selected as a lead clinical candidate

among olisaccharidic HS mimetics of the PG500 series because this modification confers improved biological activity and reduced anticoagulant activity [311]. PG545 showed antitumor activity in several murine and human solid and hematological tumor models and potent anti-metastatic effect in experimental and spontaneous metastasis models; for this reason it is currently undergoing clinical trials. However, in clinical trials on PC patients, the use of these mimetics in combination with conventional pharmacological treatments has not been successful.

5 Three-dimensional (3D) cell model

In the last 10 years the study of tumor biology has undergone a progressive development and many physiological aspects of the tumor microenvironment have been clarified, but much remains to be analyzed about the interactions between the tumor and the surrounding environment and what are the molecular mechanisms underlying that is. A tumor is made up, macroscopically, of a tumor parenchyma and a non-tumor cellular component (fibroblasts, endothelial and immune system cells), as well as a complex network of three-dimensionally arranged molecules that form the ECM. Non-parenchymal cells with ECM are called tumor stroma, and the recent findings attribute to them important functions in tumor development and growth .The study of neoplastic pathologies has been mainly conducted for years on *in vitro* systems developed in two dimensions (2D) where the cellular immortalized cultures reflecting only partially the morpho-molecular pattern of human tumor cells and also not reflecting the complexity of the microenvironment *in vivo* [312]. In this scenario, three-dimensional (3D) cell cultures represent an alternative and/or parallel approach to 2D, and they are therefore the link between traditional cell culture and *in vivo* models [313].

3D cell models can accurately reproduce the TME and mimic the regulatory mechanisms that exist between tumor and stroma. Currently they are used in several studies to identify the role of adhesion molecules in invasiveness/metastasis formation and angiogenesis, and for tissue remodeling analysis [314] and to study the penetration and action drugs.

3D cell culture model shows peculiar molecular characteristics closer to the structural architecture of the tumor *in vivo* than 2D ones. Currently, the most widespread 3D model is represented by multicellular tumor spheroids (MCTS), made up of tumor cells or a co-culture of tumor and stromal cells, which acquire a spherical symmetry organized in a three-dimensional arrangement (Fig. 5.1.1)

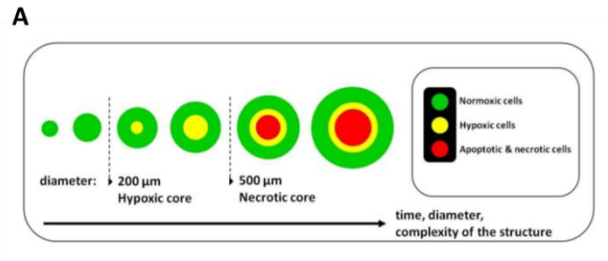

Figure 5.1.1 Spheroids architecture

The spheroid model was introduced by radio-biologists in 1970 [315]. Spheroids are generally produced by stabilized cell lines that aggregate homotypically and have morpho-physiological characteristics that favor cell-cell and cell-matrix interactions [316]. Usually small in vivo tumors show greater resistance to therapy than monolayer cultured tumor cells. The complex architecture of the solid tumor is involved in the so-called "multicellular resistance" (MCR), a phenomenon determined by different cellular mechanisms:

- the stratification in an outer proliferative layer;
- a quiescent intermediate layer;
- an hypoxic and necrotic core; above 400-500 µm in diameter, this core is formed, mainly due to the limited diffusion of oxygen and / or nutrients and the accumulation of catabolites and toxins [317];
- reduced permeability to drugs;
- inhibition of apoptosis and modulation of the expression of key proteins such as DNA repair enzymes or topoisomerases [318].

Cancer cells within the spheroid reproduce the same concentric arrangement and, at the same time, they have a growth pattern similar to early stage solid tumors not vascularized [319].

These characteristics make multicellular tumor spheroids a system closer to the tumor structure *in vivo* and make them an excellent alternative for the study of different tumors. Thanks to their peculiarities, spheroids are used to evaluate the alteration of gene expression of tumor cells during

neoplastic development, to test the effect of radiation or the sensitivity to new chemotherapeutic agents specific for different tumors. To date, the term spheroid differs from the term "aggregate" which is instead used to describe and possibly discriminate less tightly packed cells from compact spherical cultures [320].

Moreover in 2D cultures the lack of the stroma is a highly limiting factor considering that, in certain cancers, the stroma is essential for tissue remodeling. In this regard, in pancreatic cancer, about 90% of the volume is made up of stroma. Recent studies indicate that the tumor stroma critically supports tumor growth, drug response, progression and formation of metastases 8. To this end, researchers turned to 3D cell culture systems to mimic *in vivo* pancreatic tumor conditions by obtaining a 3D architecture that provides appropriate ECM proteins, cell-cell communication, nutrient gradients and hypoxic tumor regions [321; 322]. To date, few studies have showed the influence of PC cell/fibroblast 3D co-culture or monocyte in vitro.

5.1 3D culture techniques

Although in recent years different techniques have been described for the generation and culture of tumor spheroids, to date there is no standard reference tecnique to cell-contact surface interaction [323]. A strategy, well known, still widespread involves the use of continuous agitation of the cell suspension inside "spinner flasks", in this way spherical aggregates are spontaneously formed and adhesion is prevented to other substrates. A system similar to cultures in “spinner flasks” uses circular agitators or rotating tubes, which keep the cells in suspension between the rotating cylindrical walls thanks to the microgravity [324]. Both techniques allow to obtain a large number of spheroids of heterogeneous dimensions and, therefore, are suitable for large-scale production but they need a large quantities of culture medium and the availability of specific tools. Stationary culture techniques are simpler and need to seed the cell suspension to a non-adherent surface, plates coated with organic matrices such as agar, poly-HEMA, Matrigel or collagen are often used [325].The use of agar-coated 96-well U-bottom plates allows cell aggregation by sedimentation on

the well concave surface and it is then possible to monitor and manipulate the spheres separately. The variation in diameter within the plate remains below 5% for different types of spheroids and remains relatively low when the culture medium is periodically changed [322]. These methods allow for the formation of homogeneously sized spheroids and allow for the analysis of individual spheroids, but require careful handling and have the limit to product of the same.

An alternative technique is the "hanging drops" method [318; 326], which represents an effective variant for spheroids production. It is a simple tecnique, which can be used with different cell lines and allows the production of spheroids of compact homogeneous dimensions. The rounded bottom of the suspended drop, facilitates cell aggregation. The method involves the deposition of a small volume of cells (20-40µl) in the lid of a petri dish or a 96-well plate. By inverting the plate, a “hanging” drop is formed and the cells, by gravity, accumulate in the bottom of the drop, thus tending to aggregate into spheroids. To avoid evaporation of the drop, the bottom of the plate is filled with PBS [327]. This technique has the advantage of being able to form single spheroids of uniform size, does not require the use of coated plates and also does not require special equipment. However, the disadvantages are not lacking: it involves an intense manual work for the collection of the single spheroids, the volume of the suspended drop must be below 50µl, due to the surface tension that affects the drop retention, the change of the culture medium is practically impossible and, for this reason, it is only useful for short-term crops. It is therefore not a technique aimed at large-scale production nor for a long-term study. The automated methods, introduced in recent years, are instead aimed at a wider tumor spheroids production to be used for preclinical screening. Tissue engineering has solved some problems of traditional techniques, using scaffolds and bioreactors. However, the scaffolds do not intrinsically contain the signal molecules necessary to recreate the cellular microenvironment, such as collagen or matrigel [324]. The use of bioreactors has instead made it possible to provide for metabolic needs thanks to the perfusion of fluids which guarantees a continuous external gradient and / or internal nutrient, recreating the tumor micro-vasculature in vivo. However, these systems have not yet found a routine application in the new

drug validation or discovery, mainly due to the lack of a well-standardized technique on a large scale and tested.

6 Aim of the work

Pancreatic cancer (PC) is one of the most aggressive cancers in the world and it correlates to poor prognosis and high mortality due to late diagnosis. Several extracellular factors are involved in its development and metastasis to distant organs. In PC, the protein Annexin A1 (ANXA1) appears to be overexpressed and may be identified as an oncogenic factor. ANXA1 also explain its action both in intracellular and extracellular manner, also because it is a component in tumor-deriving extracellular vesicles (EVs). Indeed, these EVs are known to nourish the tumor microenvironment (TME). Some studies have highlighted that TME plays a critical role in PC chemoresistance and progression.

The general aim of this PhD project has been to investigate the paracrine effect of ANXA1 on stromal cells like fibroblasts, endothelial cells and macrophages in order to demonstrate how the ANXA1-EVs complex can stimulate and sustain the pancreatic TME, both in 2D and 3D cellular models.

Furthermore as oncogenic factor, ANXA1 can need to be inhibited, mainly by blocking its extracellular form, as a new model of cancer adjuvant therapy. Heparan sulfate (HS) is a glycosaminoglycan of the extracellular matrix known to bind growth factors and cytokines, generating a kind of reservoir in the extracellular environment. One of these molecules is represented by ANXA1. In this regard, another aim was to study the interaction between HS and ANXA1 and how this glycosaminoglycan could influence ANXA1 oncogenic action.

7 Material and methods

7.1 Cell Cultures

MIA PaCa-2 and PANC-1 cells are immortalized epithelial cells of human pancreatic carcinoma. They were purchased from ATCC (ATCC CRL-1420 and ATCC CRL-1469, respectively for MIA PaCa-2 and PANC1 cells, Manassas, VA, USA) and cultured in Dulbecco's Modified Eagle Medium (DMEM) containing L-glutamine 2 mM, 10% heat-inactivated fetal bovine serum (FBS), 10,000 U/mL penicillin, and 10 mg/mL streptomycin (Euroclone; Milan, Italy). ANXA1 knock-out (KO) MIA PaCa-2 cells were created from the wild type (WT) cells through the CRISPR/Cas9 genome editing system, as reported in [162], and kept in selection by 700 µg/mL neomycin (Euroclone; Milan, Italy). BJ cell line (human immortalized fibroblasts, ATCC CRL2522TM) were cultured in Eagle's Minimum Essential Medium (MEM) with 10% FBS, 1% L-glutamine, 1% sodium pyruvate, 1% NEAA and antibiotics. HUVEC cell line (Human umbilical vein endothelial cell) (ATCC® PCS-100-010TM, Manassas, VA, USA) was maintained as reported in [280] until passage 10. THP-1 (ATCC® TIB-202; Manassas, VA, USA) cells were maintained in Roswell Park Memorial Institute (RPMI; Euroclone; Milan, Italy) 1640 medium with 1% L-Glutamine, 10% fetal bovine serum (FBS) (Euroclone; Milan, Italy), 1% penicillin and streptomycin and βmercaptoethanol (0.05 mM; Sigma Aldrich, St. Louis, MO, USA). Human immortalized CAFs, obtained in [328] were cultured in DMEM F-12 medium supplemented with 10% FBS and 1% antibiotic-antimycotic. All cells were maintained at 37 °C in a 5% CO^2-95% air humidified atmosphere.

7.2 Exosome enrichment

The enrichment of exosomes (to which we will generally refer to as extracellular vesicles, EVs) obtained from cell culture supernatants was performed as reported in [329]. Briefly, the WT and ANXA1 KO MIA PaCa-2 cells (1.5×10^5 cm^{-2} , for a total of about 8×10^7 cells), after abundant

washing with phosphate buffered saline (PBS), were incubated for 24 h in DMEM medium without FBS. The conditioned medium was thus collected and centrifuged the first time for 5 min at 300× g at room temperature (RT) to remove the detached cells. It was recovered and centrifuged again for 10 min at 2000× g at 4 °C to remove dead cells, after which it was centrifuged once more at 10,000× g for another 30 min at 4 °C to remove cellular debris. The supernatant was transferred in tubes and ultracentrifugated for 70 min at 100,000× g at 4 °C. Subsequently, the pellet was washed in PBS and re-ultracentrifuged at 100,000× g at 4 °C for 70 min. Finally, the supernatant was removed and the pellet was re-suspended according to the experimental use. The amount of exosomes administered to the cells was normalized at 20 µg of WT and ANXA1 KO MIA PaCa-2 EVs through the Bradford assay, as reported in [163]. The normalization allowed for the administration of the same amount of EV to the cells, derived from the WT and ANXA1 KO MIA PaCa-2 cells, in all phases of the experiment. All analyses were performed on fresh isolated fractions.

7.3 Western blotting

Proteins extracted from cells and EVs were examined by Sodium Dodecyl Sulphate - PolyAcrylamide Gel Electrophoresis (SDS-PAGE). Protein content was extracted by freeze/thawing in lysis buffer containing protease inhibitors and estimated according to the Biorad protein assay (BIO-RAD, Hercules, CA, USA), as previously described [163]. A total of 20 µg of proteins were visualized using the chemioluminescence detection system (Amersham biosciences; Little Chalfont, UK) after incubation with primary antibodies against ANXA1 (rabbit polyclonal, 1:10,000; Invitrogen; Carlsbad, CA, USA), calreticulin (rabbit polyclonal, 1:1000; Elabscience; Houston, TX, USA), TSG101 (mouse monoclonal, 1:1000; ThermoFisher Scientific; Waltham, MA, USA), CD81 (mouse monoclonal, 1:200; Becton Dickinson Labware, Franklin Lakes, NJ, USA), CD63 (mouse monoclonal, 1:200; Biolegend; San Diego, CA, USA), FAP1α (rabbit polyclonal, 1:500; Santa Cruz Biotechnologies, Dallas, TX, USA), anti-cytokeratin 8 and 18 (1:1000, Santa Cruz Biotechnologies Dallas, TX, USA), antivimentin (1:1000; Santa Cruz Biotechnologies Dallas, TX, USA) and anti-E-

Cadherin (mouse monoclonal, 1:1000, Becton Dickinson Labware, Franklin Lakes, NJ), β-actin (mouse monoclonal, 1:1000; Sigma-Aldrich; St. Louis, MO, USA), GAPDH (mouse monoclonal, 1:1000; Santa Cruz Biotechnologies, Dallas, TX, USA). The blots were exposed to Las4000 (GE Healthcare Life Sciences; Little Chalfont, UK), tubulin (mouse monoclonal 1:1000; Sigma-Aldrich; St. Louis, MO, USA). The blots were exposed to Las4000 (GE Healthcare Life Sciences, Little Chalfont, UK) and the relative band intensities were determined using ImageQuant software (GE Healthcare Life Sciences). Results were considered significant if $p < 0.01$.

7.4 Wound-healing assay

The cells were seeded in a 12-well plastic plate at 5×10^5 cells for well. After 24 h at 100% cellular confluency the wound was produced at the center of the monolayer by gently scraping the cells with a sterile plastic p10 pipette tip to create a wound area of about 500 μm. After removing incubation medium and washing with PBS, cell cultures were incubated with respective treatments. All experimental points were further treated with mitomycin C (10 μg/mL, Sigma Aldrich, St. Louis, MO, USA) to ensure the block of mitosis. The wounded cells were then incubated at 37 °C in a humidified and equilibrated (5% v/v CO^2) incubation chamber of an Integrated Live Cell Workstation Leica AF-6000 LX (Leica Microsystems, Wetzlar, Germany). A 10× phase contrast objective was used to record cell movements with a frequency of acquisition of 10 min on at least 10 different positions for each experimental condition. The migration rate of individual cells was determined by measuring the wound closure from the initial time to the selected time-points (bar of distance tool, Leica ASF software, version Lite 2.3.5, Leica microsystem CMS Gmvh). For each wound 5 different positions were registered, and for each position 10 different cells were randomly selected to measure the migration distances.

7.5 Invasion assay

Cell invasiveness was studied using the Trans-well Cell Culture (12 mm diameter, 8.0-fim pore size) purchased from Corning Incorporated (New York, NY, USA), as reported in [254]. Briefly, the chambers were coated with Matrigel (Becton Dickinson Labware) that was diluted with 3 volumes of medium serum-free and stored at 37 °C until its gelation. Cells were plated in 350 µL of medium serum-free at a number of 5×10^4/insert in the upper chamber of the trans-well. the established treatment was added in 1,4 ml of medium in the lower chambers of each well in experimental points, previously addition of mitomycin C (10 µg/mL, Sigma-Aldrich;Saint Louis, MO, USA) to the arrest of mitosis. The trans-well was left for 24 h at 37 °C in 5% CO^2 -95% air humidified atmosphere. After that, the medium was aspirated, the filters were washed twice with PBS 1 × and fixed with 4% p-formaldehyde for 10 min, then with 100% methanol for 20 min. The filters so fixed, were stained with 0.5% crystal violet prepared from stock crystal violet (powder, Merck Chemicals) by distilled water and 20% methanol for 15 min. After that, the filters were washed again in PBS 1 × and cleaned with a cotton bud. The number of cells that had migrated to the lower surface was counted in 10 random fields using EVOS® light microscope (10 ×).(Life technologies Corporation).

7.6 Tube formation assay

A 24-well plate was coated with Matrigel (Becton Dickinson Labware, Franklin Lakes, NJ, USA) mixed to EGM-2 1:1 on ice and incubated at 37 °C for 30 min to allow gelation to occur. HUVEC cells were seeded to the top of the gel at a density of 2×10^4 cells/well in presence or not of the treatments. Cells were incubated at 37 °C with 5% CO^2. After 12 h, pictures were captured using EVOS® light microscope (10 ×) (Life technologies Corporation, Carlsbad, CA, USA). The length of each tube was measured, and the number of branches was calculated using ImageJ (NIH, Bethesda, MD, USA) (Angiogenesis Analyzer for ImageJ) software.

7.7 Gelatin gel zymography

The gelatinolytic activity of metalloproteinases was detected by SDS-PAGE zymography. The serum-free supernatants, mixed with a standard non reducing loading buffer for SDS-PAGE, were loaded for electrophoretic run, at 125 V, in a gel 10% polyacrylamide and 0.1% gelatin (for protease detection; Sigma Aldrich, St. Louis, MO, USA). After the electrophoresis, the gel was washed in renaturing solution (2.5% Triton X-100) for 1 h to remove SDS, following by incubation in a buffer of digestion (50 mM of Tris-HCl, pH 7.8, 200 mM of NaCl, 5 mM of CaCl2 and 5 mM of ZnCl2) for degradation of the substrate for 18 h, at 37 °C. The gels staining was with Coomassie Brilliant Blue R-250 (Sigma Aldrich, St. Louis, MO, USA) and then washed with destaining solution (10% methanol and 5% acetic acid) to reveal the areas of digestion such as a light band.

7.8 Measurement of intracellular Ca^{2+} signaling

Changes in intracellular Ca^{2+} concentration were monitored using the fluorescent probe Fluo-4 a.m. (Thermo Fisher Scientific; Waltham, MA, USA). Fluo-4 a.m. is a high-affinity Ca^{2+} indicator with an λex 470–490 nm and an λem 520–540 nm. Stock solutions (1 mM) of the AM-ester form were prepared using a solution of 20% (w/v) pluronic acid F-127 in absolute dimethyl sulphoxide (DMSO; Sigma-Aldrich; St. Louis, MO, USA). WT and ANXA KO MIA PaCa-2 cells were trypsinized, washed, and placed in 1.5 ml tubes at 1×10^6 /ml and then incubated with 2.5 μM of Fluo-4 a.m. in 3% DMSO (final concentration of DMSO in each assay, 0.06%) at 37 °C for 45 min with complete medium. After de-esterification of Fluo-4 a.m., the cells were washed three times with PBS containing or not Ca^{2+} (100 μM; Sigma-Aldrich; St. Louis, MO, USA) by centrifugation (1 min at 300 × g). The fluorescence in each sample was analyzed by a BD FACSCalibur cytometer (Becton Dickinson, Franklin Lakes, NJ, USA) using the 530/30 filter. Following the addition of N-Formylmethionyl-leucyl-phenylalanine (fMLP 50 nM; Sigma-Aldrich; St. Louis, MO, UA), Ac2-26 (1 μM), N-tert-butyloxycarbonyl-Met-Leu-Phe (Boc-1 100 μM; Bachem AG; Bubendorf, Switzerland), HS (10 μg/ml), rapid kinetic measurement of fluorescence was performed by flow

cytometry; Ca2+-ionophore (ionomycin 1 mM; Sigma-Aldrich; St. Louis, MO, USA) and the chelating agent EDTA (15 mM, 15 min; Sigma-Aldrich; St. Louis, MO, USA) served as the positive and negative control, respectively. The Ca2+ levels of PANC-1 and MIA PaCa-2 cells in PBS were recorded and considered as the baseline of Ca^{2+} concentrations.

7.9 Confocal microscopy

The cells seeded on glass bottom in multiwell plate, after each treatment, were fixed in p-formaldehyde (4% v/v with PBS; Sigma-Aldrich) for 5 min, permeabilized in Triton X-100 (0.5% v/v in PBS; Sigma-Aldrich) for 5 min, and then incubated in goat serum (20% v/v PBS; Lonza, NJ) for 30 min. Then, the cells were incubated with anti-E-cadherin antibody (mouse monoclonal; 1:500, BD Transduction Laboratories, San Jose, CA), anti-vimentin (mouse monoclonal, 1:250; Santa Cruz Biotechnologies; CA, USA), anti-vinculin (mouse monoclonal, 1:100; Santa Cruz Biotechnologies, Dallas, TX, USA), anti-COL1A (mouse monoclonal, 1:100; Santa Cruz Biotechnologies, CA, USA), anti-fibronectin (mouse monoclonal, 1:100; Santa Cruz Biotechnologies, CA, USA), anti-VE cadherin (mouse monoclonal, 1:100; Santa Cruz Biotechnologies, CA, USA), anti-cytokeratin 8 and 18 (mouse monoclonal, 1:250, Santa Cruz Biotechnologies Dallas, TX, USA), rabbit polyclonal antibodies anti-FAP1α (1:250; Santa Cruz Biotechnologies, CA, USA), anti-αSMA (1:100; Cusabio Life Science, College Park, MD, USA), anti-VEGF (rabbit polyclonal, 1:100; Santa Cruz Biotechnologies, CA, USA), anti-FGF-2 (1:100; Santa Cruz Biotechnologies, CA, USA), overnight at 4°C. F-actin was evaluated by 5 μg/ml of Phalloidin-FITC (Sigma-Aldrich; Saint Louis, MO, USA) for 30 min at RT in the dark. After two washing steps, the cells were incubated with antirabbit and/or antimouse DyLight (488- and/or 550-conjugate; 1:1,000; ImmunoReagents Inc., NC) for 2 h at RT. To detect nucleus, Hoechst 33342 nucleic acid stain (1:5,000; H1399, Molecular Probes, Thermo Fisher Scientific) was used and samples were excited with a 458 nm Ar laser. A 488 nm Ar or a 555 nm He-Ne laser was used to detect emission signals from target stains. The samples were vertically scanned from the bottom

of the coverslip with a total depth of 5 μm and a 63 × (1.40 NA) Plan-Apochromat oil-immersion objective. Images and scale bars were generated with Zeiss ZEN Confocal Software (Carl Zeiss MicroImaging GmbH, Jena, Germany). For immunofluorescence analysis and quantification, final images were generated using Adobe Photoshop CS4, version 11.0. If suitable, quantifications were performed from multichannel images obtained using a 63 × 1.4 NA objective and using the ImageJ software (NIH, Bethesda, MD), as follows. Briefly, 10 field images from a single coverslip from n = 3 biological repetitions were randomly selected and registered for each experimental condition identifying 10 distinct cells by Hoechst 33342 nuclear staining. Then, the individual cell total area was selected using the area selection tool, the fluorescence intensity value was measured and expressed as Arbitrary Unit (A.U.; the ImageJ software) subtracting background. The obtained mean value was used to compare experimental groups.

7.10 RNA isolation and quantitative Real Time-Polymerase Chain Reaction (RT-PCR)

mRNA levels of BJ and HUVEC cells were analyzed by real-time PCR using the Light Cycler 480 II instrument (Roche, Indianapolis, IN, USA). One μg of total RNA extracted from cells with Trizol reagent was reverse transcribed into cDNA with Transcriptor First Strand cDNA Synthesis Kit (Roche, Indianapolis, IN, USA). cDNAs were processed using Light Cycler 480 Syber Green I Master mix and primers for FPR-1 (Bio-Fab research; Rome, Italy) (50 -GGTGAACAGTCCAG GAGCAG-30 , 3 0 -ACCTCCCTGTGGACGACATA-50), FPR-2 (Bio-Fab research; Rome, Italy) (50 -CTGGCTACACTGTT CTGCGG-30 , 30 -AGCACCACCTGTAGTTGGAG-50), and Hypoxanthine Phosphoribosyltransferase 1 (HPRT1) (Bio-Fab research; Rome, Italy) (50 -GACCA GTCAACAGGGGACAT-30 , 30 -CCTGACC AAGGAAAGCAAAG-50) following the manufacturer's protocols. Results were analyzed using the Delta-Delta CT method. A portion (10 μL) of the RT-PCR product was electrophoresed on a 2% agarose gel in a Tris-acetate-EDTA buffer. The gel was stained with ethidium bromide and exposed to Las4000 (GE Healthcare Life Sciences; Little Chalfont, UK

7.11 Clonogenic assay

The cells were seeded 5 × 105 cells/mL in 6-well plates and after the treatment were cultured for 8 days in fresh medium. They were subsequently fixed with 4% p-formaldehyde, for 10 min, and then with 100% methanol, for 20 min (both from Sigma-Aldrich; St. Louis, MO, USA). The cellular staining was performed with crystal violet at 0.5% w/v in a v/v solution of 20% methanol / distilled water (Merck Chemicals, Darmstadt, Germany) for 30 min at RT. After washing with deionized water, the colonies were photographed, and then, the dye was dissolved in 1% SDS and measured at 570 nm by spectrophotometer (Titertek Multiskan MCC/340; Labsystems, Midland, ON, Canada), as confirmation of the result.

7.12 MTT assay

WT MIA PaCa-2, PANC-1 and HUVEC cells were harvested at the indicated times (24, 48 and 72 h) and cell viability was calculated as previously described in [13]. The optical density (OD) of each well was measured with a spectrophotometer (Titertek Multiskan MCC/340; LabX; Midland, ON, Canada) equipped with a 620 nm filter.

7.13 Macrophages generation

THP-1 monocytes differentiated into macrophages (M0) via PMA (Sigma Aldrich, St. Louis, MO, USA), 320 nM for 6 h, were allowed to recover for an additional 24 h. One dose of 20 µg of EVs was added for macrophage polarization experiments. After 24 h, the medium was collected, centrifuged to remove cellular component or debris and subjected to the ELISA test for IL10, according to the manufacturer's guidelines (Elabscience, Houston,TX, USA).

7.14 Flow cytometry

WT and ANXA1 KO MIA PaCa-2, PANC-1, BJ and HUVEC cells were harvested at a number of 1×10^6 and analyzed for FPR-1 and FPR-2, as reported in [330]; whereas THP-1 monocytes at a

number of 5 × 10^5/mL, differentiated in macrophages M0, after the treatment with PC EVs were analyzed for CD80, CD86, CD206 and CD163 expressions [331]. Briefly, pellets were incubated on ice for 1 h in PBS 1x containing a primary antibody against FPR-1 (rabbit polyclonal, 1:500, Santa Cruz Biotechnology; Dallas, TX, USA) or a primary antibody against FPR-2 (mouse monoclonal, 1:100, Genovac Gmbh; Freiburg, Germany). Then, cells incubated on ice for 1 h in 100 µl of PBS containing AlexaFluor 550 anti-rabbit (1:1000; Molecular Probes; Eugene, OR, USA) or Alexa-Fluor 550 anti-mouse (1:1000; Molecular Probes; Eugene, OR, USA). Moreover the macrophage pellets were incubated for 1 h at room temperature (RT) in PBS 1x containing FBS (2% v/v) and antihuman antibody against CD80, CD86,CD206, CD163 (1:100, Santa Cruz Biotechnologies, Dallas, TX, USA) and then for another hour with conjugated secondary antibody (1:100, antimouse). The cells were analyzed with Becton Dickinson FACScan flow cytometer (Franklin Lakes, NJ, USA) using the Cells Quest program.

7.15 hrANXA1 purification

hrANXA1 was obtained transforming BL21(DE3) competent cells with the plasmid pGEX-6-Annexin A1 (NM_000700.2 GI:733606737) purchased from MRC PPU Reagents and Services (Dundee, Scotland). The protein was overexpressed in lysogeny broth (LB) in the presence of 100 µg/ml ampicillin. 1 L of bacterial cells was grown at 37 °C to OD600 of 0.8 and induced by isopropyl-1-thio-D-galactopyranoside (IPTG, 1 mM; Sigma-Aldrich; St. Louis, MO, USA). After 6 hr at 37 °C, cells were harbored and pelleted at 5000 g for 15 min at 4 °C, finally resuspended in 40 ml of lysis buffer (PBS, pH 7.4, Euroclone; Milan, Italy), adding protease inhibitors cocktail (Sigma-Aldrich; St. Louis, MO, USA). Cells were lysed using a Vibra-Cells sonicator (Sonics; Turin, Italy), for 20 min of effective sonication (9.9 pulse/9.9 pause). Cell debris were pelleted at 10,000 g for 30 min at 4 °C and the clarified lysate was filtered using a 0.45 µm syringe filter and loaded onto a 1-mL GSTrap FF column (#17- 5130-02, GE Healthcare Life Sciences; Buckinghamshire, UK) using an AKTA purifier FPLC (GE Healthcare Life Sciences;

Buckinghamshire, UK) at the flow rate of 1 ml/min. Glutathione S-transferase (GST)-protein was eluted using the elution buffer (Tris HCl 50 mM, reduced glutathione 10 mM, both from Sigma-Aldrich; St. Louis, MO, USA, pH 8.0) over 10 column volumes. Fractions containing the GST-ANXA1 protein were confirmed by sodium dodecyl sulfate–polyacrylamide gel electrophoresis (SDS-PAGE) and then pooled. Next, the cleavage of GST was performed using the PreScission Protease (1:100 with protein; GE Healthcare Life Sciences; Buckinghamshire, UK) for 4 h at 4 °C. Analysis of cleavage reaction was performed by SDS-PAGE. The cleaved protein was then separated from the GST on the 1-ml GSTrap FF column.

7.16 Differential scanning fluorimetry (DSF)

DSF was performed with a real time (RT)-PCR Light Cycler 480 II instrument (Roche; Basilea, Switzerland). A mix containing human recombinant (hr) ANXA1, 1 μM prepared as reported above, CaCl2 (100 mM; Sigma-Aldrich; St. Louis, MO, USA), heparan sulfate (HS, Laboratori Derivati Organici -LDO- S.p.a.; Trino, VC, Italy) from 100 μM to 2 mM and freshly prepared 1x Sypro Orange dye (Sigma-Aldrich; St. Louis, MO, USA) in phosphate buffered saline 1x (PBS; Euroclone; Milan, Italy) was added to a white 96 well PCR microplate (Roche; Basilea, Switzerland). After sealing with Optical Adhesive Film (Euroclone; Milan, Italy), the plate was directly analyzed in the RT-PCR instrument with a heating cycle from 20 to 95 °C with a ramp rate of 0.06 °C and 10 acquisition per degree. First derivatives of the melting curves were calculated with LightCycler480® software release 1.5.0 SP4.

7.17 Surface plasmon resonance (SPR)

SPR analysis was performed on a Biacore 3000 system (GE Healthcare Life Sciences; Buckinghamshire, UK) equipped with research-grade CM5 sensor chip (GE Healthcare Life Sciences; Buckinghamshire, UK) as described elsewhere [18]. Briefly, the purified human recombinant full length ANXA1 (50 μg/ml in 10 mM sodium acetate, Sigma-Aldrich; St. Louis,

MO, USA, pH 5.0) and the ANXA1 N-terminal peptide, Ac2-26 (Tocris Bioscience, Bristol, UK) (60 µg/ml in 10 mM sodium acetate, pH 3.5) were immobilized at a flow rate of 10 µl/min by using standard amine-coupling protocols. A recombinant in-house protein (human Trefoil Factor 1) was used as negative control and one flow cell was left empty for background subtractions. HS was dissolved in PBS to obtain a starting solution of 8 mM (HS molar concentration was calculated considering an average molecular weight of 30 kDa) and diluted in PBS + 0.005% surfactant NP-40 (Sigma-Aldrich; St. Louis, MO, USA). Binding experiments were performed at 25 °C, by using a flow rate of 30 µl/min, with 60 s monitoring of association and 120 s monitoring of dissociation. Regeneration of the surface was performed, when necessary, by a 10 s injection of 5 mM NaOH (Sigma-Aldrich; St. Louis, MO, USA). Equilibrium dissociation constants (K_D) were derived from the ratio between kinetic dissociation (kd) and association (ka) constants obtained fitting data from all the injections at different concentrations of each compound, using the simple 1:1 Langmuir binding fit model of the BIAevaluation software (version 4.1).

7.18 Co-culture system

Transwell chambers (12 mm diameter, 8.0 fim pore size, Corning Incorporated, New York, NJ, USA) with matrigel coating (BD Biosciences, Franklin Lakes, NJ, USA) were used following the schematic representation reported in figure 7.18.1, to detect macrophage invasion to WT and ANXA1 KO conditioned medium (CM) obtained as the growth medium in contact with WT and ANXA1 KO MIA PaCa-2 cells for 48 h. These CMs were collected and centrifuged at 900 × g or 10 min to remove the cellular debris.

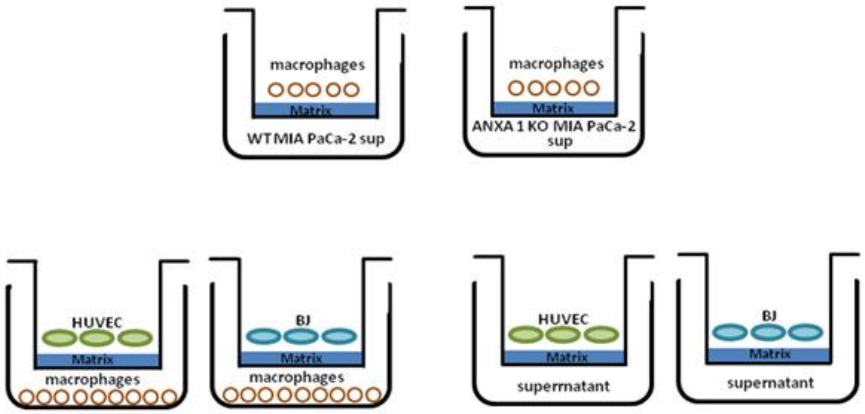

Figure 7.18.1 Schematic representation of co-culture system.

Then, the macrophages were plated in the upper chamber and in the lower chamber the CMs were put. Therefore, this co-culture system was also used to detect the BJ and HUVEC cells invasion to polarized M1 or M2 macrophages, from the upper chamber where cells were seeded at 3 × 10^4 and 4 × 10^4/insert, for BJ and HUVEC, respectively. In this case, in the lower chamber, M0 THP-1 pretreated for 24 h with Ac2-26 (1 μM, Tocris Bioscience, Bristol, UK), WT and ANXA1 KO MIA PaCa-2 EVs were plated. After 24 h, all cells were fixed and stained and analyzed as reported in [332].

7.19 ELISA for VEGF-A

After treatments with WT and ANXA1 KO EVs, THP-1 supernatants were collected, and the secreted VEGF-A amount was detected through the human VEGF-A ELISA kit, following the manufacturer's instructions (Invitrogen, Carlsbad, CA, USA).

7.20 H&E tissue staining and tissue immunofluorescence

Frozen samples of tumor and metastasis tissues were obtained from our previous in vivo study on mice [162]. In brief, SCID mice (6–8 week-old females) were obtained from Charles River (Italy) and bred under pathogen-free conditions in the Animal Facility of the University of Salerno. The orthotopic implantations were performed in the pancreas by using WT and ANXA1 KO MIA

PaCa-2 cells. After 5 weeks from the implantation, mice were sacrificed, and organs (pancreas and livers) were excised, weighed and analyzed. Metastases lesions on the liver surface were observed and quantified by gross anatomy using a dissecting microscope.

The frozen tissue sections of 6 μm, were cut on a microtome RM2125RT (Leica Microsystems, Wetzlar, Germany), mounted directly on super frost slides (Thermo Scientific, Waltham, MA, USA), and processed for haematoxylin and eosin (H&E) staining, as reported in [274] and immunofluorescence. Briefly for H&E staining, cryostat sections were dehydrated for 5 minutes with cold acetone and then rehydrated. Next, slides were placed in haematoxylin stain for 9 minutes, rinsed in alcoholic acid, differentiated in 80% alcohol and stained with eosin for 2.5 minutes, rinsed in 95% ethanol, dehydrated with absolute ethanol and cleared in xylene or 4 minutes. The images were taken through the Axio Observer microscope (20×) (Carl Zeiss MicroImaging GmbH; Jena, Germany) and analyzed using ImageJ software (NIH, Bethesda, MD, USA). Next, the sections were fixed in a solution of p-formaldehyde (4% v/v in PBS; Lonza) were permeabilized or not with Triton X-100 (0.5% v/v in PBS; Lonza), blocked with fetal bovine serum (FBS) (20% v/v in PBS, 0.5% Triton X-100; Lonza, Basilea, Swiss) and then incubated with anti-CD80 (mouse monoclonal, 1:100; Santa Cruz Biotechnologies, Dallas, TX, USA), anti-CD86 (mouse monoclonal, 1:100; Santa Cruz Biotechnologies, Dallas, TX, USA), anti-CD163 (mouse monoclonal, 1:100; Santa Cruz Biotechnologies, Dallas, TX, USA), anti-CD206 (mouse monoclonal, 1:100; Santa Cruz Biotechnologies, Dallas, TX, USA) in determined solution 0.2% Triton X-100, 3% FBS, 0.02% NaN3, overnight at 4 °C. Then, they were incubated with antimouse AlexaFluor (488 and/or 555; 1:500; Molecular Probes; Waltham, MA, USA) for 2 h at RT. After two washing steps, the slice sections were mounted, and the images were acquired using a Leica SP8 confocal microscope (Leica Microsystems, Wetzlar, Germany). The densitometry analysis was performed as reported above; in this case, a 40× objective was used, and the whole slide was evaluated to count nuclei and the related protein signal for each data set. The obtained mean value

was used to compare experimental groups. Fifteen sections from six animals (three for each condition of implantation) were selected.

7.21 Monocytes isolation

Human peripheral blood was obtained from “Etablissement Francais du Sang” (EFS). Peripheral blood mononuclear cells (PBMCs) were isolated from healthy donors' buffy coats by centrifugation on a density gradient (400 × g for 40 min in Ficoll-Paque Plus, Amersham Biosciences Corp), as described previously [333]. Following centrifugation, the layer of PBMC was aspirated carefully, washed and centrifuged at 250 × g for 7 minutes several time in order to remove platelets from PBMC and have a clear suspension. The PBMCs, resuspended in 20 mL of RPMI complete medium, were counted (by Vi-CELL™ XR Cell Viability Analyzer, Beckman Coulter) and then taken the necessary number of cells (10×10^6 cells) in suspension and centrifuged. The pellet was suspended in 80 uL of buffer (PBS, 0.5% BSA and 2mM EDTA) and used for monocyte isolation thanks to positive selection by CD14 beads using autoMACS® Pro Separator (Miltenyi Biotec)

7.22 3D model generation and area analysis

3D co-cultures model were performed by 96 well U-bottom plates (Corning® Costar®, #3799). In this plate, 5000 tumor cells were seeded per well for mono-culture and 5000 tumor cells and 5000 CAFs fibroblasts and on day 3 10,000 monocytes per well for co-cultures were added. 3D monocultures and co-cultures models were incubated for 10 days at 37°C with 5% CO^2 and monitored in the Incucyte® Live-Cell Analysis System (Sartorius) (6 h repeat scanning, up to the end) until spheroid formation. After the spheroid growth and shrinkage its size was reported in real time based on DF-Brightfield image analysis thanks to Incucyte® Spheroid Software Module (Sartorius).

7.23 Counting live cells in 3D model

After 10 days the cells in 3D models were first dissociated using PBS 1× with 10% Trypsin and then they were counted and analyzed through Vi-CELL™ XR Cell Viability Analyzer (Beckman Coulter). The Vi-CELL™ Cell Viability Analyzer provides an automatic means to perform the Trypan Blue Dye Exclusion method.

7.24 Cell viability for 3D model

Cell viability was measured using CellTiterGlo (Promega,) on day 10 according to the supplier's instructions. Briefly, equal volume of CellTiterGlo reagent was added to the wells containing mono/co-cultures with and without monocytes in medium and incubated for 45 min at RT on a shaker. The cell suspension was then transferred to a black 96 well clear flat bottom plate and the relative luminescence units (RLU) were measured using a microplate reader (Synergy 2 Plate reader, Bio-Tek).

7.25 Statistical analysis

Data analysis and statistical evaluations were carried out using Microsoft Excel; the number of independent experiments and p-values are indicated in the figure legends. All results are the mean ± standard deviation of at least 3 experiments performed in triplicate. Statistical comparisons between the experimental points were performed using two-tailed t-test comparing two variables. Differences were considered significant if $p < 0.05$, $p < 0.01$ and $p < 0.001$.

8 Results

8.1 Effects of extracellular vesicles (EVs) from wild type (WT) and ANXA1 knock-out (KO) MIA PaCa-2 cells on fibroblast migration and invasion

In order to investigate the role of ANXA1 on EVs-dependent metastatic potential of PC cells, we studied the paracrine effects of EVs derived by WT and ANXA1 KO MIA PaCa-2 cells, obtained by CRISPR/Cas9 genome editing system, on BJ fibroblasts, one of the cellular components of the tumor microenvironment [334; 335]. First, the EVs obtained from PC MIA PaCa-2 cells were characterized by the presence of TSG101 or the absence of calreticulin, used as positive and negative controls respectively, as previously described [163]. We also showed the exclusive and abundant expression in EVs of tetraspanins CD63 and CD81, often used for the detection of secreted microvesicles. Our results also confirmed the different expression of ANXA1, as revealed by the lack of ANXA1 KO total and EV protein extracts, for both full length and cleaved forms (Fig. 8.1A).

Once validated, the EV effects on HUVEC motility [163], the BJ cell migration was analyzed by wound-healing assay as well as the capability of invasion through the coating of Matrigel in transwells. As shown in Figure 8.1B, and C, BJ cells invaded and migrated more rapidly in the presence of EVs isolated from WT MIA PaCa-2 cells when compared to those obtained from ANXA1 KO cells and to the untreated controls. In order to support the results obtained with the invasion assay, we performed a gel zymography to assess the activity of metalloproteinases 2 (MMP2) (e.g., gelatinolytic enzymes), secreted by the cells. The degrading activity of BJ MMP2 was significantly increased in the presence of EVs from WT MIA PaCa-2 compared to the EVs released by ANXA1 KO cells. This kind of signal appeared evident after 48 and 72 h of treatment (Fig. 8.1D). Furthermore, the activation of fibroblasts triggers their switch into myofibroblasts. This phenomenon is related to the increase of the expression of specific protein markers, particularly relevant of which is the fibroblast activated protein 1α (FAP1α), a member of the group II integral

serine proteases, and vinculin, a cytoskeletal protein of the focal adhesion plaques [336; 337]. BJ cells showed a notable increase of levels of FAP1α expression when treated with EVs from WT MIA PaCa-2, more than ANXA1 KO EV. The WT EV treatment triggered a marked increase of traction stresses, with an increase in the expression of vinculin not only with respect to the control cells, but also with respect to the ANXA1 KO EV treated cells. Furthermore, by this confocal analysis, we proved that fibroblasts acquired more precise and parallel directionality in the presence of WT EVs than in the presence of ANXA1 KO EV treated cells (Fig. 8.1E).

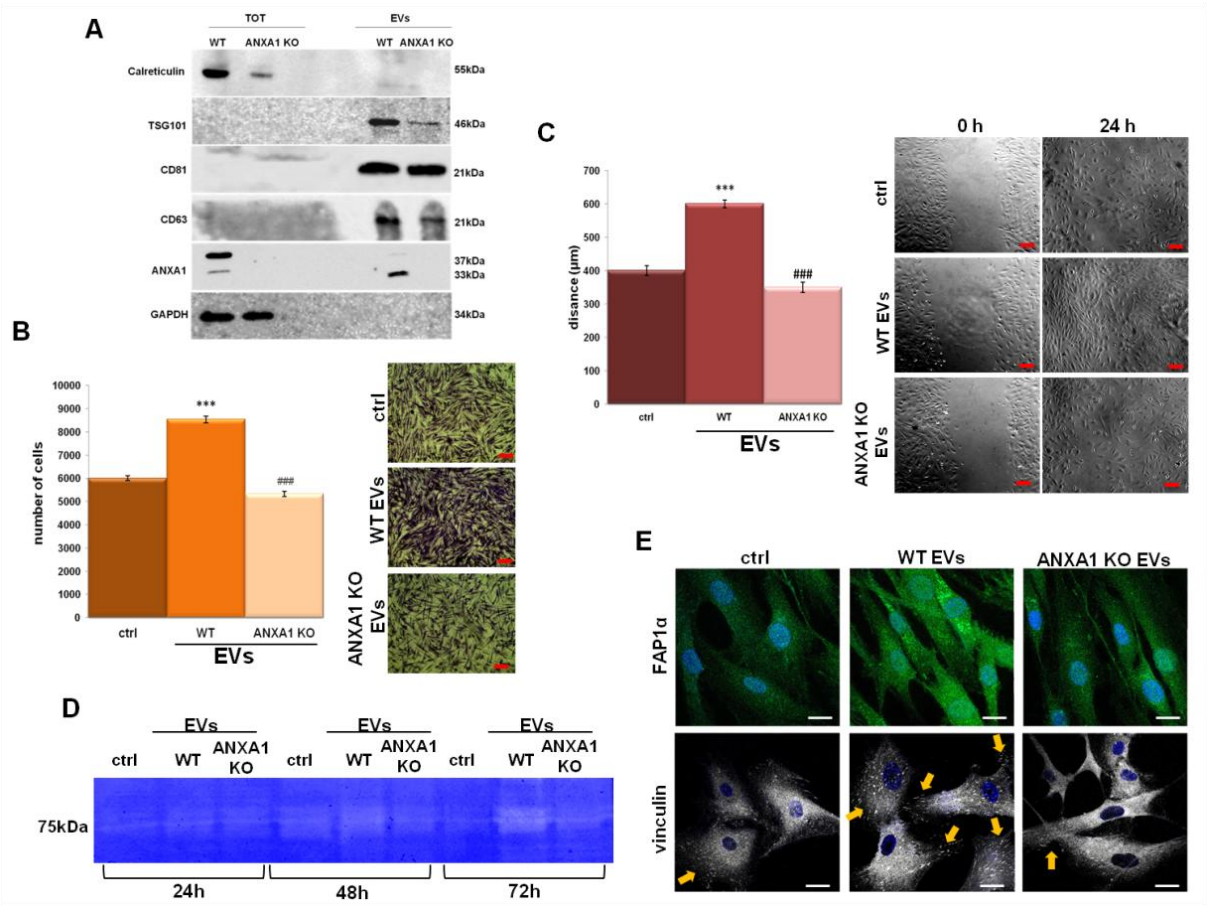

Figure 8.1 MIA PaCa-2 extracellular vesicles (EV) effects on BJ cells. (**A**) Western blot using antibodies against calreticulin, TSG 101. CD63, CD81, and ANXA1 on the protein content of total cell lysates and EV fractions extracted from the WT and ANXA1 KO MIA PaCa-2 cells. Protein normalization and the check of the sample quality were performed on GAPDH levels. Analysis of (**B**) invasion and (**C**) migration distance of BJ cells treated with EVs from wild type (WT) and ANXA1 knock-out (KO) MIA PaCa-2 cells with relative bright field images. Bar = 50 µm. (**D**) Gelatin zymography showing increased gelatinolytic activity of MMP-2 of BJ cells. Zymography was performed using 0.1% gelatin gel followed by Coomassie blue staining. (**E**) Immunofluorescence analysis to detect Fibroblast Activated Protein 1α (FAP1α) and vinculin. Nuclei were stained with Hoechst 33342 1:1000 for 30 min at room temperature (RT) in the dark. Magnification 63 × 1.4 numerical aperture (NA). Bar = 100 µm. Data represent the mean of three independent experiments ± standard deviation with similar results. *** $p < 0.001$ treated cells vs. untreated controls; ### $p < 0.001$ for each point of ANXA1 KO MIA PaCa-2 cells vs. WT one

8.2 Ac2-26 peptide promoted fibroblasts and endothelial cells motility through FPRs

Once validated the EVs effects on motility and activation of BJ cells in precence of ANXA1, we focused on the mechanism by which the ANXA1-EVs complex could stimulate stromal cells and promote their mesenchymal switches.

It has been observed that the secreted form of ANXA1 stimulates a more aggressive phenotype in cancer cells by its interaction with FPRs [162; 274; 199]. Particularly, the N-terminal mimetic peptide of ANXA1, Ac2-26, is known to be involved in cell migration and invasion by acting on these receptors [162; 251].

In this study we assessed these processes on BJ and HUVEC cells, showing an increase in migration speed (Fig.8.2A and B, for BJ and HUVEC cells, respectively) and invasion ability (Fig.1C and D, for BJ and HUVEC cells, respectively) of cells treated with Ac2-26 or with the natural FPR agonist fMLP (formyl-Methionine-Leucine-Phenylalanine), compared to controls. The FPRs antagonist Boc-1 (*N-tert*-butyloxycarbonyl-Met-Leu-Phe) significantly inhibited basal and Ac2-26 or fMLP-stimulated migration. About the *in vitro* angiogenesis on HUVEC cells, these ones showed a higher tendency to form capillary-like structures when treated with Ac2-26 and fMLP to a greater extent than control cells. Additionally, Boc-1 negatively influences angiogenic activity, with or without treatment (Fig. 8.2E). These events have been further corroborated by the analysis of the number of branching points and of the relative tube length.

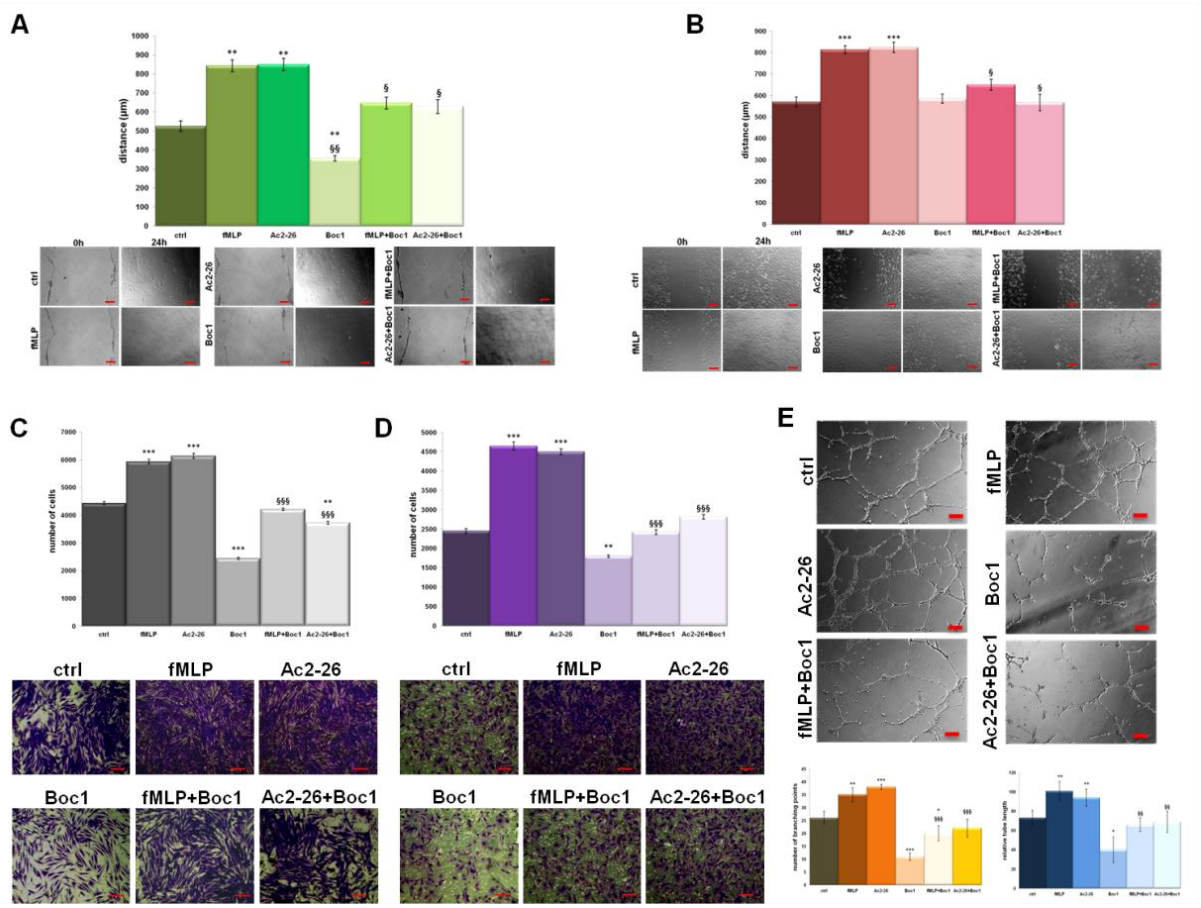

Figure 8.2 Effects of Formyl peptide receptors (FPRs) agonists and antagonists on BJ and Human umbilical vein endothelial cell (HUVEC) cells. Results of Wound-Healing assay on (**A**) BJ and (**B**) HUVEC cells treated with formyl-Methionine-Leucine-Phenylalanine (fMLP) (50 nM), Ac2-26 (1 µM), and N-tert-butyloxycarbonyl-Met-Leu-Phe (Boc1) (100 µM), with related images. Analysis of invasion distance of BJ (**C**) and HUVEC (**D**) with relative bright field images treated or not with FPR agonists and antagonist at the same concentration. Bar = 50 µm. (**E**) Representative images of tube formation by HUVEC cells seeded for 12 h on Matrigel: Endothelial Cell Growth Basal Medium-2 (EBM-2) 1:1 with the same treatment. Analysis of tube length and number of branches calculated by ImageJ (Angiogenesis Analyzer tool) software. Bar = 100 µm. Data represent the mean of three independent experiments ± standard deviation with similar results.* $p < 0.05$; ** $p < 0.01$; *** $p < 0.001$ treated cells *vs*. untreated controls; § $p < 0.05$; §§ $p < 0.01$; §§§ $p < 0.001$ for each point of EVs + Boc-1 *vs*. Boc-1 alone.

8.3 PC cells-EVs interact with FPRs on human fibroblasts

Once evaluated the activation of FPRs, the mechanism by which PC cells-deriving EVs might induce the motility of human fibroblasts was investigated. First, we assessed by cytofluorimetric analysis that FPR-1 and FPR-2 expression on BJ cells does not change in presence of WT and ANXA1 KO EVs (Fig. 8.3A). We confirmed this data through the RT-PCR (Fig. 8.3B). Next, we examined the migration and invasion distances of these cells treated with EVs derived from WT and ANXA1 KO MIA PaCa-2 cells with or without Boc-1. The results in figure 8.3C and D show that fibroblasts treated with WT EVs together with Boc-1 migrated and invaded more than the control, but less than the WT EVs treated cells. The motility effects were inhibited by co-administration of ANXA1 KO EVs plus Boc-1. Finally, to support the results obtained by invasion assay, we performed gel zymography reporting the activation of MMP2 in BJ cell supernatants. Gel degradation increased in presence of WT EVs and Boc-1 if compared to not treated and Boc-1 treated cells but also when the FPR-antagonist is co-administered ANXA1 KO EVs (Fig. 8.3E).

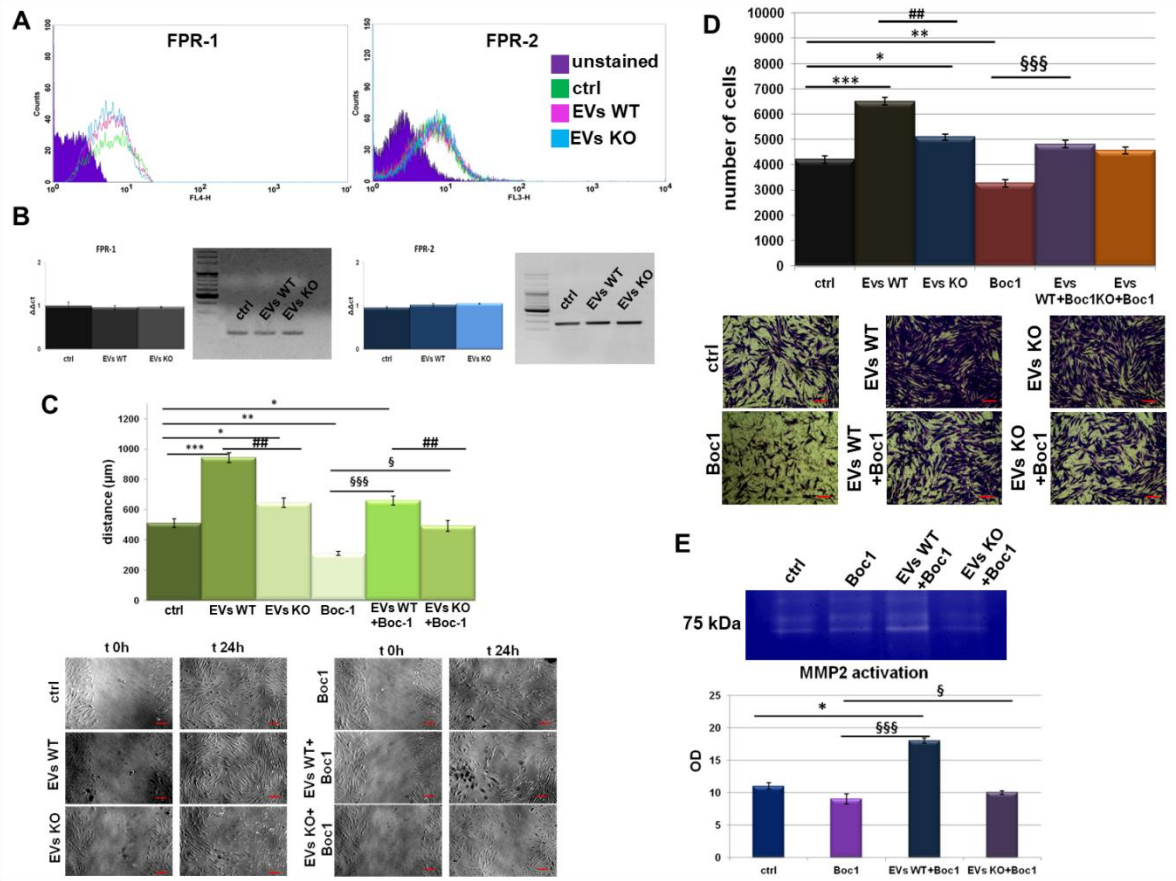

Figure 8.3 EVs interact with FPRs on fibroblasts. (**A**) Expression of FPR-1 and FPR-2 on BJ cells were analyzed by flow cytometry. The violet areas in the plots are relative to unstained fibroblasts. FPR-1 and FPR-2 signals are showed in green for ctrl, in pink for WT EVs and in light blue for ANXA1 KO EVs treated cells for 24 h. (**B**) Real Time-Polymerase Chain Reaction (RT-PCR) for FPR-1 and FPR-2, mRNA expression measured on levels of HPRT1. Values refer to the same experimental points of flow cytometry analysis and are expressed using the delta-delta Ct method to derive relative fold change. It is also shown the electrophoresis of the FPR-1 and FPR-2 RT-PCR products on 2% agarose gel stained with ethidium bromide. Results of Wound-Healing assay and (**C**) invasion analysis with relative bright field images of BJ cells, treated or not with EVs from WT and ANXA1 KO MIA PaCa-2 cells and Boc1 (100 µM). Bar = 50 µm. (**D**) Gelatin zymography showing gelatinolytic activity of MMP-2 of BJ supernatants. (**E**) Data represent the mean of four independent experiments ± standard deviation with similar results.* $p < 0.05$; ** $p < 0.01$; *** $p < 0.001$ treated cells *vs*. untreated controls; ## $p < 0.01$; for each point of ANXA1 KO MIA PaCa-2 cells *vs*. WT one; § $p < 0.05$; §§§ $p < 0.001$ for each point of EVs + Boc-1 *vs*. Boc-1 alone.

8.4 ANXA1-containing EVs interact with FPRs on endothelial cells

As for human fibroblasts, FPR-1 and FPR-2 expression remained unmodified also in HUVEC cells in presence of both WT and ANXA1 KO EVs (Fig. 8.4A, B).

Additionally, as shown for BJ cells, EVs induced a signal transduction via FPRs in HUVEC cells as well. The addition of Boc-1 to WT EVs determined a significant slowdown of the migration and invasion distances compared to cells treated with WT EVs alone. The same trend, but much less pronounced, has been observed when Boc-1 was added ANXA1 KO EVs (Fig. 8.4C, D). Finally, the inhibition of FPRs through Boc-1 presented a significant effect also on *in vitro* angiogenesis, for which we found a rescue of WT EVs action more than ANXA1 KO EVs (Fig. 8.4E).

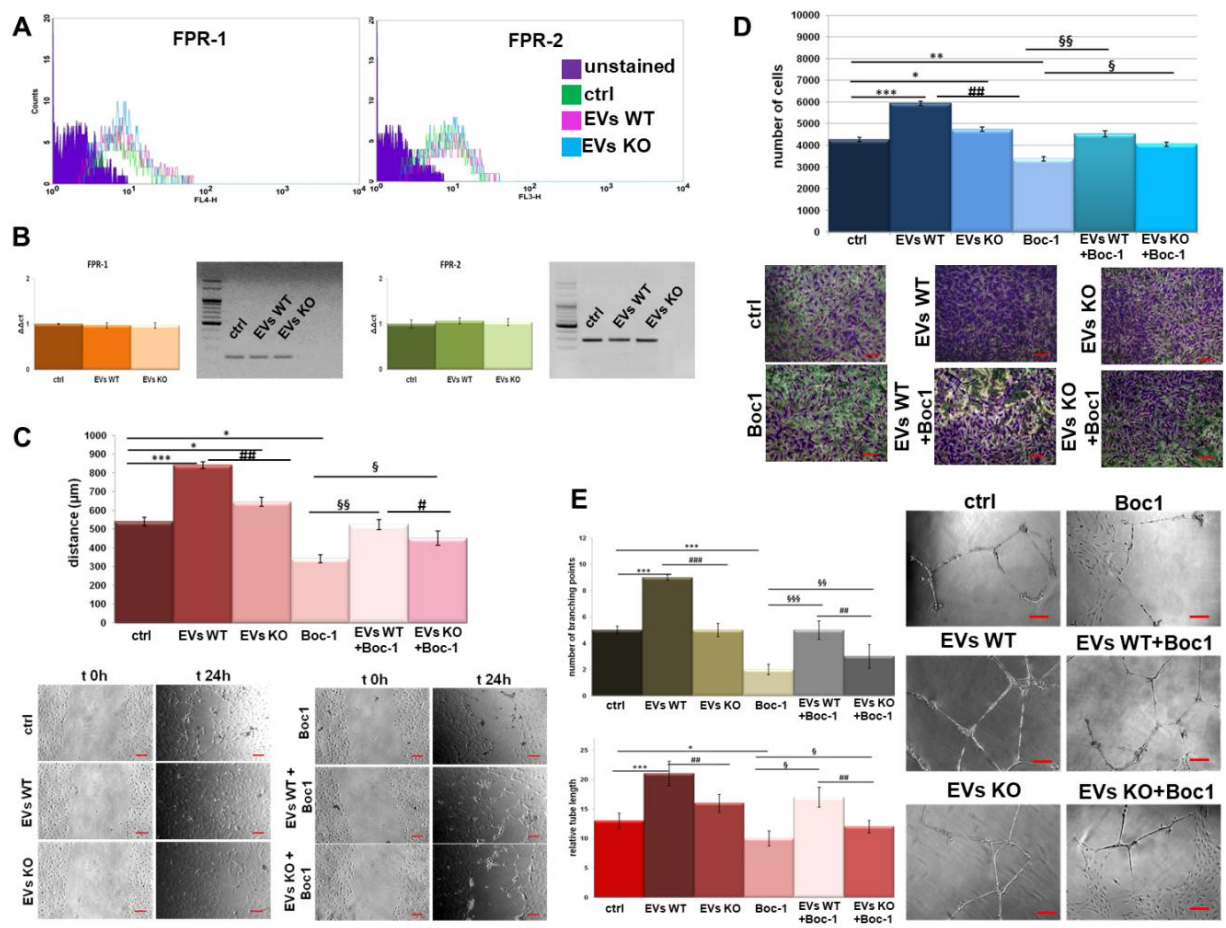

Figure 8.4 EVs interact with FPRs on endothelial cells. (**A**) Expression of FPR-1 and FPR-2 on HUVEC cells was analyzed by flow cytometry. The violet areas in the plots are relative to unstained fibroblasts. FPR-1 and FPR-2 signals are showed in green for ctrl, in pink for WT EVs and in light blue for ANXA1 KO EVs treated cells for 24 h. (**B**) RT-PCR for FPR-1 and FPR-2, mRNA expression measured on levels of HPRT1. Values refer to the same experimental points of flow cytometry analysis are expressed using the delta-delta Ct method to derive relative fold change. It is also

shown the electrophoresis of the FPR-1 and FPR-2 RT-PCR products on 2% agarose gel stained with ethidium bromide. Results of HUVEC (**C**) migration and (**D**) invasion in presence of WT and ANXA1 KO EVs with or without Boc-1 (100 μM) with relative bright field images. Bar = 50 μm. (**E**) Representative images of tube formation by HUVEC cells with the related analysis of tube length and number of branches. Bar = 100 μm. Data represent the mean of four independent experiments ± standard deviation with similar results. * $p < 0.05$; ** $p < 0.01$; *** $p < 0.001$ for treated cells *vs*. untreated controls; # $p < 0.05$, ## $p < 0.01$; ### $p < 0.001$ for each point of ANXA1 KO MIA PaCa-2 cells *vs*. WT one; § $p < 0.05$; §§ $p < 0.01$; §§§ $p < 0.001$ for each point of EVs + Boc-1 *vs*. Boc-1 alone.

8.5 WT EVs promoted the fibroblasts switch more than ANXA1 KO EVs

In TME fibroblasts can differentiate into myofibroblasts forming a tumor-responsive stroma. Analyzing some of the principal mesenchymal markers, we showed in BJ cells a notable increase of expression of FAP1α, Collagen type I alpha1 (COL1A) and Fibroblasts Growth Factor 2 (FGF2) when treated with EVs from WT MIA PaCa-2 than when treated with ANXA1 KO EVs (Fig. 8.5, panels y-a', a-c and m-o, respectively).

In presence of Boc-1, the levels of these proteins appeared strongly reduced (panels b', d, p, respectively). When this antagonist has been administered together with ANXA1 KO EVs the signal for these markers became very similar to the untreated cells (panels d', e and q, respectively), while an intermediate intensity has been revealed in case of Boc-1/WT EVs (panels c', d and p).

Here we found a significant increase of well-organized stress fibers, as revealed by phalloidin staining of F-actin, when the cells were treated with WT EVs. Actin polymerization reached an intermediate situation between ctrl and WT EVs when BJ have been treated with ANXA1 KO EVs. Again, Boc-1 negatively affected this process and interfered more with WT EVs than with ANXA1 KO EVs (panel g-l). A very similar trend has been observed for vinculin expression, for which WT and ANXA1 KO EVs confirmed its increase (panels e'-g'). On the other hand, Boc-1 determined a different formation of vinculin adhesion plaques. Moreover, in case of co-administration, Boc-1 plus WT EVs, this inversion appeared higher than the addition of the mix Boc-1/ANXA1 KO EVs (panels h'-j'). Furthermore, the expression of vimentin resulted not affected by treatments, but interestingly, this protein appeared much better structured in presence of WT EVs than in presence of ANXA1 KO EVs. Vimentin organization has been strongly affected by Boc-1 added together

with WT EVs than with ANXA1 KO EVs (panels s-x). Finally, the confocal analysis allowed us to show an elongated form and a parallel-organized pattern in almost 100% of the seeded population in the presence of WT EVs, but less with ANXA1 KO EVs. The untreated cells and the cells treated with Boc-1 resulted in being disorganized and randomly orientated. As far as the expression markers are concerned, the co-administration of EVs and Boc-1 led to an intermediated behavior.

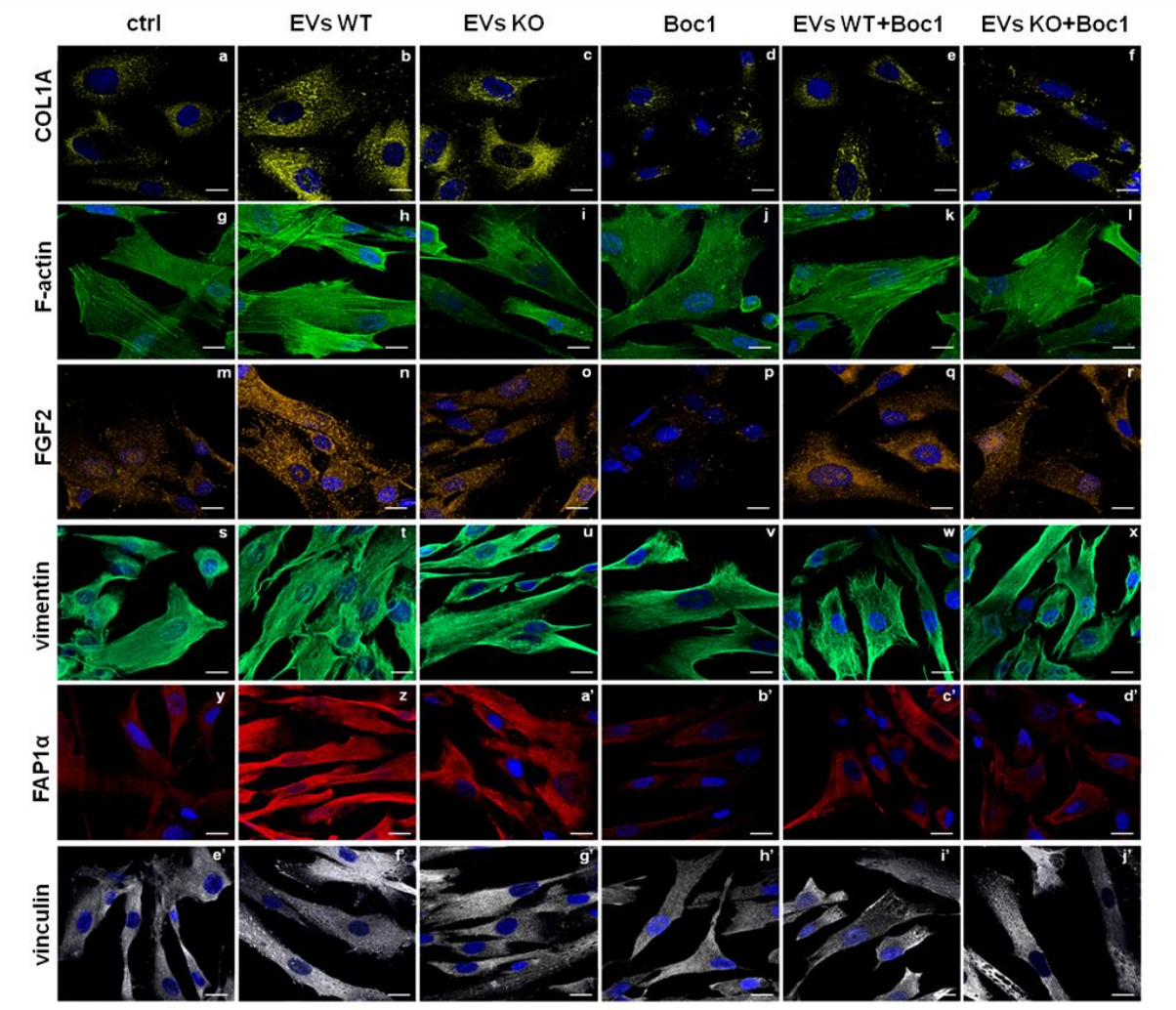

Figure 8.5 Fibroblasts activation induced by ANXA1-containing EVs. Fibroblasts activation induced by ANXA1-containing EVs. Immunofluorescence analysis on BJ cells to detect: COL1A (panels a–f), F-actin (panels g–l), FGF2 (panels m–r), vimentin (panels s–x), FAP1α (panels y–d') and vinculin (panels e'–j'). Nuclei were stained with Hoechst 33342 1:1000 for 30 min at RT in the dark. Magnification 63 × 1.4 NA. Bar = 100 µm.

8.6 WT EVs is able to induce the EndMT through FPRs

In direct response to vesicles released from a primary tumour, the endothelium can undergo the Endothelial-to-Mesenchimal Transition (EndMT), acquiring a mesenchymal phenotype. For this reason, we have investigated by confocal microscopy the effects of EVs from WT and ANXA1 KO MIA PaCa-2 cells on HUVEC cells. In figure 8.6, in presence of WT EVs, HUVEC disclosed a greater expression of Vascular Endothelial Growth Factor (VEGF), α-Smooth Muscle Actin (αSMA), FAP1α and fibronectin (Fig. 8.6, panels a-b, m-n, y-z, and e'-f', respectively), considered altogether as markers of EndMT.

Furthermore, the expression of these proteins underwent a smaller increase in presence of EVs from ANXA1 KO clones (panels c, o, a', g', respectively). Accordingly, Boc-1 was more effective when FPRs were stimulated by WT EVs than by ANXA1 KO (panels d-f, p-r, b'-d', h'-j', respectively for VEGF, αSMA, FAP1α, fibronectin). Again, Vascular Endothelial (VE)-cadherin showed an increased cytosolic expression with WT EVs, than with ANXA1 KO EVs; Boc-1 blocked these effects and the protein remained linked to cell membrane despite the vesicles stimulation (panels s-x). Finally, the phalloidin staining allowed us to show the F-actin fibers more sharply with WT EVs compared to ANXA1 KO EVs.

The intermediate behavior for each related treatment has been reached in presence of the FPRs antagonist, as for the other markers considered (panels g-l).

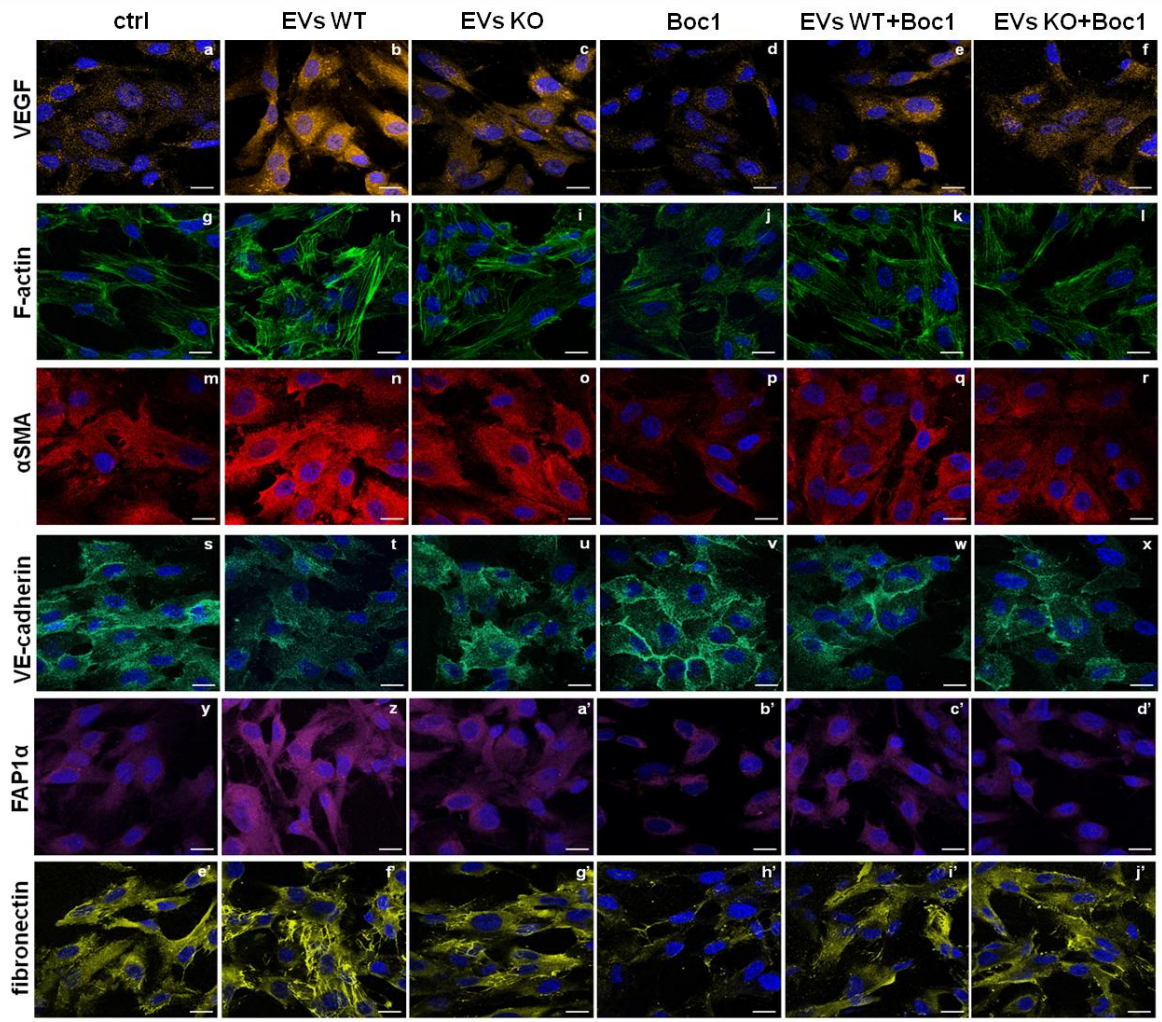

Figure 8.6 EndMT induced by ANXA1-containing EVs. Confocal analysis for HUVEC cells in presence of WT and ANXA1 KO EVs with and without Boc-1, for: VEGF (panels a-f), F-actin (panels g-l), αSMA (panels m-r), VE-cadherin (panels s-x), FAP1α (panels y-d'), fibronectin (panels e'-j'). Nuclei were stained with Hoechst 33,342 1:1000 for 30 min at RT in the dark. Magnification 63 × 1.4 NA. Bar = 100 μm.

8.7 The PC cell-derived EVs influence the macrophage polarization

The exosomes released by cancer cells preserve an immunomodulatory capability, also promoting macrophage polarization, mainly as M2-like phenotype. In order to investigate the paracrine effects of these vesicles on the recruitment of M2 macrophage, we have used the THP-1 monocyte cells. These cells have been pretreated with the phorbol-12myristate-13-acetate (PMA), 320nM for 6 h which allowed the M0 macrophagic polarization mainly confirmed by cell adhesion [338]. Then, the M0 population has been treated with a normalized amount of EVs derived from WT and ANXA1 KO MIA PaCa-2 cells. After 24 h of treatment, THP-1 cells were harvested, and the surface markers were detected by flow cytometry to distinguish the two subpopulations: CD80/86 for M1 and CD163/206 for M2. Thus, figure 8.7A displayed a strong polarization of macrophages treated with PC EVs into M1 or M2 subpopulation. In particular, WT EVs induced a high expression mainly of M2 markers compared to the treatment with IL-4 and IL-13 used as controls. The administration of Ac2-26 proved that this differentiation is due to ANXA1. On the other hand, ANXA1 KO EVs were able to induce phenotype switch in M1 population with high levels of its markers as seen in presence of LPS and INFγ, as technical controls.

The respective analyses of plots have been highlighted by histograms in figure 8.7B. To confirm that the WT EVs induced the polarization of macrophages to M2 phenotype, we measured the production of the cytokine IL-10 (a well-known M2 cytokine) by ELISA (Fig. 8.7C). Actually, a significant increase of IL-10 amount was found in PC cell-derived EVs-treated macrophages with respect of ANXA1 KO EVs and interestingly also more than the stimulus induced by the controls IL-4 and IL-13.

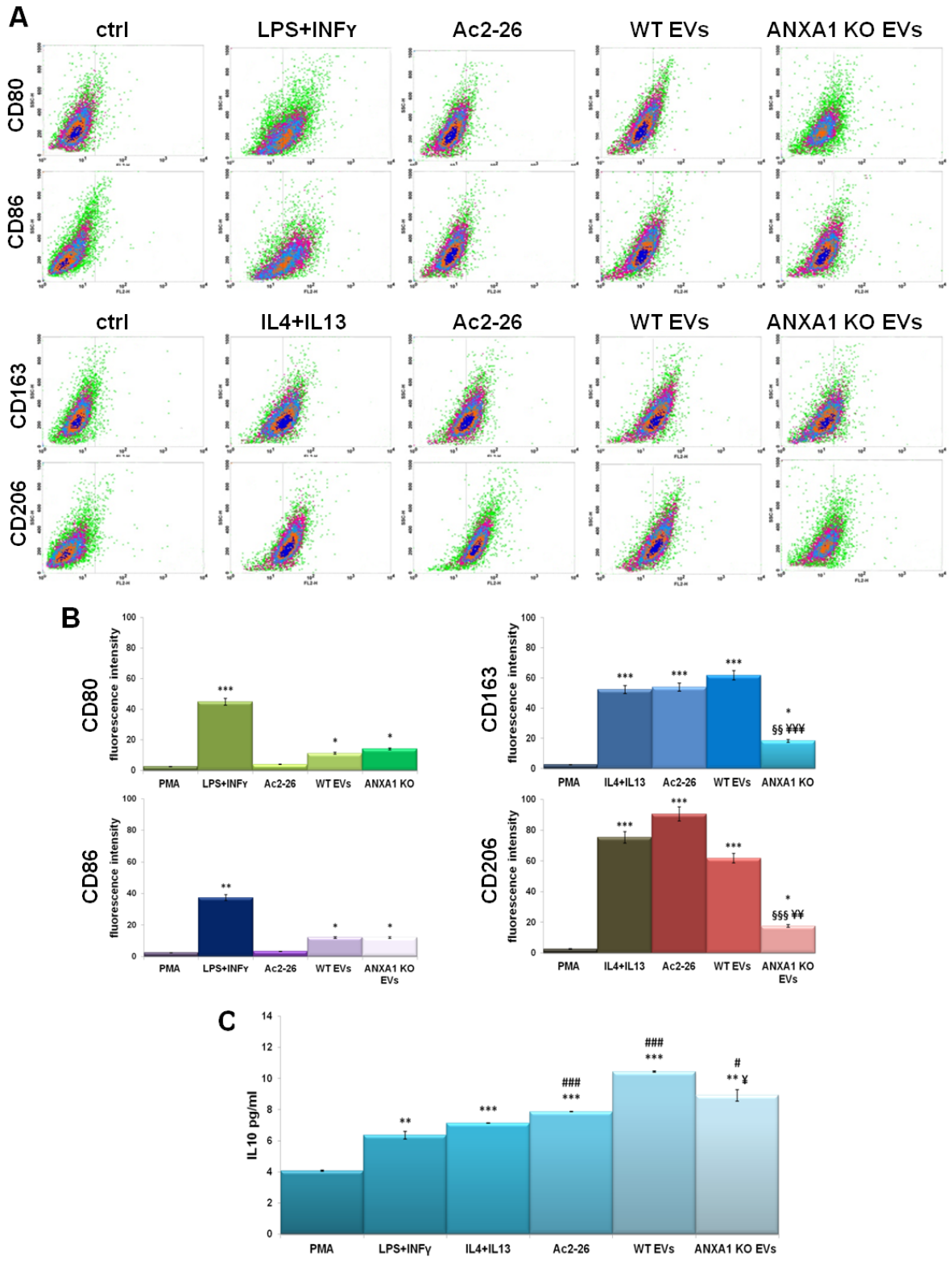

Figure 8.7 Macrophage polarization. (**A**) Flow cytometry analysis of M1 cell surface markers (CD80 and CD86) and M2 (CD163 and CD206) cell surface markers on THP-1 macrophages incubated with LPS+INF-γ (M1 induction cytokines), IL4+IL13 (M2 induction cytokines), Ac2-26 (1 μM) and WT and ANXA1 KO EVs for 24 h. (**B**) The histograms showed the expression of these markers on total cells analyzed through flow cytometry. (**C**) ELISA analysis of IL10 cytokine expression in THP-1 macrophages treated with LPS+INFγ (M1 induction cytokines), IL4+IL13 (M2 induction cytokines) and WT and ANXA1 KO EVs for 24 h. Data represent the mean of five independent experiments ± standard deviation with similar results. * $p < 0.05$; ** $p < 0.01$; *** $p < 0.001$ for treated cells vs. PMA treated controls; §§ $p < 0.01$; §§§ $p < 0.001$ for the point with ANXA1 KO EVs vs. Ac2-26; ¥ $p < 0.05$, ¥¥ $p < 0.01$, ¥¥¥ $p < 0.001$ for ANXA1 KO EVs vs WT EVs; # $p < 0.05$; ## $p < 0.01$; and ### $p < 0.001$ for each point vs. IL-4+IL-13.

8.8 The effects of EVs from WT and ANXA1 KO MIA PaCa-2 cells on macrophage migration and invasion.

The metastatic potential of ANXA1, secreted *via* EVs, has previously studied on endothelial cells and fibroblasts. Here, we focused on the M0 macrophage motility assessing migration and invasion processes. As shown in figure 8.8A and C, cells migrated and invaded more rapidly in presence of WT EVs than with ANXA1 KO EVs, both compared to untreated controls (Fig. 8.8B and D representative bright field images of wound healing and invasion assay, respectively, are reported). Also, in this case, Ac2-26 confirmed that the exogenous ANXA1 was able to induce very similar effects of WT EVs. Furthermore, we have proved that the WT EVs promoted the proliferation of these M0 macrophages through a colony formation assay, performed as reported in Material and methods section. We further distinctly reported as the ANXA1 KO EVs were less able to support cell growth. These results are described both in the bright field images (Fig. 7.8E) and in the histogram analysis (Fig. 7.8F) obtained from the SDS dissolution of cell-adsorbed crystal violet.

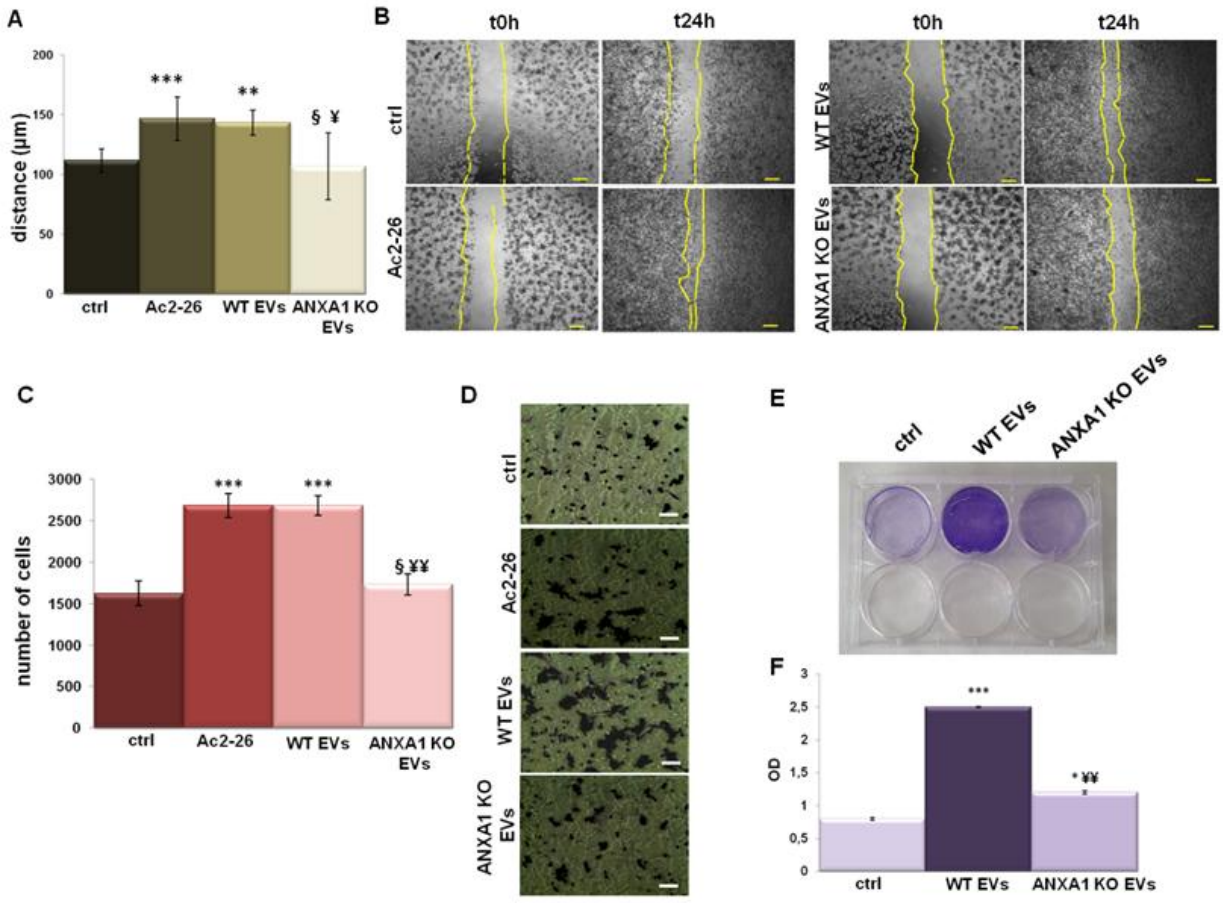

Figure 8.8 EVs effects on THP-1 macrophages. Analysis of (**A**) migration and (**C**) invasion speed of THP-1 macrophages treated with EVs from WT and ANXA1 KO MIA PaCa-2 cells with relative bright field images in (**B**) and (**D**), for migration and invasion respectively. Bar = 50µm. (**E**) Representative images of the clonogenic assay performed on THP1-macrophages in presence of WT and ANXA1 KO EVs for 24 hrs. (**F**) Histogram referring to the optical density (OD) obtained from 1% SDS cell dissolution and read to spectrophotometer. Data represent the mean of three independent experiments ± standard deviation with similar results. * $p<0.05$; ** $p<0.01$; *** $p<0.001$ for treated cells vs. untreated controls; § $p<0.05$ for the point with ANXA1 KO EVs vs. Ac2-26; ¥ $p<0.05$; ¥¥ $p<0.01$ for each point with ANXA1 KO EVs vs. WT EVs.

8.9 ANXA1 affects the tumor microenvironment

In TME, cancer cells can activate and recruit other cellular elements that contribute to tumor progression. In order to investigate the role of extracellular ANXA1, indirect co-culture systems were established between supernatants of WT and ANXA1 KO MIA PaCa-2 cells and macrophages and between EVs-treated macrophages and BJ or HUVEC, as described in Material and methods section. Thus, we have demonstrated that the conditioned medium (CM) harvested from the WT MIA PaCa-2 cells induced the macrophage recruitment in a more significant manner if compared with the ANXA1 KO MIA PaCa-2 one. The histogram referred to the panels a, c and e (Fig. 8.9A) which represent the macrophages in the bottom of the lower chamber in response to CM from WT and ANXA1 KO cells. In the same figure 8.9B, panels b, d and f are representative of the correspondent cells stained by crystal violet in the matrigel coating in the upper chamber of generated system. These last panels confirm that THP-1 cells invaded more rapidly in presence of the WT cells CM compared to the ANXA1 KO cells one, in line with which we reported above. Furthermore, the white arrows indicate that in presence of the CM from WT cells, the activated macrophages produced the typical ejections indispensible for the amoeboid movement capacity (Fig. 8.9A, panel c). On the contrary, when stimulated with ANXA1 KO cells-CM, macrophages remained mostly with a rounded monocyte-like appearance, like the untreated condition (Fig. 8.9A, panel e and a, respectively).

Finally, we have studied that polarized macrophages, obtained by the pretreatment with WT and ANXA1 KO EVs, were differently able to recruit fibroblasts and endothelial cells. To confirm the peculiar role of the extracellular ANXA1 in this process, we also used M0 macrophages treated with Ac2-26 as positive control. Figure 8.9B and C show the invasion of HUVEC and BJ, respectively. In both cases, as evident by histograms and bright field images, cell enrolment was significantly enhanced by M2 macrophages compared to M1 ones and mainly to the untreated control. These results were also confirmed using the supernatant (sup.) of M1 and M2 macrophages

polarized by WT and ANXA1 KO EVs. Furthermore, we studied the ability of polarized macrophages in M2, following the pretreatment with WT EVs for 24 hours, and M1, thanks to ANXA1 KO ones, to activate BJ and HUVEC motility. To confirm that this process is influenced by externalized ANXA1, we also used M0 macrophages treated with Ac2-26 as positive control. HUVEC and BJ invasion was significantly enhanced and affected by M2 macrophages compared to M1 and untreated control. The results were confirmed using only the supernatant (sup.) of M1 and M2 macrophages polarized by WT and ANXA1 KO EVs.

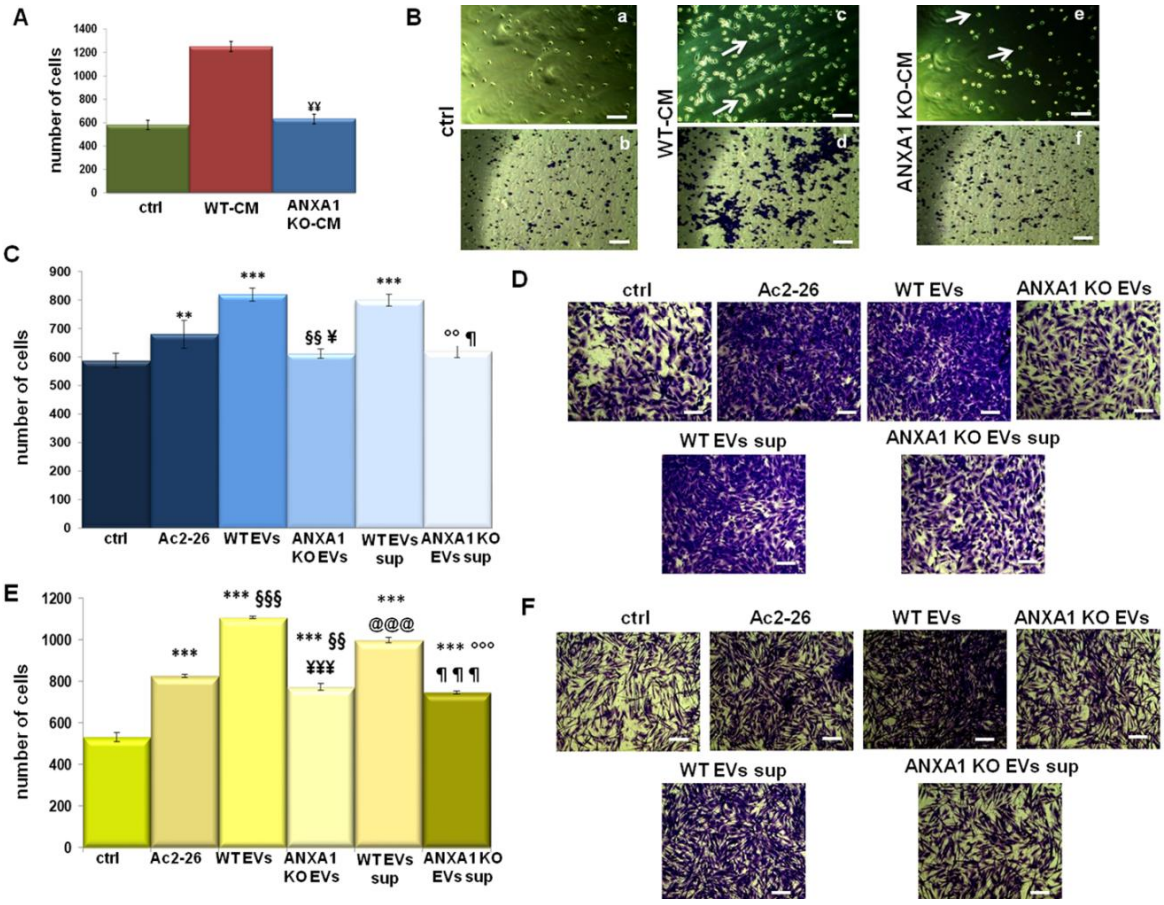

Figure 8.9 ANXA1 effects on TME. (**A**) Co-colture system performed by THP-1 macrophage invasion assay to WT and ANXA1 KO conditioned medium (CM). (**B**) Bright filed images of THP-1 cells captured in the bottom of the lower chamber of transwell (panels a, c and e) and representative images of macrophages in the same experimental points stained by crystal violet in the matrigel coating in the upper chamber of the generated invasion system (panels b, d and f). Results of (**C**) HUVEC and (**E**) BJ cells invasion to polarized M1 or M2 macrophages pretreated for 24 hrs with WT and ANXA1 KO MIA PaCa-2 EVs, with Ac2-26 (1µM) and with the supernatants of THP-1 pretreated for 24 hrs with WT and ANXA1 KO MIA PaCa-2 EVs. The relative bright field images were showed in (**D**) for HUVEC and in (**F**) for BJ, respectively. Bar = 50µm. Data represent the mean of four independent experiments ± standard deviation with similar results. ** p<0.01; *** p<0.001 for treated cells *vs*. untreated controls; §§ p<0.01; §§§ p<0.001 for each point with ANXA1 KO EVs *vs*. Ac2-26; ¥ p<0.05; ¥¥ p<0.01; ¥¥¥ p<0.001 for each point with ANXA1 KO EVs *vs*. WT EVs; °° p<0.01; °°° p<0.001 for ANXA1 KO EVs sup *vs*. Ac2-26; ¶¶ p<0.01; ¶¶¶ p<0.001 for ANXA1 KO EVs sup *vs*. WT EVs sup; @@@ p<0.001 for WT EVs sup *vs*. Ac2-26.

8.10 WT MIA PaCa-2 EVs influence the endothelial cell activation

The significant association between TAMs and angiogenesis in several cancers is a well-known issue [339; 340]. Additionally, the promotion of this process by ANXA1 in EVs has already been studied [247]. Thus, we have investigated how polarized M1 or M2 macrophages could influence the activation of endothelial cells and promote the angiogenesis. Since the vascular endothelial growth factor-A (VEGF-A) has one of the major mediators of angiogenesis, we measured its production by ELISA finding a notable increase in the supernatant of macrophages treated with EVs. In particular, WT EVs acted more efficiently than ANXA1 KO ones with a significant difference both if compared to each other and compared to control both at baseline (only following treatment with PMA for 6 h) and after 24 h more from the seeding with growth medium. Interestingly, M2 macrophages with WT EVs treatment have secreted more VEGF-A than ANXA1 KO ones. Additionally, the positive effect of Ac2-26 about the induction of VEGF-A section has been strongly evaluated (Fig. 8.10A). Later, we focused on cell motility evaluating that HUVEC migrated more rapidly if treated with supernatant of M2 macrophages (WT sup. – obtained from macrophages after a pre-treatment with WT EVs) compared to M1 supernatant (ANXA1 KO sup. – harvested from differentiated THP-1 pre-treated with ANXA1 KO EVs) (Fig. 8.10B and C for representative images). Furthermore, also for the *in vitro* angiogenesis the capability of macrophage supernatant to strongly stimulate this process was confirmed.

Notably, the WT EVs sup. promoted a significant number of branching points and the relative tube length com-pared to ANXA1 KO EVs sup. and the untreated control (Fig. 8.10D and E for bright field images). The macrophage supernatant containing Ac2-26 (Ac2-26 sup.) again confirmed its positive action in a very similar manner to WT EVs sup. stimulus (Fig. 8.10D and E). Finally, based on the variation of HUVEC migration speed, we studied their cytoskeletal reorganization through confocal analysis. Thanks to phalloidin staining, we observed a well-organized cytoskeleton with more evident F-actin fibers in cells treated with WT EVs sup. when

compared to other ones (Fig. 8.10F, panels a-d). In this same experimental point, we inversely found that VE-cadherin expression was significantly reduced compared to the control but also respect to the ANXA1 KO EVs sup. treated points (Fig. 8.10F, panels e-h). Also, in this case, we used as control the endothelial cells in presence of their own growth medium (ctrl) and with HUVEC medium: macrophage growth medium 1:1 (ctrl sup). The experimental point with Ac2-26 was already shown above. These results highlighted by the fluorescence images have been also proved by the histograms representing the densitometry analysis (Fig. 8.10G).

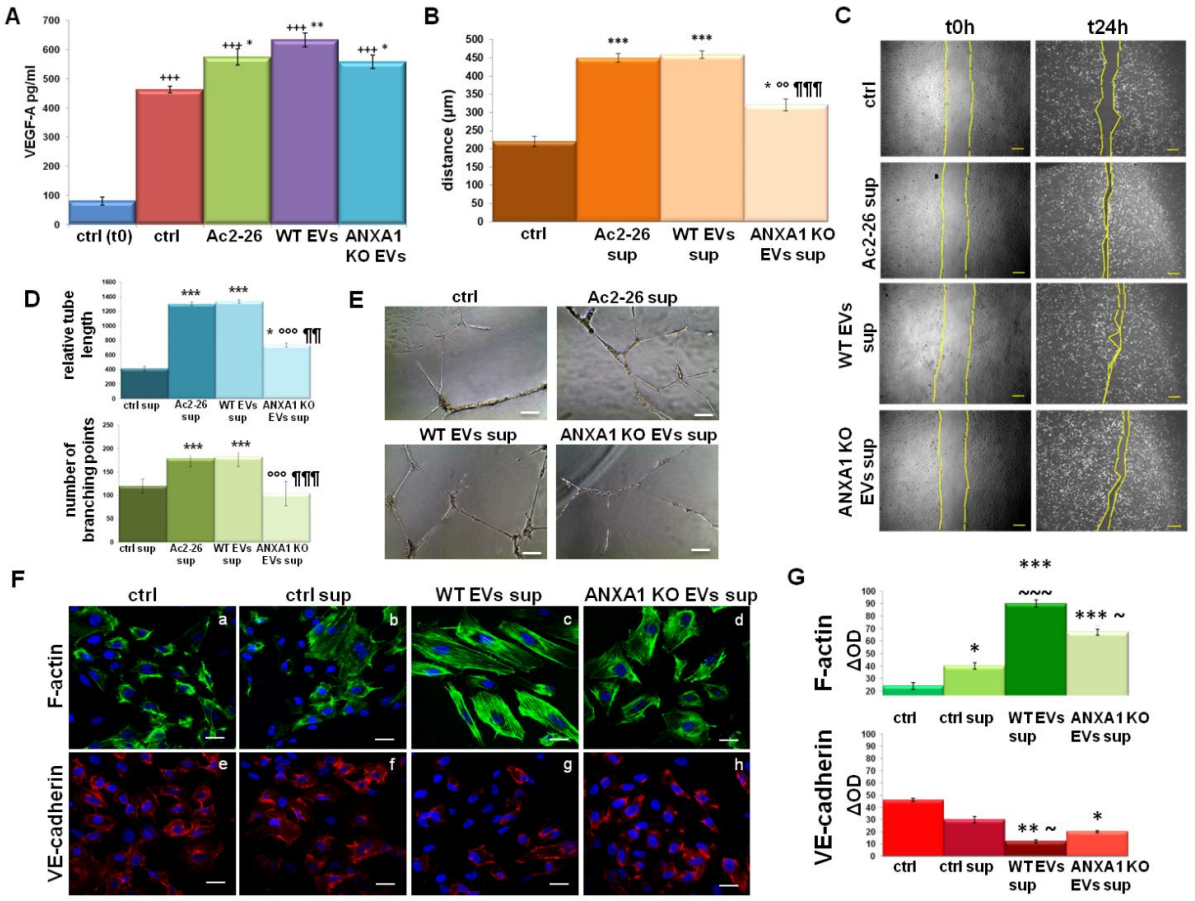

Figure 8.10 Endothelial cells activation induced by M2 macrophages. (**A**) ELISA analysis of VEGF-A expression in the supernatants of macrophages treated with Ac2-26 (1µM) and WT and ANXA1 KO EVs for 24 hrs. Result of HUVEC (**B**) migration and (**D**) in vitro angiogenesis in presence of THP-1 supernatants pretreated for 24 hrs with WT and ANXA1 KO MIA PaCa-2 EVs and Ac2-26 (1µM). The relative bright field images are reported in (**C**) for migration assay (Bar = 50µm) and in (**E**) for angiogenesis one (Bar = 100 µm). (**F**) Confocal analysis for HUVEC cells: F-actin (panels a-d) and VE-cadherin (panels e-h) with the related densitometry evaluation in (**G**). Nuclei were stained with DAPI 1:1000 for 30 min at RT in the dark. Magnification 63× 1.4 numerical aperture (NA). Bar = 100 µm. Data represent the mean of three independent experiments ± standard deviation with similar results. * p<0.05; ** p<0.01; *** p<0.001 for treated cells *vs*. untreated controls; § p<0.05; §§ p<0.01; §§§ p<0.001 for ANXA1 KO EVs *vs*. Ac2-26; ¥¥ p<0.01; ¥¥¥ p<0.001 for each point with ANXA1 KO EVs *vs*. WT EVs; +++ p<0.001 for each experimental point *vs*. baseline control t0 meaning the treatment exclusively with PMA (320nM) for 6 hrs; °° p<0.01; °°° p<0.001 for ANXA1 KO EVs sup *vs*. Ac2-26 sup; ¶¶ p<0.01; ¶¶¶ p<0.001 for ANXA1 KO EVs sup *vs*. WT EVs sup; ~ p<0.05; ~~~ p<0.001 for ANXA1 KO EVs sup and WT EVs sup *vs*. ctrl sup

8.11 TAMs support the fibroblast activation

As shown in figure 8.11 (A and B), the BJ cells migrated more rapidly in presence both of Ac2-26 and of WT EVs sup. than to those with ANXA1 KO EVs sup. and to untreated control. In order to support this result, we performed a gel zymography assessing the activity of MMPs secreted by fibroblasts to degrade the extracellular matrix. Differently from MMP2 whose signal appeared overall unchanged, the MMP9 underwent a very prominent increase, after 24 h of WT-EVs sup. treatment as compared to the ANXA1 KO-EVs sup. (Fig. 8.11C). Furthermore, activated fibroblasts are characterized by cytoskeletal changes, as revealed in this case through the marked increase of well-organized F-actin stress fibers and acquisition of more precise and parallel directionally not only respect to the control cells but also respect to the ANXA1 KO EVs sup. treated cells (Fig. 8.11E, panels a-d). Another important signal of fibroblast differentiation is the increase of the expression levels of FAP1α. In BJ cells, this expression notable increase when treated with WT EVs sup, more than ANXA1 KO EVs sup. (Fig. 8.11E, panels e-h). As for HUVEC cells, we used two technical controls: the first one constituted by the BJ in presence of the growth medium and the second one by BJ growth medium: macrophage growth medium 1:1 (ctrl sup). Also in this case, we have not illustrated the experimental point treated with Ac2-26 that was shown previously. This information appeared evident not only in fluorescence images but also through the densitometry analysis (Fig. 8.11F). Moreover, the western blotting reported in figure 8.11G, further confirm the different levels of FAP1α expression which appears absolutely in line with confocal results.

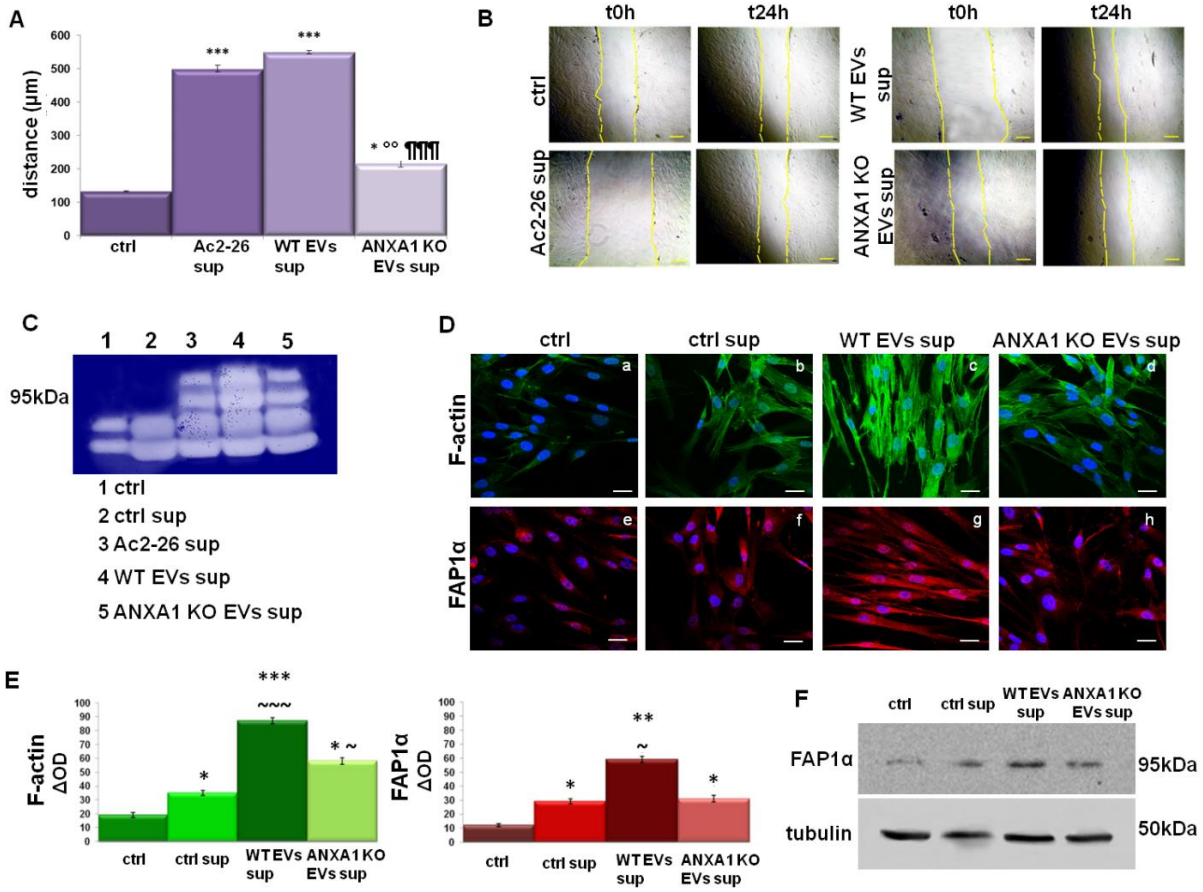

Figure 8.11 Fibroblasts activation induced by M2 macrophages. Results of (**A**) wound-healing assay and relative bright field images (**B**) of BJ cells with THP-1 supernatants obtained after 24 h with WT and ANXA1 KO MIA PaCa-2 EVs, and Ac2-26 (1 µM). Bar = 50 µm. (**C**) Gelatin zymography showing gelatinolytic activity of MMP-9 of BJ supernatants. (**D**) Immunofluorescence assay on BJ to detect: F-actin (panels a–d) and FAP1α (panels e–h) with the related densitometry analysis (**E**). Magnification 63 × 1.4 NA. Bar = 100 µm. (**F**) Western blot using antibodies against FAP1α on protein content of fibroblasts. Protein normalization was performed on tubulin levels. Data represent the mean of three independent experiments ± standard deviation with similar results. * $p < 0.05$; ** $p < 0.01$; and *** $p < 0.001$ for treated cells vs. untreated controls; °° $p < 0.01$ for ANXA1 KO EVs sup. vs. Ac2-26 sup; ¶¶¶ $p < 0.001$ for ANXA1 KO EVs sup. vs. WT EVs sup; ~ $p < 0.05$; ~~~ $p < 0.001$ for ANXA1 KO EVs sup. and WT EVs sup. vs. ctrl sup.

8.12 Characterization of macrophage infiltration in WT and ANXA1 KO tumor and metastases

TAMs are pre-dominantly anti-inflammatory M2-macrophages. Thus, in order to assess the main phenotype, the WT and ANXA1 KO tissues from mice pancreas and liver, obtained from our previous study [162], have been analyzed through H&E staining. First, pancreas WT sections generally displayed multiple injuries, infiltrating ductal-like structures and extensive desmoplastic stromal reactions (Fig. 8.12A, panel a, star), attributable to high macrophage infiltration (Fig. 8.12A, panel a, white arrows) compared to the ANXA1 KO ones (Fig. 8.12A, panel b). We also determined whether ANXA1 depletion could affect the stromal infiltration in metastasis formation. Therefore, we analyzed the liver section because it represents one of the first affected organs by the PC metastatic process. The H&E staining displayed a high infiltration of macrophages in WT livers (Fig. 8.12A, panel c, white arrows), which were particularly notable in the metastatic niche in the section, signed by the lost structural integrity and reduced compactness. On the other hand, the ANXA1 KO liver sections retained their red color, integrity and tissue density and showed much less macrophage infiltration in metastasis lesion (Fig. 8.12A, panel d).

Next, in order to confirm the phenotype of TAMs in tumor and metastasis tissues, their characterization has been performed by an immunofluorescence assay. As shown in figure 8.12B, a large number of CD206 and CD163 positive macrophages more than CD80 and CD86 were observed in the WT pancreatic tumor and in the corresponding liver metastasis sections, suggesting the relevant presence of M2 macrophages. In contrast, low levels of CD206 and CD163 positive macrophages were detected in the ANXA1 KO tumor (panels e-h) and metastasis (panels m-p) tissues, where the main macrophage phenotype was the M1 one, as revealed by CD80 and CD86 signals (panels a, b and i, j for CD80; b, f and k, l for CD86; e, f and m, n for CD163; g, h and o, p for CD206). These results have been also confirmed by densitometry analysis shown in figure 8.12C.

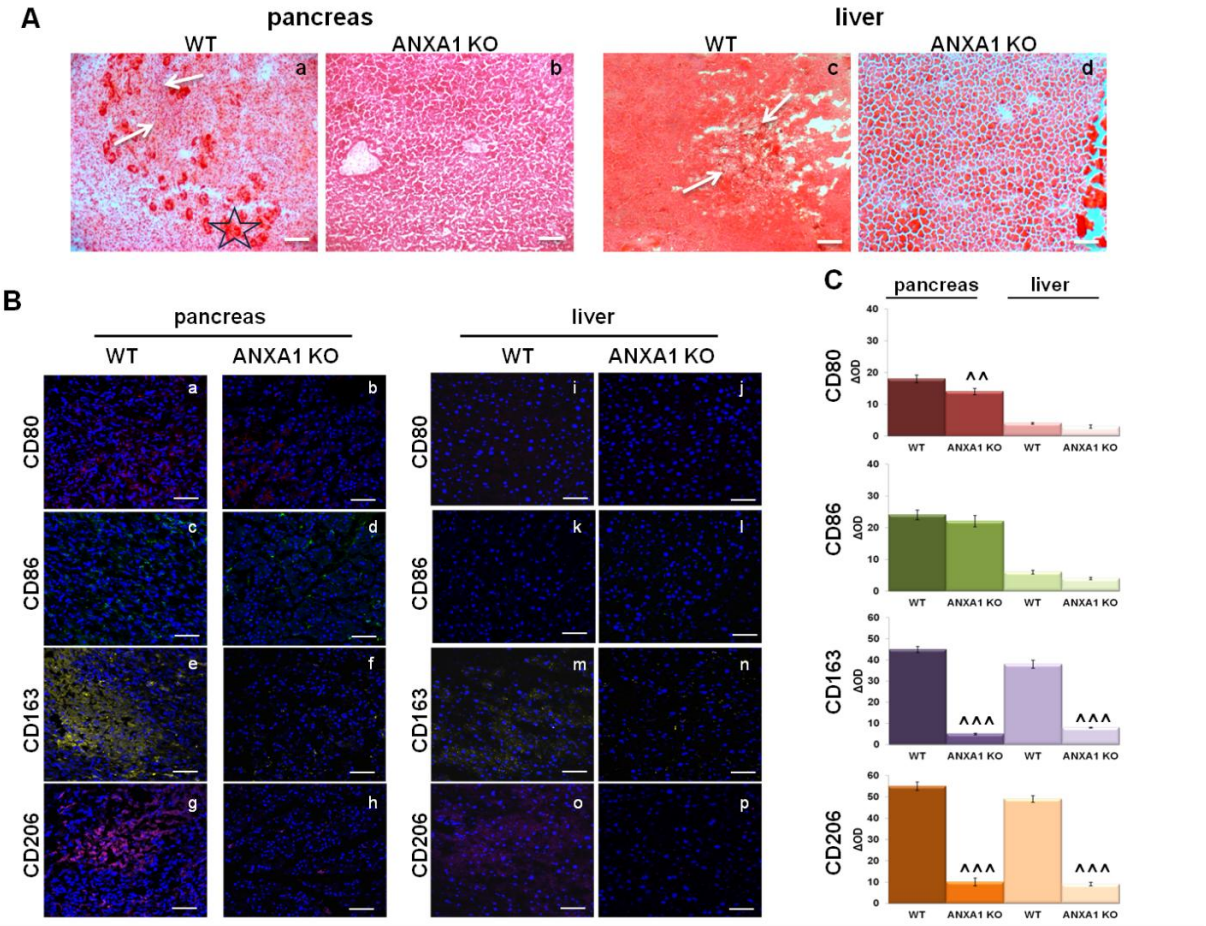

Figure 8.12 Macrophage infiltration in SCID mice sections derived from primary pancreatic tumors and livers after intrapancreatic implantation of WT and ANXA1 KO MIA PaCa-2 cells. In detail, we indicated as WT and ANXA1 KO pancreas the sections derived from mice in whose pancreas we have previously implanted WT and ANXA1 KO MIA PaCa-2 cells, respectively, and in which primary tumors have been developed. Additionally, WT and ANXA1 KO livers represented the hepatic sections in which we had found significantly more metastatic lesions deriving from tumors originating from WT MIA PaCa-2 cells compared to ANXA1 KO ones. (**A**) Pancreas (panels a and b) and liver (panels c and d) sections have been stained by H&E. Infiltrating ductal-like structures were labeled by star; macrophage infiltrations were marked by white arrows. Bar = 100 μm. (**B**) Representative images of CD80 (panels a and b; i and j), CD86 (panels c and d; k and l) (M1 macrophage markers) and CD163 (panels e and f; m and n) and CD206 (panels g and h; o and p) (M2 macrophage markers) staining by immunofluorescence in WT and ANXA1 KO mice pancreas and liver (livers in which we have found metastatic lesions derived from intrapancreatic injection of WT MIA PaCa-2 cells) sections. (**C**) The histograms showed the densitometry analysis on immunofluorescence images based on the intensity of each signal compared to the total number of nuclei. Nuclei were stained with DAPI 1:1000 for 30 min at room temperature (RT) in the dark. Magnification 40 × 1.4 NA. Bar = 100 μm. Data represent the mean of three independent experiments ± standard deviation with similar results. ^^ $p < 0.01$; ^^^ $p < 0.001$ for ANXA1 KO vs. WT cells xenografts.

8.13 The ability of ANXA1 to affect tumor 3D model

In order to investigate how the ANXA1 can affects the TME, 3D model both in mono and co-culture were established between WT and ANXA1 KO MIA PaCa-2 cells, CAFs and monocytes, as described in Material and methods section. In figure 8.13.1A we have demonstrated that MIA PaCa-2 cells, after 10 days, form a compact spheroid with an outer proliferative layer and a hypoxic and necrotic core that means the cellular interactions as well as compactness. On the other hand, though the ANXA1 KO MIA PaCa-2 cells show themselves how "aggregate" which describe less tightly packed cells from compact spherical cultures like spheroids (Fig. 8.13.1B).

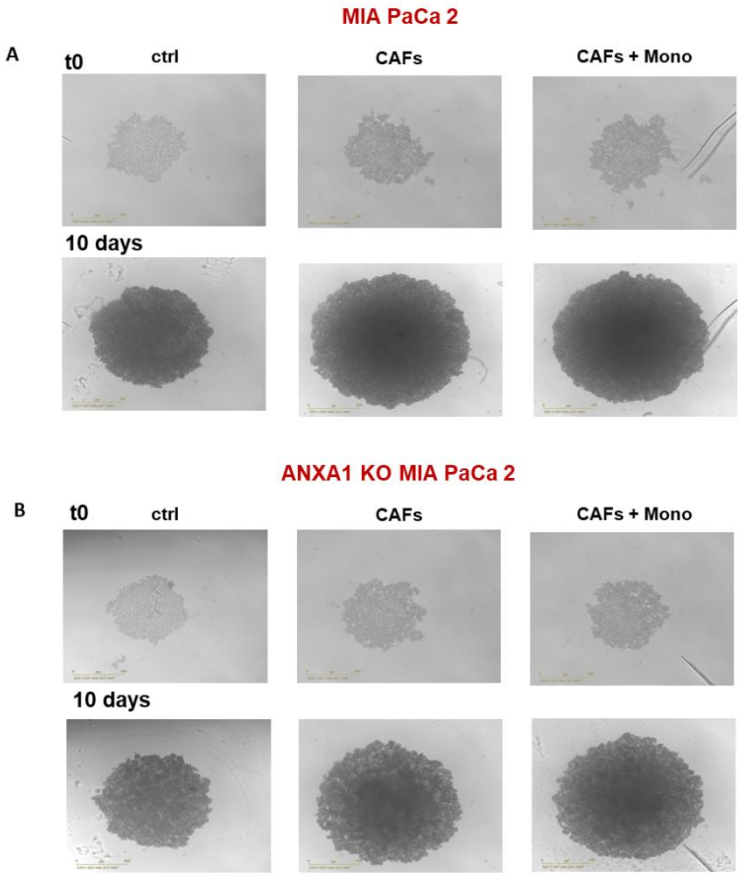

Figure 7.13.1 ANXA1 effects on tumor 3D model. (**A**) 3D model in mono and co-colture system performed by WT cells and ANXA1 KO ones (**B**) in 96 well U-bottom plates.

Furthermore, the presence of CAFs in the co-culture with WT tumor cells, compared to ANXA1 KO ones, considerably increased the spheroid formation, also confirmed by the analysis of the

number of cells, size and viability (Fig. 8.13.2A-F). All tumor cell lines showed increased proliferation and survival in co-culture with CAFs compared to tumor monocultures. To determinate the influence of monocyte addition to 3D model co-culture formation, viability and proliferation, WT and ANXA1 KO MIA PaCa-2 cells and CAFs were co-cultured for 3 days to form spheroids and freshly isolated monocytes were added (Fig. 8.13.1).

Tumor cells/CAFs/monocytes were incubated for 7 days; then the analysis of the number of cells, size and viability were performed (Fig. 8.13.2 A-F). As show in figure 8.13.2 the presence of monocytes in co-culture 3D model did not influence this system if compared with presence of CAFs, both for WT and ANXA1 KO MIA PaCa-2 3D models.

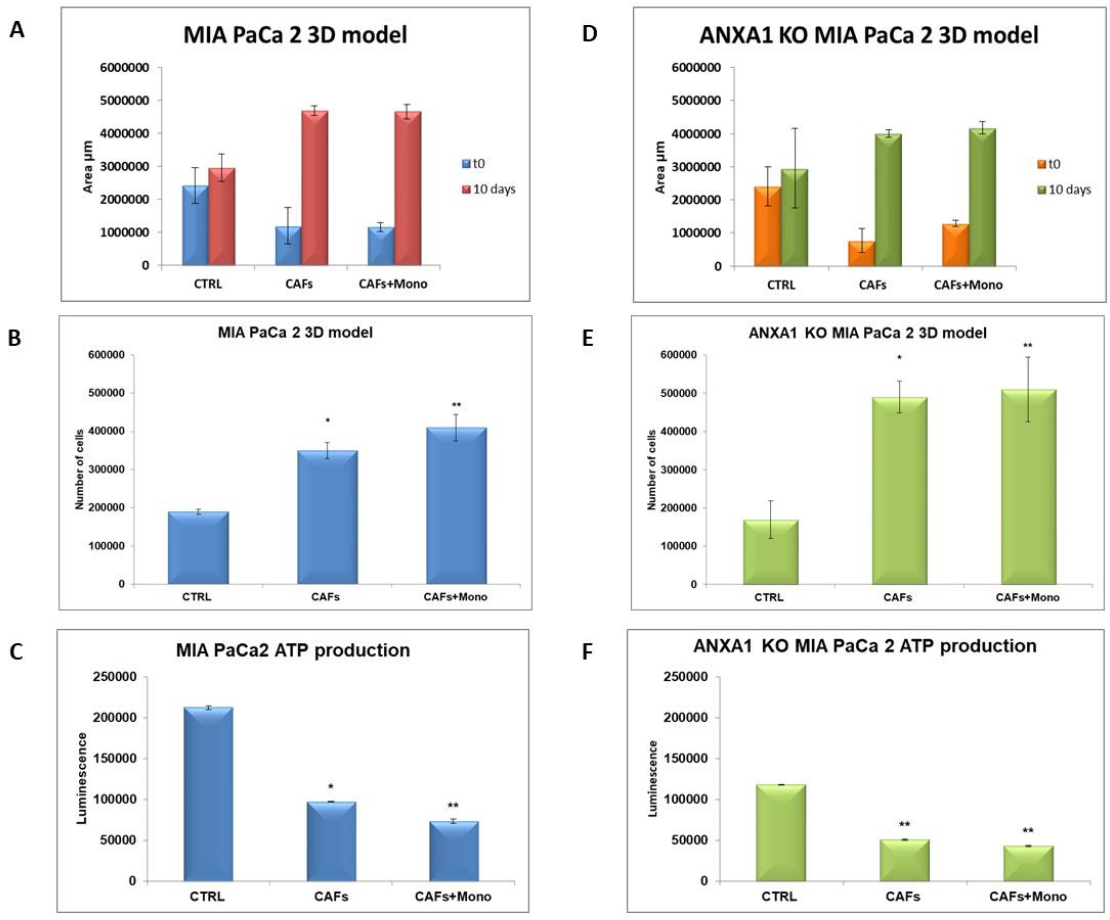

Figure 8.13.2 Analysis of WT and ANXA1 KO tumor 3D model. (**A-D**) Area analysis of 3D model in mono and co-colture system performed by WT cells and ANXA1 KO ones, with CAFs and monocytes; (**B-E**) Count of number of WT and ANXA1 KO MIA PaCa2 cells; (**C-F**) Analysis of viability by CellTiterGlo (Promega). Data represent the mean of three independent experiments ± standard deviation with similar results. * $p < 0.05$; ** $p < 0.01$; and *** $p < 0.001$ for treated cells vs. untreated controls.

8.14 HS directly interacts with ANXA1 N-terminal peptide

ANXA1 is involved in PC progression, mainly the extracellular form. Thus, the need to inhibit its action, has become an appealing cue for the anti-cancer research. Heparan sulfate (HS) is a glycosaminoglycan of the extracellular matrix known to bind several molecules, as growth factors and cytokines, generating a kind of reservoir in the extracellular environment. Here, we started our study by showing the physical calcium-dependent interaction between HS and ANXA1 as both full-length protein and Ac2-26 by biophysical techniques. The direct binding of ANXA1 to a series of sulfated oligosaccharides was recently assessed as a calcium-dependent interaction [279]. A DSF analysis, based on the shift of protein melting temperature upon specific ligand binding, was first used to explore the interaction of our human recombinant ANXA1 and our HS preparation. As shown in Fig. 8.14A, B, we observed a 4.76 $^{\circ}$C temperature shift in presence of Ca^{2+} ions and progressively growing melting temperatures (Tm) at increasing concentrations of HS. We did not observe any temperature shift in absence of Ca^{2+} ions. Since the presence of calcium is known to induce a conformational change that exposes the N-terminal domain from the core with a consequent activation of the protein [341], we decided to explore the direct involvement of the N-terminal domain in the binding to HS. To test this hypothesis, we took advantage of the SPR technique immobilizing on a sensor chip both the human full length ANXA1 and the N-terminal peptide Ac2-26. As shown in figure 8.14C, D, the associations and dissociations curves of HS injections showed concentration-dependent responses indicating a direct binding between both the full-length ANXA1 (K_D = 1.3 ± 1.0 10^{-4} M) and the N-terminal peptide K_D = 1.5 ± 1.5 10^{-4} M. The direct binding of ANXA1 to a series of sulfated oligosaccharides was recently assessed as a calcium-dependent interaction. This binding has been confirmed in my research laboratory through DSF and SPR technique both for full-length hrANXA1 and Ac2-26. We continued the study evaluating the effects of the HS on migration (Fig. 8.14A) and invasion (Fig. 8.14B) processes of WT and ANXA1 KO MIA PaCa-2. ANXA1 KO clone did not undergo the action of HS.

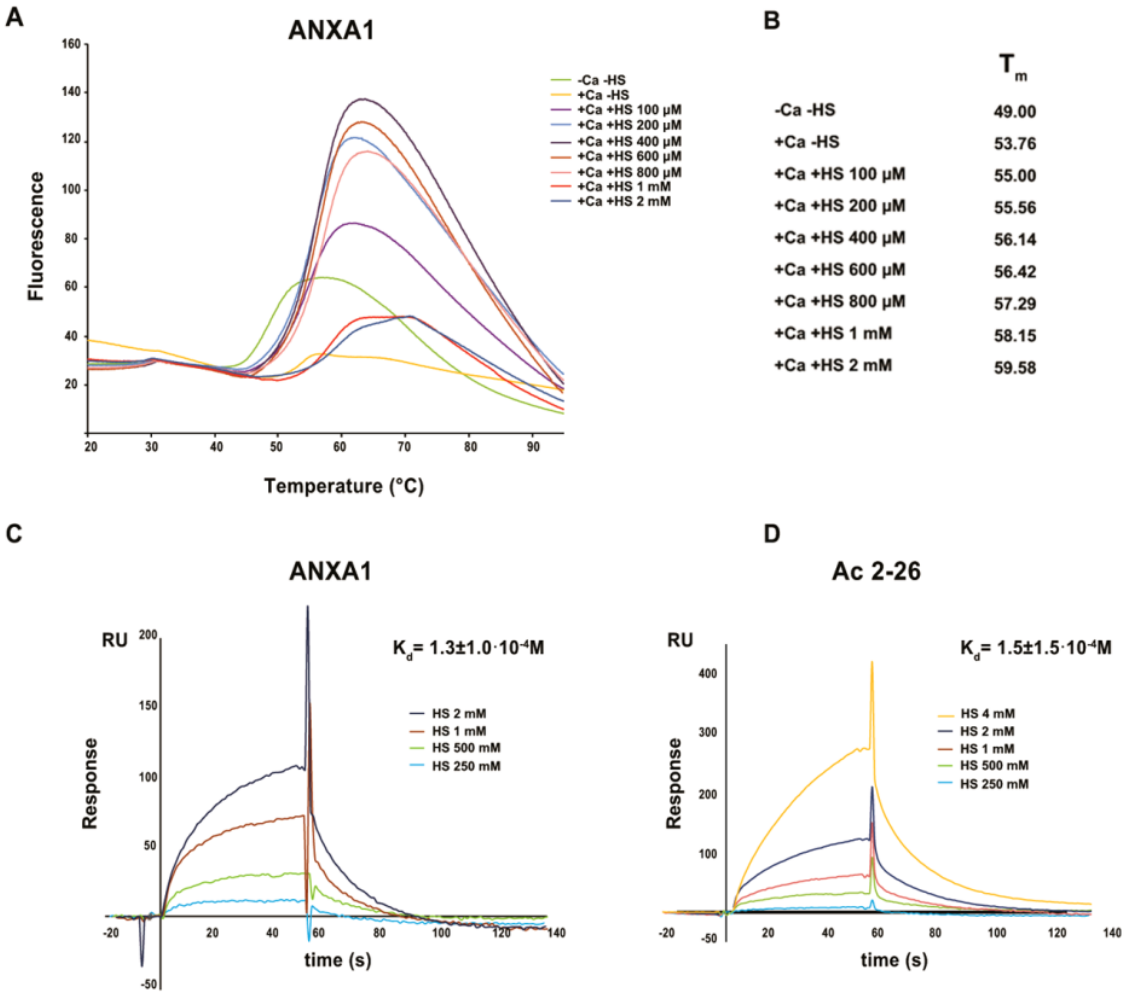

Figure 8.14 Heparan sulphate binding to the full length ANXA1 and the N-terminal peptide Ac2-26. (**A**) DSF analysis of the full length ANXA1 protein with different concentrations of HS and Ca^{2+} ions as indicated. (**B**) ANXA1 melting Temperatures (Tm) of the conditions reported in (**A**). Sensorgrams obtained from the SPR interaction analysis of HS binding to immobilized full length ANXA1 (**C**) and the N-terminal peptide Ac 2–26 (**D**).

8.15 HS inhibits the migration and invasion rate of WT MIA PaCa-2 cells and not of ANXA1 KO clone

The role of ANXA1 in PC cell motility has been previously elucidated [162; 254]. Once established the interaction between HS and ANXA1, we continued the study evaluating the effects of the GAG on migration (Fig. 8.15A and B) and invasion (Fig. 8.15C and D) processes of WT and ANXA1 KO MIA PaCa-2. Once confirmed the significant slowed motility of MIA PaCa-2 cells lacking ANXA1, we assisted to a strong decrease induced by HS on both biological processes only on WT MIA PaCa-2. Indeed, ANXA1 KO clone did not undergo the action of HS. The concentration of this molecule (10 µg/ml) has been chosen through previous migration tests performed on WT and ANXA1 KO MIA PaCa-2 cells.

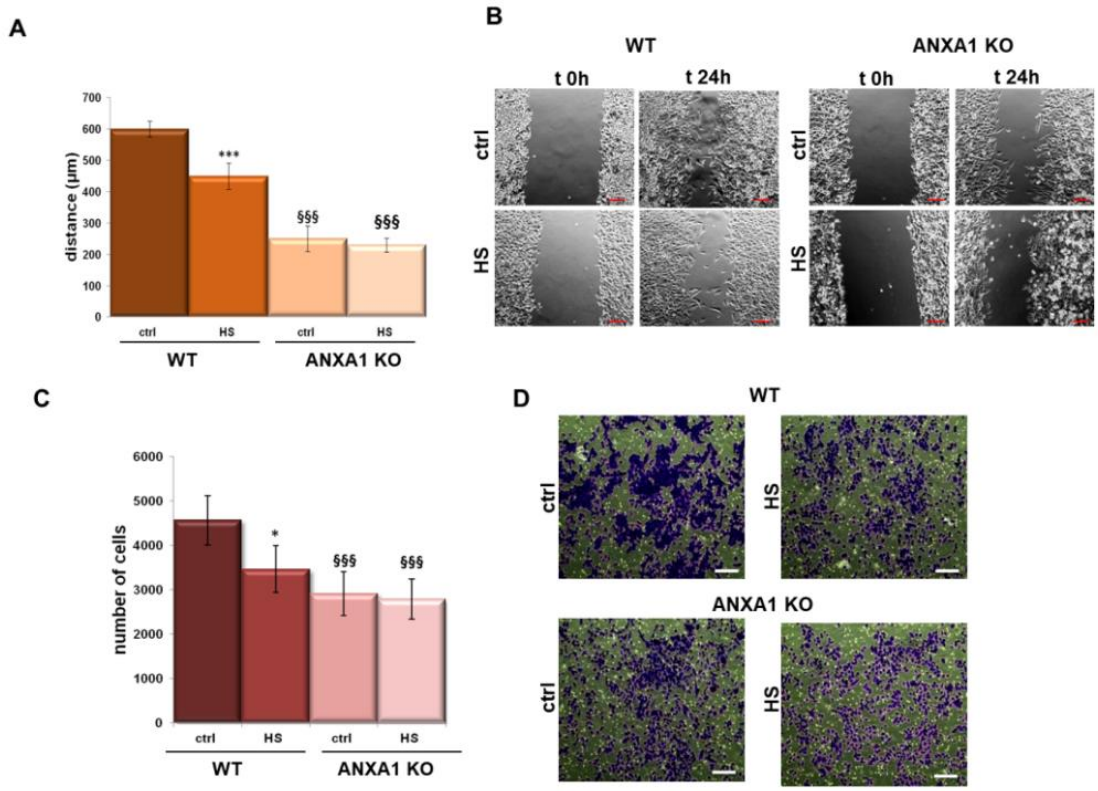

Figure 8.15 Evaluation of migration/invasion rate of WT and ANXA1 KO MIA PaCa-2 cells in presence of HS. (**A**) Results from the scratch wound healing assay on WT and ANXA1 KO MIA PaCa-2 cells treated or not with HS (10 µg/ml). (**B**) Representative bright field images captured by Time Lapse microscope (Leica AF-6000 LX; Leica Microsystems) of WT and ANXA1 KO MIA PaCa-2 cells at 0 (coincident with the HS administration) and 24 hr from produced wounds. Magnification 10×. Bar = 100 µm. ***p < 0.001 versus untreated controls; §§§p < 0.001 versus WT not treated cells. The migration rate was determined by measuring the distances covered by individual cells from the

initial time to the selected time points (bar of distance tool, Leica ASF software). The data are representative of n = 3 independent experiments ± SEM. (**C**) Results of the invasion assay on WT and ANXA1 KO MIA PaCa-2 cells treated or not with HS (10 μg/ml). The data represent the sum of cells of 15 separate fields per well of n = 5 experiments. *p < 0.05 versus untreated controls; §§§p < 0.001 versus WT not treated cells. (**D**) Representative images of analyzed fields of the invasion assay captured after 24 hr from the start of the invasion experiment, coincident with the HS administration. Magnification 20×. Bar = 150 μm

8.16 HS reduces the pro-migratory and invasive effects of ANXA1

The Western blot analysis showed in figure 8.16A confirmed the presence of ANXA1 only in the total and supernatant protein extracts of WT MIA PaCa-2 cells. Thus, we replaced the growth medium of ANXA1 KO cells with WT supernatants, conditioned on cells for 24 h, in presence or not of HS. As reported in figure 8.16B and 2C, when treated with WT cells medium, containing ANXA1, the migration and invasion speed of KO MIA PaCa-2 notably increased. Moreover, we assisted to a significant rescue when WT supernatant has been administered to ANXA1 KO cells together with HS (Fig. 8.16B and C).

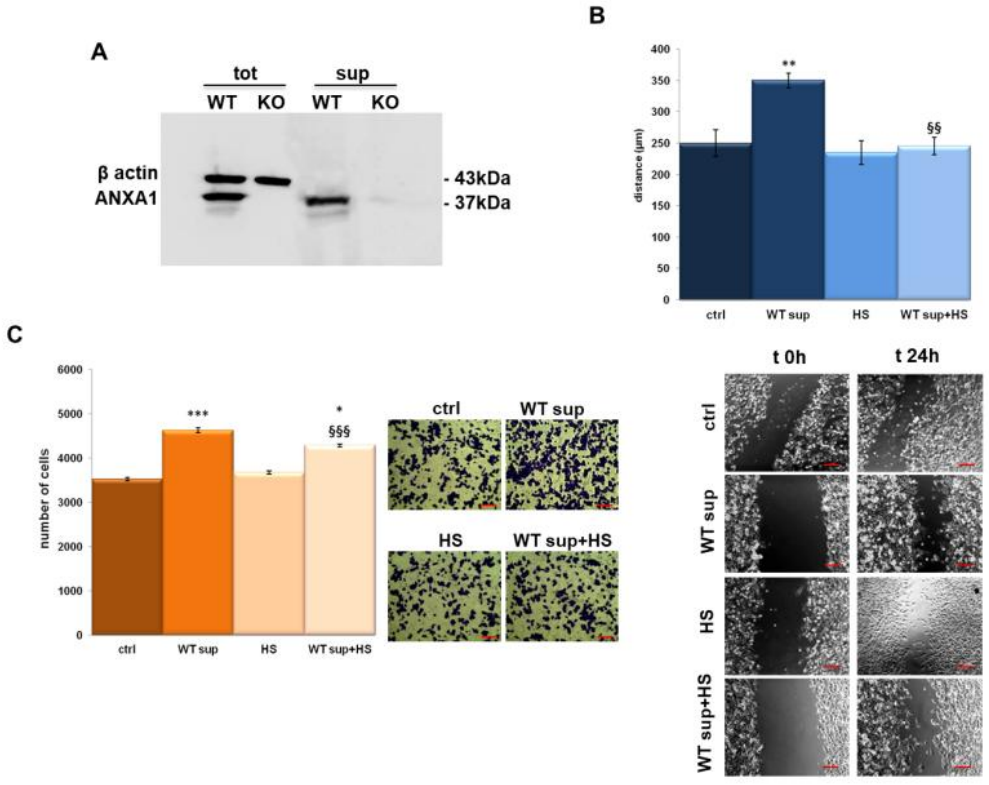

Figure 8.16 HS effects on ANXA1 KO MIA PaCa-2 cells in presence of WT cells conditioned medium. (**A**) Western blot analysis of total and supernatant protein extract from WT and ANXA1 KO MIA PaCa-2 cells. (**B**) Results from the scratch wound healing assay on ANXA1 KO MIA PaCa-2 cells treated or not with HS (10 μg/ml) and/or the medium of

WT MIA PaCa-2 in which cells have grown for 24 h (WT sup). Representative bright field images captured by Time Lapse microscope (Leica AF-6000 LX; Leica Microsystems) of ANXA1 KO MIA PaCa-2 cells at 0 and 24 h from produced wounds. Magnification 10×. Bar = 100 μm. **p < 0.01 versus untreated controls; §§p < 0.01 versus cells treated with WT supernatants. The migration rate was determined by measuring the distances covered by individual cells from the initial time to the selected time points (bar of distance tool, Leica ASF software). The data are representative of n = 3 independent experiments ± SEM. (**C**) Results of the invasion assay on ANXA1 KO MIA PaCa-2 cells treated or not with HS (10 μg/ml) and/or the WT sup. The data represent the sum of cells of 15 separate fields per well of n = 3 experiments. **p < 0.01 and ***p < 0.001 versus untreated controls; §§§p < 0.001 versus cells treated with WT supernatants. Representative images of analyzed fields of the invasion assay captured after 24 hr from the start of the invasion experiment. Magnification 20×. Bar = 150 μm.

8.17 The effects of Ac2-26 on WT MIA PaCa-2 cells are inhibited by HS

The induction of Ca^{2+} release from the intracellular compartments by ANXA1 and its N-terminal peptide Ac2-26 is a well-known concept [184; 342]. In order to focus our efforts on the HS effects on ANXA1, we continued our analysis on WT MIA PaCa-2 cells. Therefore, the Fluo-4 a. m. cytofluorimetric assay confirmed the activation of Ca^{2+} intracellular transition when Ac2-26 has been externally added to cells. Moreover, in case of co-administration of Ac2-26 and HS, the effects of the ANXA1 mimetic peptide has been strongly abrogated. Furthermore, HS interfered with Ca^{2+} release also when provided alone (Fig. 8.17A). Ionomycin and EDTA have been used as technical controls. Since Ca^{2+} mobilization represents a crucial moment for cell motility [28,29], we further assessed migration and invasion assays on WT MIA PaCa-2 cells. As expected, Ac2-26 has been able to induce both processes. However, when this peptide has been added together with HS, this ability has been significantly abolished (Fig. 8.17B and C).

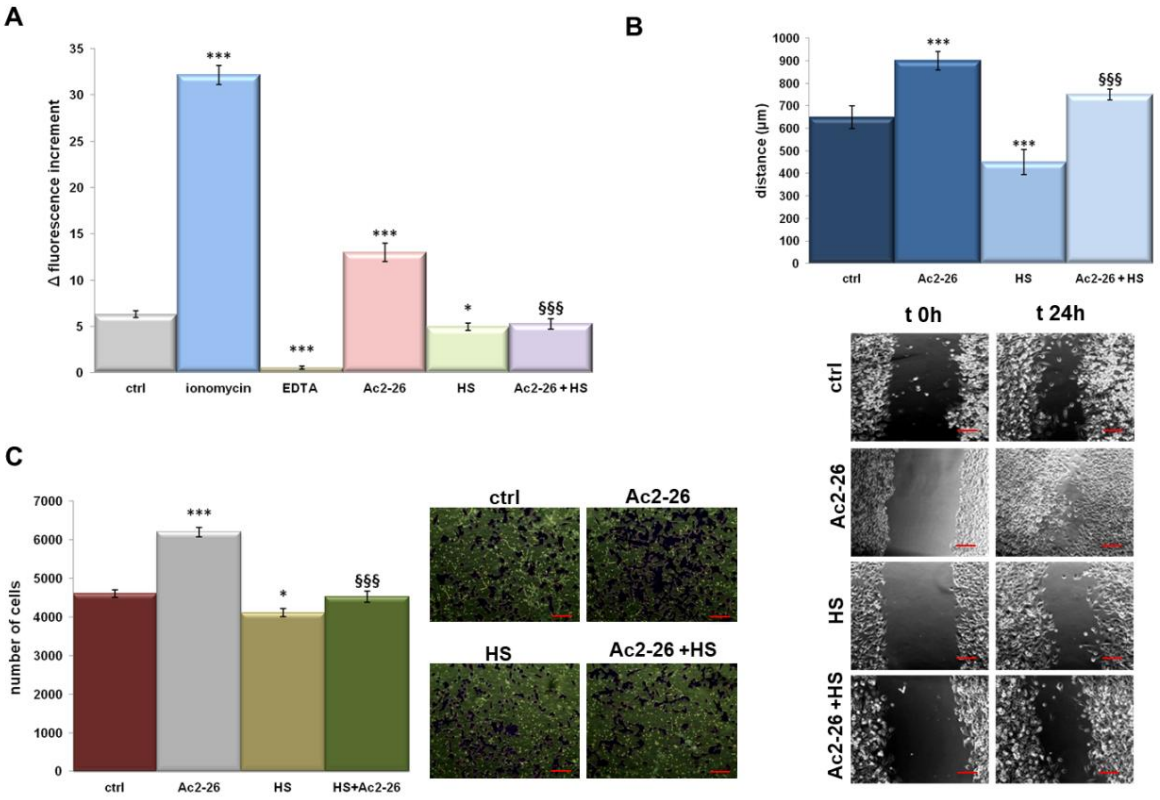

Figure 8.17 Assessment of HS action on Ac2-26 on WT MIA PaCa-2 cells. (**A**) Effects of ionomycin (1 mM), EDTA (15 mM), as technical controls, Ac2-26 (1 µM) with or without HS (10 µg/ml) on rise in intracellular Ca^{2+} in WT MIA PaCa-2 cells.*p<0.05; ***p<0.001 versus not treated control; §§§p<0.001 versus Ac2-26. (**B**) Scratch wound healing assay and invasion assay (**C**) on WT MIA PaCa-2 treated for 24hr with Ac2-26 (1µM) and/or HS (10 µg/ml). **p<0.01 versus untreated controls; ***p<0.001 versus untreated controls; §§p<0.01 versus cells treated with WT supernatants; §§§p<0.001 versus AC2-26 treated cells.

8.18 The mesenchymal phenotype of WT MIA PaCa-2 cells is reverted by HS

WT MIA PaCa-2 cells are characterized by a marked mesenchymal phenotype which is further amplified by ANXA1 [343; 344]. In this study, we found the loss of the epithelial cytokeratins 8 (CK8) and 18 (CK18) in presence of Ac2-26, accompanied by an increased expression induced by HS. Finally, an intermediate condition has been highlighted when Ac2-26 and HS have been administered together (Fig. 8.18A, panels a-d for CK8 and panels e-h for CK18). No differences in terms of expression were found for vimentin even if a better filamentous-like organization has been retained for Ac2-26. This organization, which was lost when cells have been treated by HS, reached an intermediate feature in presence of both treatments (Fig. 8.18A, panels i-l). These results are corroborated by the western blot in figure 8.18B. Next, we have studied the capability of WT MIA PaCa-2 to form spheroids in particularly conditions. We could find that after 24 h, WT MIA PaCa-2 cells continued to stay in a huge aggregate when the spheroid was treated with Ac2-26. On the contrary, the cell mass scattered in presence of HS. Therefore, we analyzed the spheroids/aggregates areas by the microscopic images and we evaluated an intermediate situation with HS that reached very similar features to control cells. Moreover, to confirm the aggressive behavior of PC cells we analyzed their ability to growth forming colonies proving [345] that the ANXA1 mimetic peptide promoted the formation of WT MIA PaCa-2 cells colonies, behavior inhibited by HS both alone and together with Ac2-26 (Fig.8.18D). It has been possible to observe these results in the bright field image and in the histogram related to the dissolution by SDS of cell-adsorbed crystal violet (Fig. 8.18D). Finally, MTT assay in Fig. 8.18E shows that cell proliferation is affected by no kind of treatment at 24, 48 and 72 h.

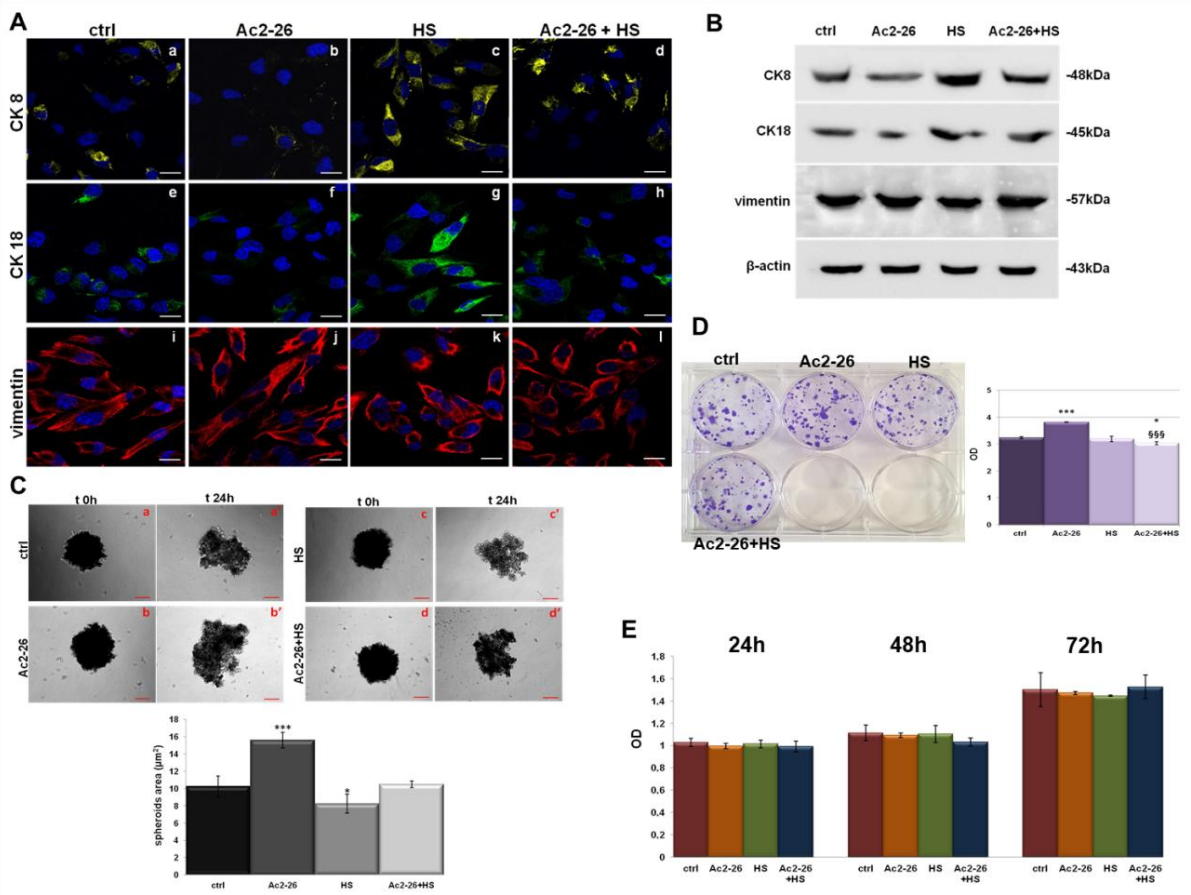

Figure 8.18 Analysis of HS effects on MIA PaCa-2 cell aggressiveness. (**A**) Confocal analysis on WT MIA PaCa-2 cells not treated and treated with HS 10 µg/ml and or Ac2- 26 1 µM for 24 hr for CK8 (panels a-d), CK18 (panels e-h) and vimentin (panels i-l). Magnification 63× 1.4NA. Bar = 10 µm. (**B**) Western blot on protein extract from MIA PaCa-2 cells analyzed for CK8, CK18, vimentin and β-actin, this latter used as housekeeping. The shown blots are representative of n = 3 experiments with similar results. (**C**) Spheroids grown in hanging methylcellulose drops for 7 days. Panels a-d refers to images taken immediately after seeding the spheroids in plate; panels a'-d' are related to treatments at 24 hr. Magnification 10×. Bar = 50 µm. Spheroids/aggregates area has been calculated. *p < 0.05 **p < 0.01. The shown results are representative of n = 3 independent experiments. (**D**) Representative images of the clonogenic assay performed on WT MIA PaCa-2 cells in presence or not of Ac2-26 (1 µM) and/or HS (10 µg/ml) for 24 hr. The histograms refers to the optical density (OD) obtained from 1% SDS dissolution and read to spectrophotometer. (**E**) Histogram reported the mean of n = 5 MTT analysis at 24, 48 and 72 hr on MIA PaCa-2 cells.

8.19 The Ac2-26-enhanced aggressive behavior of PANC-1 cells is reduced by HS

In order to amplify the knowledge about the *in vitro* HS action on PC activity, we have performed functional assays on PANC-1 cell line that have been described to express ANXA1 but to not secrete it [161]. First, we assessed the calcium mobilization in presence of Ac2-26 with or without HS. As found on MIA PaCa-2 cells, Ac2-26 confirmed its ability to promote the Ca^{2+} intracellular transition, this effect is notably reverted in presence of HS. Interestingly, when administered alone, HS presents no relevant action with respect to the not treated cells (Fig. 8.19A). The highly aggressive behavior of PANC-1 cells, similarly to MIA PaCa-2 ones, has been previously evaluated. Particularly, the main EMT markers like E-cadherin and vimentin have been used to show the pronounced mesenchymal phenotype of this cell line [161; 346]. Here, we used the immunofluorescence and western blot analysis of these proteins evaluating that Ac2-26 is responsible to stimulate the EMT features, proved by the decrease of the E-cadherin levels but the vimentin expression does not change s (Fig. 8.19D, western blot and panel b and f). Furthermore the confocal analysis highlights a cell fibroblast-like shape (Fig. 8.19D, panel f), typically associated to a mesenchymal phenotype. Even if we did not find any significant modification about migration and invasion processes induced by HS, this GAG seems able to cause a slight increase of E-cadherin and a more pronounced decrease of vimentin (Fig. 8.19D, panels c and g). Interestingly, it produces a rescue of Ac2-26 effects on the levels of both proteins which return very similar to not treated cells (Fig. 8.19D, panels d and h). Finally, as reported for MIA PaCa-2 cell line, Ac2-26 and HS induce no effects on proliferation at 24, 48 and 72 h, either as single treatment or in coadministration (Fig. 8.19E).

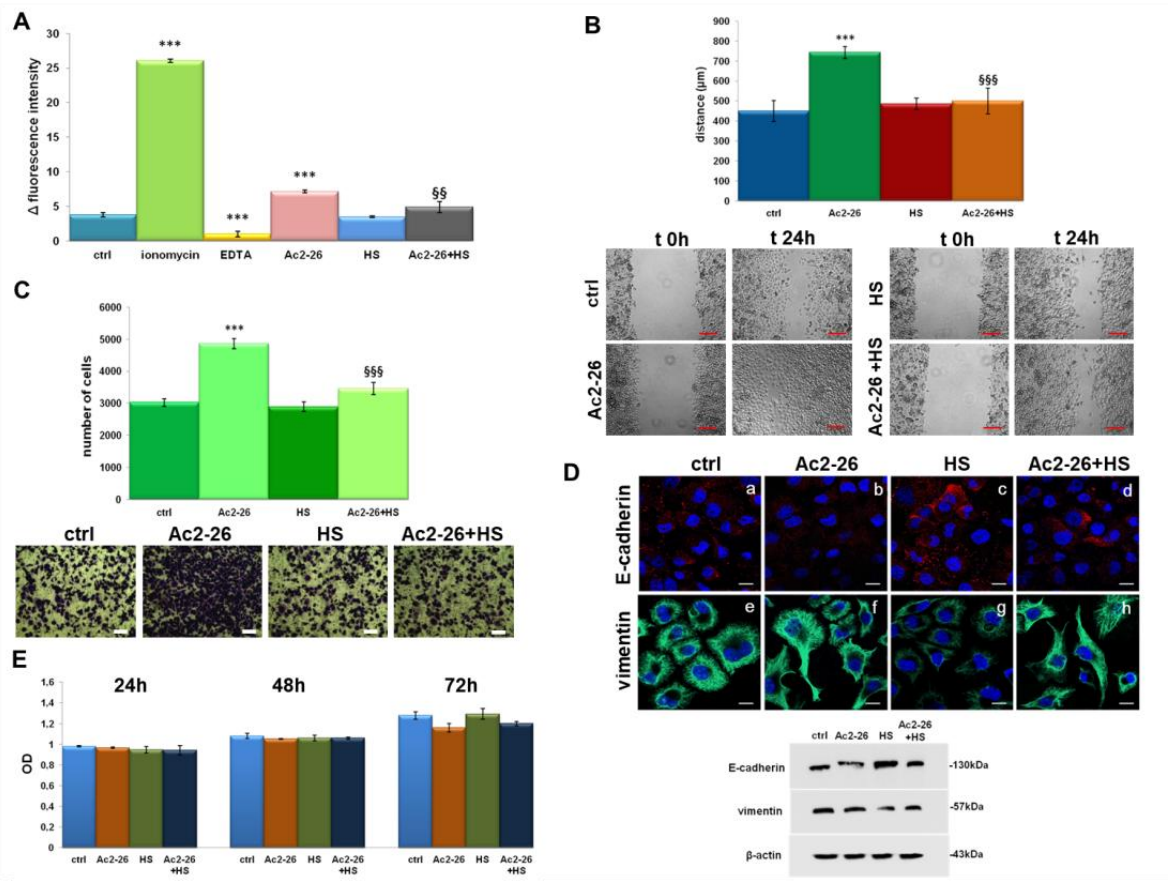

Figure 8.19 Investigation of the HS effects on PANC-1 cells behavior. Investigation of the HS effects on PANC-1 cells behavior. (A) Effects of ionomycin (1 mM), EDTA (15 mM), Ac2-26 (1 μM) with or without HS (10 μg/ml) on rise in intracellular Ca2+ in PANC-1 cells. The histogram shows the fluorescence increment related to calcium intracellular amount. Data are means ± SEM of n = 3 experiments with similar results. ***p < 0.001 versus not treated control; §§p < 0.01 versus Ac2-26. (B) Scratch wound healing assay on PANC-1 cells treated or not with Ac2-26 (1 μM) and/or HS (10 μg/ml). Representative bright field images captured by Time Lapse microscope (Leica AF-6000 LX; Leica Microsystems) of PANC-1 cells at 0 and 24 h from produced wounds. Magnification 10×. Bar = 100 μm. ***p < 0.001 versus untreated controls; §§§p < 0.001 versus Ac2-26 treated cells. The migration rate was determined by measuring the distances covered by individual cells from the initial time to the selected time points (bar of distance tool, Leica ASF software). The data are representative of n = 3 independent experiments ± SEM. (C) Results of the invasion assay on PANC-1 cells treated or not with Ac2-26 (1 μM) and/or HS (10 μg/ml). The data represent the sum of cells of 15 separate fields per well of n = 3 experiments. ***p < 0.001 versus untreated controls; §§§p < 0.001 versus Ac2-26 treated cells. Representative images of analyzed fields of the invasion assay. Magnification 20 × . Bar = 150 μm. (D) Confocal analysis on PANC-1 cells not treated and treated with HS 10 μg/ml and or Ac2-26 1 μM for 24 hr for E-cadherin (panels a-d) and vimentin (panels e-h). Magnification 63× 1.4NA. Bar = 10 μm. Western blot on protein extract from PANC-1 cells analyzed for E-cadherin, vimentin and β-actin, this latter used as housekeeping. The shown blots are representative of n = 3 experiments with similar results. (E) MTT analysis at 24, 48 and 72 h on PANC-1 cells treated or not with Ac2-26 (1 μM) and/or HS (10 μg/ml). The data derived from the mean of n = 5 experiments with similar results.

8.20 The activation of HUVEC cells, enhanced in presence of Ac2-26, is notably inhibited when the ANXA1 peptide is administered together with HS

The pro-angiogenic action of intra- and extracellular ANXA1 has been previously highlighted [347;348]. In this work, the study of angiogenesis started with the evaluation of HUVEC cell migration and invasion promoted by Ac2-26. In these two processes, as found for WT MIA PaCa-2 cells, HS did not have a significant action on cell speed but was able to revert the positive effect of ANXA1 mimetic peptide (Fig. 8.20A and B). Next, the tube formation assay revealed us that, even if HS alone did not interfere with the in vitro angiogenesis, it blocked the pro-angiogenic action of Ac2-26. Particularly, this result is highlighted by the images of capillary-like structures formed on matrigel coating by HUVEC cells and it is further corroborated by the analysis of the number of branching points and of the relative tube length calculated as reported in Material and methods section (Fig. 8.20C). As revealed for PC cells, also HUVEC proliferation appeared not affected by any treatment at 24, 48 and 72 hours (Fig. 8.20D).

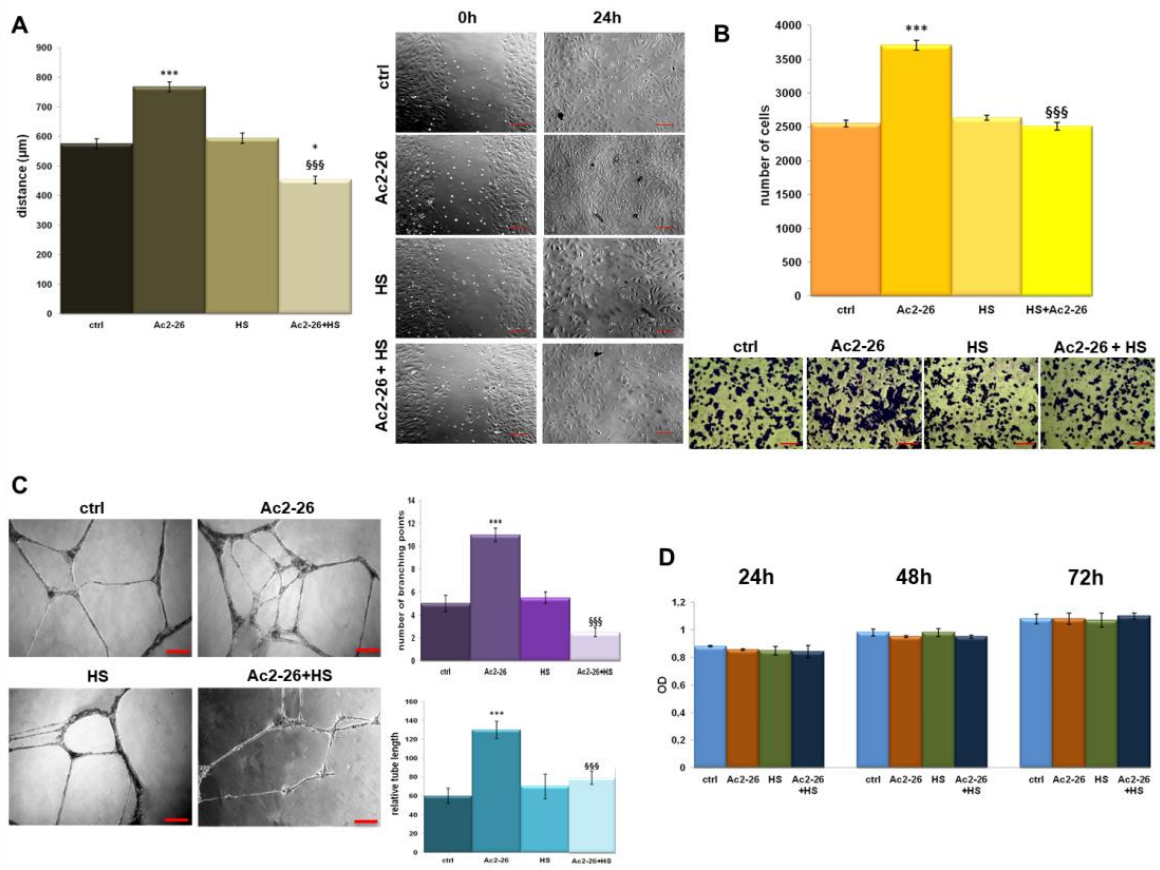

Figure 8.20 Analysis of migration/invasion rate and in vitro tube formation of endothelial cells with HS and Ac2-26. (**A**) Results from the scratch wound healing assay on HUVEC cells treated or not with Ac2-26 (1 µM) and/or HS (10 µg/ml). Representative bright field images captured by Time Lapse microscope (Leica AF-6000 LX; Leica Microsystems) of HUVEC cells at 0 and 24 hr from produced wounds. Magnification 10×. Bar = 100 µm. *p < 0.05; ***p < 0.001 versus untreated controls; §§§p < 0.001 versus Ac2-26 treated cells. The migration rate was determined by measuring the distances covered by individual cells from the initial time to the selected time points (bar of distance tool, Leica ASF software). The data are representative of n = 3 independent experiments ± SEM. (**B**) Results of the invasion assay on HUVEC cells treated or not with Ac2-26 (1 µM) and/or HS (10 µg/ml). The data represent the sum of cells of 15 separate fields per well of n = 3 experiments. ***p < 0.001 versus untreated controls; §§§p < 0.001 versus Ac2-26 treated cells. Representative images of analyzed fields of the invasion assay. Magnification 20×. Bar = 150 µm. (**C**) Analysis of tube length and number of branches calculated by ImageJ (Angiogenesis Analyzer tool) software on the same experimental points of scratch wound healing and invasion assays. The data represent a mean of n = 3 independent experiments ± SEM, ***p < 0.001 versus untreated control; §§p < 0.01; §§§p < 0.001 versus HS treated cells. Representative images of tube formation by HUVEC cells seeded for 12 hr on matrigel and EBM2 1:1. Bar = 100 µm. (**D**) MTT analysis at 24, 48 and 72 hr on HUVEC cells treated or not with Ac2-26 (1 µM) and/or HS (10 µg/ml). The data derived from the mean of n = 5 experiments with similar results.

8.21 HS blocks the interaction of ANXA1 with FPRs

As reported above, Ac2-26 induces Ca^{2+} release in WT MIA PaCa-2 cells. It is known that this effect is mediated by its interaction with FPRs [162; 219; 349]. Once assessed by cytofluorimetric assay that HS does not affect the expression of FPR-1 and FPR-2 isoforms on WT, ANXA1 KO MIA PaCa-2 and PANC-1 cells (Fig. 8.21A, C, D), we focused on the evaluation of the receptor activation. In this case, using fMLP as FPR agonist and Boc-1 as antagonist, we showed that Ac2-26 triggered the receptor activation on the three cell lines. Particularly, on these cells Boc-1 confirmed its ability to revert the effects of fMLP and Ac2-26. On the other hand, the decrease of fluorescent signal appeared evident only when HS has been added together with Ac2-26 and not with fMLP (Fig. 8.21B for WT MIA PaCa-2 cells, D for ANXA1 KO ones and F for PANC-1). This aspect underlines the specificity for HS to bind Ac2-26 and not fMLP. Furthermore, the effect of HS taken alone was significant with respect to not treated cells only on WT MIA PaCa-2 cells and not on ANXA1 KO clone and on PANC-1 cell line.

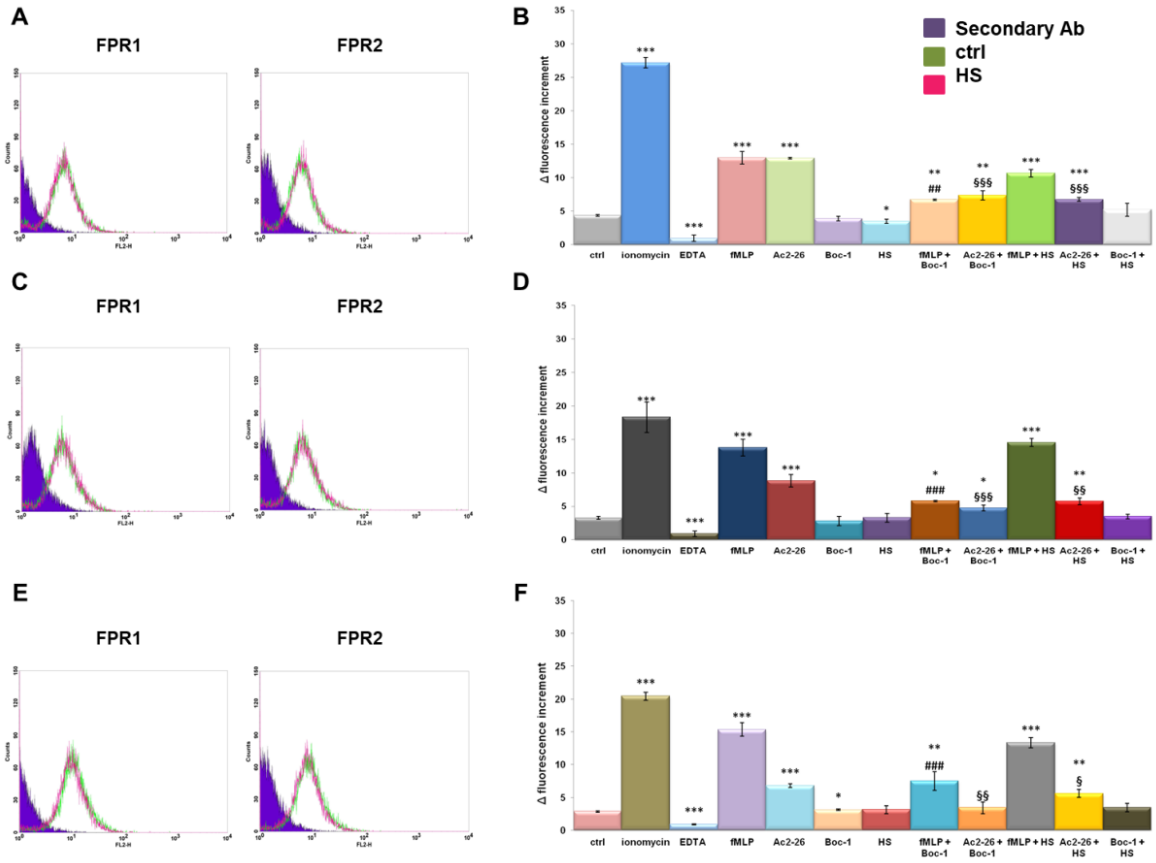

Figure 8.21 Evaluation of the effects of HS on Ac2-26 for Ca2+ mobilization. Cell surface expression of FPR-1 and FPR-2 in (**A**) WT, (**C**) ANXA1 KO MIA PaCa-2 and (**E**) PANC-1 cells was analyzed by flow cytometry. The violet areas in the plots are relative to secondary antibody alone. FPR-1 and FPR-2 signals are showed in green for ctrl and in pink for HS (10 µg/ml) treated cells for 48 h. The histograms obtained by Fluo-4 a.m. cytofluorimetric approach represent the effects of ionomycin (1 mM), EDTA (15 mM), fMLP (50 nM), Ac2-26 (1 µM), Boc-1 (100 µM), HS (10 µg/ml) on rise in intracellular Ca2+ in WT (**B**) and ANXA1 KO (**D**) MIA PaCa-2 and (**F**) PANC-1 cells. Data are means ± SEM of n = 3 experiments with similar results. *p < 0.05; **p < 0.01; ***p < 0.001 versus not treated control; ##p < 0.01; ###p < 0.001; §§p < 0.01 versus fMLP; §§§p < 0.001 versus Ac2-26. (For interpretation of the references to colour in this figure legend, the reader is referred to the web version of this article.)

9 Discussion

PC microenvironment strongly favors malignancy and plays a critical role in tumor progression [350], revealing a strong relationship between its organization, metastasis and chemoresistance. The tissue surrounding the PC cells consists of the same cancer cells and stromal ones, e.g. fibroblasts, endothelial cells, immune cells as lymphocytes and macrophages, and extracellular components, such as EVs, that sustain the primary tumor in autocrine and paracrine manner. EVs, enriched in exosomes, released by cancer cells are functional carriers necessary to guarantee cell-cell communication and their content can have strong effects on the recipient cells. Interesting evidences have demonstrated that in many models of cancer, including PC [164], exosomes contribute to tumor progression by the formation of pre-metastatic niches [351; 352]. This finding raised much interest and led many researchers to implement studies aiming to increase the knowledge of these structures. Among the most significant elements, ANXA1 was identified as one of the proteins associated with PC metastasis in multiple organs, mainly in liver [340]. In parallel, our previous works demonstrated that ANXA1, in its intracellular and extracellular forms, promotes PC progression respectively acting as a cytoskeletal remodeling factor and as an agonist of FPRs [161; 162]. Moreover, in our last work we have shown that ANXA1 is a key actor of EVs isolated from MIA PaCa-2 PC cells, revealing its importance in the production and/or secretion of these microvesicles [163].

In this study based on the fact that (i) the extracellular microvesicles have an important role in PC progression, (ii) ANXA1 is involved in the exosomes biogenesis and/or effects and (iii) the extracellular counterpart of this protein is able to trigger cell motility [161-163], we decided to investigate the *in vitro* action of ANXA1/EVs on fibroblasts and endothelial cells and macrophages as recipient stromal cells. The use of the ANXA1 KO MIA PaCa-2, compared to WT one, confirmed to be a good in vitro model to preliminarily describe the action of the protein of our interest on tumor microenvironment.

The different degree of fibroblasts activation depending on the presence of ANXA1 in PC deriving EVs was analyzed, showing their switch into myofibroblasts-like features, as highlighted by the induced cell motility, metalloproteinases action and increased expression of FAP1α and vinculin.

The interaction of the secreted form of ANXA1 with a FPR receptor partner family is known, as commonly observed in both physiological and pathological models [196]. This binding is able to trigger calcium mobilization, actin polymerization, adhesion, invasion and focused migration [161; 162; 349]. Therefore, we have used molecules such as fMLP and Ac2-26 as endogenous ligands and Boc-1 as antagonist to show the main biological events triggered by FPRs leading to a more aggressive cell phenotype. Once tested the expression and activation of the receptor isoforms 1 (FPR1) and 2 (FPR2) on both BJ and HUVEC cells, it has been possible to show the mechanism by which the EVs obtained from MIA PaCa-2 were able to bring about a significant variation in the recipient cell behavior, especially if containing ANXA1. These activities have been assessed in term of acquisition of a mesenchymal phenotype, which is essential for tumor metastasis [162; 353]. Fibroblasts are known to play an important role on cancer progression, not only in term of chemoresistance, as consistent physical block against chemotherapeutic agents, mainly because they can switch into CAFs mimicking the features of myofibroblasts [354-358]. This phenotype is generally represented by a well-organized rearrangement of cytoskeleton in a parallel cell orientation. In this study, the action of ANXA1 in EVs on FPRs was assessed by the inhibitory effect on the migratory and invasive speed in presence of the receptor pan-inhibitor Boc-1. Hence, this result demonstrates that Boc-1 is able to block the ANXA1 effects, as for the classical FPRs agonists, even if this protein is part of microvesicles. Moreover, these particular responses leading to a mesenchymal phenotype have also been examined by evaluating the increased expression of COL1A, FGF2, vinculin and FAP1α and the more structured orientation of vimentin and F-actin. On the other hand, the involvement of both ANXA1 and tumor-derived EVs as pro-angiogenic elements, already widely described in literature [359; 360] confirm the previously described

interaction of EVs-containing ANXA1 with FPRs [163]. In particularly, here we report the main biological changes triggering angiogenesis, such as cell functional migration and invasion and EndMT [359], a process evaluated by the increase of several protein markers such as VEGF, αSMA, FAP1α and fibronectin and the loss of plasma membrane localization of the adhesion molecule VE-cadherin. All these aspects have been modified in presence of Boc-1 more extensively in case of WT MIA PaCa-2 cells-deriving EVs as compared to ANXA1 KO cells, highlighting one more time the involvement of ANXA1 in EVs on FPRs, also on endothelial cells. In this study, we can say that an important issue was explained about the involvement of EVs as vehicle of ANXA1 externalization, which for a long time has been considered essential for disclosure of protein behavior [199]. On the other hand, until today the precise mechanism of interaction of ANXA1/EVs with target cells remains controversial. In this scenario, as suggested for other biological systems [196], we propose that the presence of ANXA1 on the external side of the membrane of vesicles allows these ones to directly interact with FPRs, triggering the activation of receptor-related downstream events. However, it is not still clear if the EVs are endocytosed by the receiving cells, as an alternative or even an additional mechanism, which will be investigated for the identification of ANXA1 as a potential target for therapy/prevention of PC dissemination. Furthermore, we could suggest that this FPR-dependent cascade is able to induce a positive loop, culminating in the increase of microvesicles production and release, which could favor tumor development.

Based on these findings, another important issue brought about is the involvement of tumor EVs in modulation of the immune response [361-363] influencing immune cells like macrophages. These latter are known as TAMs when associated to TME, mainly following switch into M2 phenotype, due to specific stimuli. Among these latter, the protein ANXA1 plays an important immunomodulatory role [364]. Thus, we have investigated the ANXA1 effect, as cargo of EVs, on THP-1 macrophages highlighting its extracellular role in regulating the macrophages polarization in M2 subpopulation rather than in M1. THP-1 are an immortalized cell line of human leukemic monocytes and represent a good model for studying monocyte/macrophage differentiation process

since strongly show up M0 / M1/ M2 features. Also in this case, we preferred to prove the action of externalized ANXA1 using both its single form, as Ac2-26, [196; 353] and as content of EVs. In this way, we could hypothesize that the ability of the protein to regulate macrophage behavior could be due to a paracrine action that the PC deriving secreted form of the protein is able to trigger. Interestingly, we found very similar results, about the acquisition of a more aggressive behavior. Indeed, the ANXA1 KO EVs are significantly less impacting about this action. These activities have been evaluated in terms of acquisition of a higher macrophages speed of migration, invasion and proliferation, all processes strongly involved in the formation of a TME particularly favorable for tumor progression [68-72; 162;]. Since we have previously demonstrated that the complex ANXA1/EVs is able to activate endothelial cells and fibroblasts *via* FPR, we hypothesized that ANXA1 could also affect the macrophages by activating its receptor FPR, as described in hepatocellular carcinoma where this protein is able to enhance the differentiation into M2 macrophages activating FPR2 and supports their expression of IL-10 [365]. In consideration of the crucial role of each single cellular TME component, we studied a three-ways cross-talk among PC cells and TAMs and endothelial cells/fibroblasts. This triple kind of interactions appeared to be notably mediated by ANXA1 which first induces macrophages polarization into M2 and then, this subpopulation in turn supports the other stromal cellular components also by secreting a series of factors. Among them, one important factor is just VEGF-A whose secretion by TAMs interestingly correlates to ANXA1 stimulus [365]. We have also associated this finding to the activation of endothelial cells within the TME, revealed through the induction of migration/invasion processes and mainly the *in vitro* formation of capillary-like structures. The significant effects of M2 supernatants, obtained in turn by the effects of Ac2-26 and WT EVs, rather than ANXA1 KO ones, suggests the strong action of this protein in the promotion of pro-tumor action by the endothelial cells in TME. On the other hand, CAFs are activated fibroblasts that arise in the TME and playing an important role on cancer progression [337; 354-357]. Moreover, Cho and colleagues have shown that CAFs can promote monocyte differentiation into pro-invasive TAMs by secreted factors as

GM-CSF and IL6 [366]. Instead, in this study, as for the endothelial cells, we have found that fibroblasts are importantly influenced by M2 macrophages effects as found through the evaluation of MMP-9 secretion, FAP1α expression, F-actin structures and migration/invasion processes suggesting, once again, and indirect role of ANXA1 [367]. Furthermore, *ex vivo* analysis on previously obtained tissue sections, specifically both pancreatic tumors and liver metastasis, were warranted to confirm the predominant M2 macrophage infiltration in both cases. In this way, we have confirmed how the presence of ANXA1 can markedly influence the differentiation and/or the recruitment of M2 macrophages into both primary tumor and metastasis.

Thus, this work contributes to add another important tile in the knowledge about the role of extracellular ANXA1 in PC progression [162; 163; 208; 280]. This specific action manifests in an autocrine way and also in a paracrine manner on endothelial cells, fibroblasts and macrophages. Moreover, we proved that this paracrine effect is further mediated by the macrophage TME subpopulation. Thus, ANXA1 has been revealed to directly induce M2, as pro-tumor, phenotype and, through these cells, indirectly promotes the activation of PC stroma. In the light of all these data, it is necessary to understand more the mechanisms operating in TME in order to define suitable PC therapies and overcome resistance. Therefore, crosstalk between different cells in the tumor microenvironment plays an important role in tumor growth and tumor-mediated immune suppression.

2D *in vitro* models are widely used for the study of cellular physiology and tumorigenesis Nevertheless, they retain many limits about specific investigation, as for the evaluation of response to pharmacological treatments, because of several undefined changes that cells, in monolayers, can acquire losing their original phenotypic and functional characteristics. These limiting features have been overcome by the establishment of *in vivo* systems which, in turn, possess important ethic obstacles and do not allow a factual predictive analysis of human tumor progression and therapies efficacy, especially about the evaluation of the influence of TME. In this scenario, it has become necessary the development of new experimental models reflecting in a superior way the *in vivo*

situation. The 3D co-culture systems show peculiar molecular characteristics that are closer to the structural architecture of the tumor *in vivo*. 3D cell models can accurately reproduce the tumor, the TME and mimic the regulatory mechanisms that exist between tumor and stroma; in particular these models are able to provide critical insight on interaction between tumoral cells, desmoplastic fibroblasts as well as with immune cells involved in cancer progression and therapy resistance. Currently they are used in several studies to identify the role of adhesion molecules in invasiveness/metastasis formation and angiogenesis, and for tissue remodeling analysis [314] and to study the penetration and action drugs. To establish 3D models, most studies focus on one or two cell lines to observe cell-cell interaction, but to achieve a more realistic *in vivo* situation, not only tumor cells and fibroblasts, but also immune cells have to be kept into account [324]. Fibroblasts and immune cells have been reported to play a key role in tumor initiation, progression and metastasis of PC and various strategies including immunotherapies are currently being tested [318; 325; 368]. In this regard, we have proved that ANXA1 affects the spheroid formation, because the WT cells have a greater ability to form this 3D model both in moculture and especially in co-culture with CAFs, if compared to ANXA1 KO ones. These data show that WT cells, thanks to the presence of ANXA1, are more prone to aggregation and interaction with other cellular components and that CAFs support spheroid formation and cell survival, in order to improve the formation of the dense stroma of the TME.

Moreover upon addition of monocytes to our 3D tumor cell/CAFs co-culture, we could not observe a direct effect on spheroid, so on tumor growth and survival. This data will lead us to analyze also in this case the effect of extracellular ANXA1 on monocytes phenotype and differentation, and cytokine profile of the co-cultures.

Generally, the extracellular form of ANXA1 has been detected in human sera in several conditions. In case of inflammation ANXA1 containing-EVs have proved to raise pro-repair and anti-inflammatory effects and to represent a diagnostic biomarker. Moreover, the prospect of ANXA1-containing nanoparticles to deliver therapeutic benefit has also been investigated [369].

Additionally, the identification of ANXA1 as circulating molecule in sera of cancer-affected patients has been considered as prognostic factor because of its correlation with clinicopathological conditions [370]. Therefore, as oncogenic factor, ANXA1 needs to be inhibited, mainly by blocking its extracellular form, as a new model of PC adjuvant therapy. Blocking its activity has been a fascinating research goal in recent years to confirm the biological role of ANXA1, but, surprisingly, despite the deep information about ANXA1 structure and performances in a broad variety of biological processes, from the inflammation to cancer, no inhibitor molecules have been already identified. The assessment of the interaction between ANXA1 and HS shown by Horlacher and colleagues [279] has been the starting point of our investigation focusing on the effects that this binding could have on the involvement of ANXA1 in PC and endothelial cells. Moreover, previous studies have reported that HS mimetics can affect tumor biological behavior by exerting pleiotropic effects through a specific mechanism of action based not only on heparanase inhibition, but also on the HS functions. We confirmed the direct association of HS with the full length protein using both DSF and SPR techniques. Interestingly, for the first time, SPR experiments also revealed a direct interaction between the GAG and the ANXA1 N-terminal mimetic peptide, Ac2-26, showing a concentration-dependent response. Our analysis established that this interaction results to be calcium-dependent presumably because of the implication that these ions have on protein folding [371] and for guaranteeing the electrostatic binding with the HS sulfate groups. The GAGs play an important role in tumor-stroma cross-talk during cancer development, transformation, growth, and metastasis [372; 373]. For example, in PC progression glypican-1 and syndecan-1 have been described to be involved in vesicle trafficking and stroma dysregulation [373-377]. On the other hand, HS as component of the ECM is largely known to interact with other elements of the extracellular environment such as growth factors and cytokines leading to numerous biological events, including pathological ones [378; 379]. The major part of information about HS in physiopathological events is related to the use of synthetic mimic molecules or mainly to the HSPGs. Thus, the use of HS as free molecule administered exogenously to the cells appears as an

uncommon expedient. Here, the *in vitro* tests have proven that the interaction ANXA1/HS affects the protein functions as oncogenic factor in PC development. Initially, by the administration of an exogenous free form of HS, we showed its significant inhibitory effects on the motility of WT MIA PaCa-2 cells, in contrast to the related and well characterized ANXA1 KO clone. This finding allowed us to assess the specificity of the HS action just on this protein. Furthermore, the administration of WT MIA PaCa-2 cells supernatant on the KO counterpart confirmed the pro-migratory and invasive effects of the endogenous extracellular ANXA1. The rescue induced by HS reveals the ability of this macromolecule to sequester the protein in the extracellular environment. Additionally, these effects are evident also on the Ac2-26 and not only limited to the cell motility but also regarding the main *in vitro* features of PC aggressiveness. In this context, we considered the ability of MIA PaCa-2 cells to retain and increase, in presence of Ac2-26, a significant mesenchymal phenotype confirmed by the lack of cytokeratins 8 and 18, by the well-organized vimentin cytoskeleton, and the formation of colonies and spheroids. Interestingly, HS is strongly capable to overall revert PC cell aggressive behavior by inhibiting ANXA1 peptide effects and also when administered alone, probably because of the interference with the endogenous ANXA1 secreted by cells, as stated above [161-163]. These *in vitro* analyses have been deepened using PANC-1 cells, as another human primary PC epithelial cell line. It is shown that these cells do not secrete ANXA1 [161]. Thus, the lack of significant effects of HS on all the examined processes can be reasonably explained by the absence of ANXA1 in the supernatants. Nevertheless, this GAG remarkably reverts what the ANXA1 mimetic peptide is able to induce about calcium mobilization, cell speed and EMT. HS critically regulates the formation endothelial tubes by playing a pro-angiogenic role. On the endothelial cell-surface, HS is described as responsible for facilitating various growth factors that in turn mediate endothelial growth signaling. Therefore, this “bank” of pro-angiogenic factors is represented by the polysaccharide conjugated with protein cores on cell membrane [380]. Surprisingly, when administered as free exogenous molecule on our *in vitro* model, HS does not affect the HUVEC cells motility and it reports no consequences on capillary

formation. Also in this case, the interference with the ANXA1 pro-angiogenic effects could be explained by the notably evident rescue of Ac2-26 action. Finally, the interference of calcium mobilization is one of the ANXA1 autocrine/paracrine effects which are inhibited by HS. Particularly, the ability of this GAG to block selectively Ac2-26 and not fMLP, both of them promoters of calcium release, confirms the specific affinity of HS for ANXA1 and its mimetic peptide. Furthermore, this capability explains the mechanism by which this binding is able to hinder the effects of extracellular ANXA1 by preventing the interaction of this protein with FPR, its well-known receptor partner. Taken together, these findings represent an appealing issue to further consideration. It is important to underline that GAGs can be characterized by diverse types of monomeric unit, linkages between each monomer, the position of sulfate groups, and the degree of sulfation, among the different classes [381]. However, inside the same class, the molecules can appear with different features: HS occurs naturally in all cells and varies enormously in terms of degree of sulfation and chain length, which depend on its biological origin. Thus, it would be interesting to characterize these features, which probably could influence the ANXA1/HS complex formation. In the first case, the number and the type of sulfation points could modify the electrostatic strength of the binding. On the other hand, the length of HS chains and the related different outcomes can be due to the heparanase, the enzyme known to cleave this polymer. These enzymes have been described to be involved in PC progression, since, as it appears also in other kind of solid tumors, the cleavage of the HS chains alters the structure and function of HSPG and gives an important contribution both to the remodeling of the ECM and of the molecules linked to the cellular surface. Heparanase can also indirectly contribute to neoangiogenesis by the loss of matrix integrity and the release and diffusion of pro-angiogenic molecules linked to the ECM [382; 383]. MIA PaCa-2 cells express high levels of heparanase which correlates with cell aggressive behavior [384]. Thus, it would be interesting to evaluate if the HS we added on PC and endothelial cells undergoes proteolytic cleavages, how this eventual action could interfere with the binding with ANXA1and to study the action that the complex ANXA1/HS can have *in vivo*. In conclusion,

targeting oncogenic factors is one of the most pursued strategies in the anti-cancer research. Here, we showed that the physical interaction between HS and ANXA1 is able to inhibit the effects of this protein on PC cells motility and maintenance of mesenchymal phenotype and on *in vitro* angiogenesis. Particularly, HS selectively prevents the activation of FPRs by the N-terminal mimetic ANXA1 peptide. These findings can represent a very appealing issue with an encouraging impact on the knowledge about the therapeutic approach in PC. Indeed, this study proposes to lay the basis for the creation of new synthetic molecules with an HS mimetic function playing the specific role of blocking ANXA1 and its pro-tumor effects. Therefore, ongoing clinical trial in phase I and II trials in combinational anti-cancer therapy with HS mimetics in metastatic PC, despite having given promising signs, yielded no significant effects in overall survival [385; 386].

Finally, we have proved that (i) the extracellular microvesicles have an important role in tumor-stroma comunication, mainly in PC progression and metastatis, (ii) extracellular ANXA1, via EVs, effects on the cellular counterpart of TME, activating fibroblats in myofibroblasts, inducing the EndMT for the endothelial cells and macrophage polarization into M2 subpopulation, (iii) this protein is able to induce spheroids formation. All these data make ANXA1 as a key mediator of PC bad behavior suggesting as this protein could become an interesting target to consider in diagnosis/prognosis phases and/or therapy ones.

Bibliography

1. Edlund H. Developmental biology of the pancreas. Diabetes. 2001; 50(1):S5-9.
2. Hepatobiliary and Pancreas Surgery Surgical Options for Biliary Injuries and Pancreas Disease. http://www.cpmc.org/advanced/liver/patients/topics/PP-hepatobiliary.html.
3. Hruban R.H, Pitman M.B, Klimstra D.S. Atlas of Tumor Pathology, Fourth Series, Fascicle Tumors of the pancreas. American Registry of Pathology, Washington, DC. 2007.
4. Bockman D.E. Anatomy of the Pancreas. The Pancreas: Biology, Pathobiology, and Disease, 1993, Raven Press Ltd.
5. Kern H.F. Fine Structure of the Human Exocrine Pancreas. The Pancreas: Biology, Pathobiology, and Disease, 1993, Raven Press Ltd.
6. Valentijn K, Valentijn J.A, Jamieson J.D. Role of actin in regulated exocytosis and compensatory membrane retrieval: insights from an old acquaintance. Biochem Biophys Res Commun. 1999; 266(3): 652-661.
7. Reichert M, Rustgi AK. Pancreatic ductal cells in development, regeneration, and neoplasia. J Clin Invest. 2011121(12):4572-8.
8. Daniel S. Longnecker. Anatomy and Histology of the Pancreas Pancreapedia: Exocrine Pancreas Knowledge Base. 2014; 10.3998/panc.2014.3.
9. Gorelick FS and Jamieson JD,. Physiology of the gastrointestinal tract. 2006. Elsevier Academic.
10. Lai KC, Cheng CH, Leung PS. The ghrelin system in acinar cells: localization, expression, and regulation in the exocrine pancreas. Pancreas. 2007; 35(3):e1-8.
11. Zimmermann B. Endocrine function of the pancreas. Blackwell Scientific publication. 1952; The Ryerson.
12. Korc M. Normal Function of the Endocrine Pancreas. The Pancreas: Biology, Pathobiology, and Disease, 1993, Raven Press Ltd.
13. Rutter GA, Pullen TJ, Hodson DJ, Martinez-Sanchez A. Pancreatic β-cell identity, glucose sensing and the control of insulin secretion. Biochem J. 2015; 466(2):203-18.
14. Madeb R, Koniaris LG, Schwartz SI. The discovery of insulin: the Rochester, New York, connection. Ann Intern Med. 2005; 143(12):907-12.
15. Nussey S, Whitehead S. Endocrinology: An Integrated Approach. BIOS Scientific Publishers. 2001
16. Brunton L L., Chabner B A., Knollmann B C. The Pharmacological Basis of Therapeutics, 2011. Goodman & Gilman's
17. McGuigan A, Kelly P, Turkington RC, Jones C, Coleman HG, McCain RS. Pancreatic cancer: A review of clinical diagnosis, epidemiology, treatment and outcomes. World J Gastroenterol. 2018; 24:4846–4861.
18. Siegel RL, Miller KD, Jemal A. 2015 Cancer statistics. CA Cancer J Clin. 201565(1):5-29.
19. Ferlay J, Soerjomataram I, Dikshit R, Eser S, Mathers C, Rebelo M, Parkin DM, Forman D, Bray F. Cancer incidence and mortality worldwide: sources, methods and major patterns in GLOBOCAN 2012. Int J Cancer. 2015; 136(5):E359-86.
20. Matsuoka L, Selby R, Genyk Y. The surgical management of pancreatic cancer. Gastroenterol Clin North Am. 2012; 41(1):211-21.
21. Fuchs CS, Colditz GA, Stampfer MJ, Giovannucci EL, Hunter DJ, Rimm EB, Willett WC, Speizer FE. A prospective study of cigarette smoking and the risk of pancreatic cancer. Arch Intern Med. 1996; 156(19):2255-60.
22. Pezzilli R, Pagano N. Is diabetes mellitus a risk factor for pancreatic cancer? World J Gastroenterol. 2013; 19(30):4861-6.
23. Michaud DS, Giovannucci E, Willett WC, Colditz GA, Stampfer MJ, Fuchs CS. Physical activity, obesity, height, and the risk of pancreatic cancer. JAMA. 2001; 286(8):921-9.

24. Olsen GW, Mandel JS, Gibson RW, Wattenberg LW, Schuman LM. A case-control study of pancreatic cancer and cigarettes, alcohol, coffee and diet. Am J Public Health. 1989; 79(8):1016-9
25. Nutritional aspects of the development of cancer. Report of the Working Group on Diet and Cancer of the Committee on Medical Aspects of Food and Nutrition Policy. Rep Health Soc Subj; 1998; 48:i-xiv, 1-274.
26. Tersmette AC, Petersen GM, Offerhaus GJ, Falatko FC, Brune KA, Goggins M, Rozenblum E, Wilentz RE, Yeo CJ, Cameron JL, Kern SE, Hruban RH. Increased risk of incident pancreatic cancer among firstdegree relatives of patients with familial pancreatic cancer. Clin Cancer Res. 2001; 7(3):738-44.
27. Weiss FU. Pancreatic cancer risk in hereditary pancreatitis. Front Physiol. 2014; 5:70.
28. Lynch HT, Smyrk T, Kern SE, Hruban RH, Lightdale CJ, Lemon SJ, Lynch JF, Fusaro LR, Fusaro RM, Ghadirian P. Familial pancreatic cancer: a review. Semin Oncol. 1996; 23(2):251-75.
29. Hidalgo M. Pancreatic cancer. N Engl J Med. 2010; 362(17):1605-17
30. Chang MC, Wong JM, Chang YT. Screening and early detection of pancreatic cancer in high risk population. World J Gastroenterol. 2014; 20:2358–2364.
31. Ghiorzo P. Genetic predisposition to pancreatic cancer. World J Gastroenterol. 2014; 20:10778–10789.
32. Bond-Smith G, Banga N, Hammond TM, Imber CJ. Pancreatic adenocarcinoma. BMJ. 2012; 344:e2476.
33. Loc WS, Smith JP, Matters G, Kester M, Adair JH. Novel strategies for managing pancreatic cancer. World J Gastroenterol. 2014; 20(40):14717-25.
34. Reynolds R B, & Folloder J. Clinical Management of Pancreatic Cancer. J Adv Pract Oncol. 2014; 5(5): 356–364.
35. Strobel O, Dor Y, Alsina J, Stirman A, Lauwers G, Trainor A, Castillo CF, Warshaw AL, Thayer SP. In vivo lineage tracing defines the role of acinar-to-ductal transdifferentiation in inflammatory ductal metaplasia. Gastroenterology. 2007; 133(6):1999-2009.
36. Means AL, Meszoely IM, Suzuki K, Miyamoto Y, Rustgi AK, Coffey RJ Jr, Wright CV, Stoffers DA, Leach SD. Pancreatic epithelial plasticity mediated by acinar cell transdifferentiation and generation of nestin-positive intermediates. Development. 2005; 132(16):3767-76.
37. Zhu L, Shi G, Schmidt CM, Hruban RH, Konieczny SF. Acinar cells contribute to the molecular heterogeneity of pancreatic intraepithelial neoplasia. Am J Pathol. 2007; 171(1):263-73.
38. Miyamoto Y, Maitra A, Ghosh B, Zechner U, Argani P, IacobuzioDonahue CA, Sriuranpong V, Iso T, Meszoely IM, Wolfe MS, Hruban RH, Ball DW, Schmid RM, Leach SD. Notch mediates TGF alpha-induced changes in epithelial differentiation during pancreatic tumorigenesis. Cancer Cell. 2003; 3(6):565-76.
39. Jones S, Zhang X, Parsons DW, et al. Core signaling pathways in human pancreatic cancers revealed by global genomic analyses. Science. 2008; 321:1801–06.
40. Rozenblum E, Schutte M, Goggins M, Hahn S A, Panzer S, Zahurak M, Goodman S N, Sohn T A, Hruban R H, Yeo C J, Kern S E. Tumor-suppressive pathways in pancreatic carcinoma. Cancer Res. 1997; 57:1731–34.
41. van Heek NT, Meeker AK, Kern SE, Charles J Yeo, Lillemoe K D, Cameron J L, Offerhaus G J A, Hicks J L, Wilentz R E, Goggins M G, De Marzo A M, Hruban R H, Maitra A. Telomere shortening is nearly universal in pancreatic intraepithelial neoplasia. Am J Pathol. 2002;161:1541–47.
42. Hong SM, Heaphy CM, Shi C, et al. Telomeres are shortened in acinar-to-ductal metaplasia lesions associated with pancreatic intraepithelial neoplasia but not in isolated acinar-to-ductal metaplasias. Mod Pathol. 2010; 24(2):256-66.
43. Hruban RH, Goggins M, Parsons J, Kern SE. Progression model for pancreatic cancer. Clin Cancer Res. 2000; 6:2969–72.
44. Hruban RH, Maitra A, Goggins M. Update on pancreatic intraepithelial neoplasia. Int J Clin Exp Pathol. 2008; 1:306–16.

45. Jones S, Zhang X, Parsons DW, et al. Core signaling pathways in human pancreatic cancers revealed by global genomic analyses. Science. 2008; 321:1801–06
46. Carter H, Samayoa J, Hruban RH, Karchin R. Prioritization of driver mutations in pancreatic cancer using cancer-specific high-throughput annotation of somatic mutations (CHASM) Cancer Biol Ther. 2010; 10:582–87.
47. Hingorani SR, Wang LF, Multani AS, et al. Trp53(R172H) and KraS(G12D) cooperate to promote chromosomal instability and widely metastatic pancreatic ductal adenocarcinoma in mice. Cancer Cell. 2005; 7:469–83.
48. Omura N, Goggins M. Epigenetics and epigenetic alterations in pancreatic cancer. Int J Clin Exp Pathol. 2009; 2:310–26.
49. Schutte M, Hruban RH, Geradts J, et al. Abrogation of the Rb/p16 tumor-suppressive pathway in virtually all pancreatic carcinomas. Cancer Res. 1997; 57:3126–30.
50. Sato N, Matsubayashi H, Abe T, Fukushima N, Goggins M. Epigenetic down-regulation of CDKN1C/p57KIP2 in pancreatic ductal neoplasms identified by gene expression profiling. Clin Cancer Res. 2005; 11:4681–88.
51. Sato N, Fukushima N, Hruban RH, Goggins M. CpG island methylation profile of pancreatic intraepithelial neoplasia. Mod Pathol. 2008; 21:238–44.
52. Sato N, Fukushima N, Maitra A, et al. Discovery of novel targets for aberrant methylation in pancreatic carcinoma using high-throughput microarrays. Cancer Res. 2003; 63:3735–42.
53. Sato N, Fukushima N, Chang R, Matsubayashi H, Goggins M. Differential and epigenetic gene expression profiling identifies frequent disruption of the RELN pathway in pancreatic cancers. Gastroenterology. 2006; 130:548–65.
54. Sato N, Fukushima N, Maehara N, et al. SPARC/osteonectin is a frequent target for aberrant methylation in pancreatic adenocarcinoma and a mediator of tumor-stromal interactions. Oncogene. 2003; 22:5021–30.
55. Parsi MA, Li A, Li CP, Goggins M. DNA methylation alterations in endoscopic retrograde cholangiopancreatography brush samples of patients with suspected pancreaticobiliary disease. Clin Gastroenterol Hepatol. 2008; 6:1270–78.
56. Sato N, Maitra A, Fukushima N, et al. Frequent hypomethylation of multiple genes overexpressed in pancreatic ductal adenocarcinoma. Cancer Res. 2003; 63:4158–66.
57. Vincent A, Ducourouble MP, Van Seuningen I. Epigenetic regulation of the human mucin gene MUC4 in epithelial cancer cell lines involves both DNA methylation and histone modifications mediated by DNA methyltransferases and histone deacetylases. FASEB J. 2008; 22:3035–45.
58. Matsubayashi H, Canto M, Sato N, et al. DNA methylation alterations in the pancreatic juice of patients with suspected pancreatic disease. Cancer Res. 2006; 66:1208–17.
59. Szafranska AE, Doleshal M, Edmunds HS, et al. Analysis of microRNAs in pancreatic fine-needle aspirates can classify benign and malignant tissues. Clin Chem. 2008; 54:1716–24.
60. Li A, Omura N, Hong SM, et al. Pancreatic cancers epigenetically silence SIP1 and hypomethylate and overexpress miR-200a/200b in association with elevated circulating miR-200a and miR-200b levels. Cancer Res. 2010; 70:5226–37.
61. Bloomston M, Frankel WL, Petrocca F, et al. MicroRNA expression patterns to differentiate pancreatic adenocarcinoma from normal pancreas and chronic pancreatitis. JAMA. 2007; 297:1901–08.
62. Kent OA, Mullendore M, Wentzel EA, et al. A resource for analysis of microRNA expression and function in pancreatic ductal adenocarcinoma cells. Cancer Biol Ther. 2009; 8:2013–24.
63. Hussain, Z.; Nigri, J.; Tomasini, R. The Cellular and Biological Impact of Extracellular Vesicles in Pancreatic Cancer. Cancers. 2021; 13, 3040.
64. Ren, B.; Cui, M.; Yang, G.; Wang, H.; Feng, M.; You, L.; Zhao, Y. Tumor microenvironment participates in metastasis of pancreatic cancer. Mol Cancer. 2018, 17:108,

65. Nielsen MF, Mortensen MB, Detlefsen S. Key players in pancreatic cancer-stroma interaction: Cancer-associated fibroblasts, endothelial and inflammatory cells. World J Gastroenterol. 2016; 22: 2678-700
66. Feig, C., Gopinathan, A., Neesse, A., Chan, D. S., Cook, N., and Tuveson, D. A. The Pancreas Cancer Microenvironment. Clin. Cancer Res. 2012. 18, 4266–4276.
67. Zhang, Z., Ji, S., Zhang, B., Liu, J., Qin, Y., Xu, J., et al. Role of Angiogenesis in Pancreatic Cancer Biology and Therapy. Biomed. Pharmacother. 2018. 108, 1135–1140.
68. Tarique, A.A.; Logan, J.; Thomas, E.; Holt, P.G.; Sly, P.D.; Fantino, E. Phenotypic, functional, and plasticity features of classical and alternatively activated human macrophages. Am J Respir Cell Mol Biol. 2015; 53:676–688.
69. Di Caro, G.; Cortese, N; Castino, G. F.; Grizzi, F.; Gavazzi, F.; Ridolfi, C.; Capretti, G.; Mineri, R.; Todoric, J.; Zerbi, A.; Allavena, P.; Mantovani, A.; Marchesi, F. Dual prognostic significance of tumour-associated macrophages in human pancreatic adenocarcinoma treated or untreated with chemotherapy. Gut. 2016; 65(10):1710-20.
70. Helm, O.; Held-Feindt, J.; Schäfer, H., Sebens S. M1 and M2: there is no "good" and "bad"- How macrophages promote malignancy-associated features in tumorigenesis. Oncoimmunology. 2014; 3:e946818.
71. Lankadasari M.B., Mukhopadhyay P., Mohammed S., Harikumar K.B. TAMing pancreatic cancer: combat with a double edged sword. Mol Cancer. 2019; 18(1):48.
72. Ye H; Zhou Q; Zheng S; Li G; Lin Q; Wei L; Fu Z; Zhang B; Liu Y; Li Z; Chen R. Tumor-associated macrophages promote progression and the Warburg effect via CCL18/NF-kB/VCAM-1 pathway in pancreatic ductal adenocarcinoma. Cell Death Dis. 2018; 9:453.
73. Hu H; Hang JJ; Han T; Zhuo M; Jiao F; Wang LW. The M2 phenotype of tumor-associated macrophages in the stroma confers a poor prognosis in pancreatic cancer. Tumour Biol. 2016; 37:8657–8664.
74. Buchholz, S. M., Goetze, R. G., Singh, S. K., Ammer-Herrmenau, C., Richards, F. M., Jodrell, D. I., et al. Depletion of Macrophages Improves Therapeutic Response to Gemcitabine in Murine Pancreas Cancer. Cancers. 2020. 12, 1978.
75. Candido, J. B., Morton, J. P., Bailey, P., Campbell, A. D., Karim, S. A., Jamieson, T., et al. CSF1R+ Macrophages Sustain Pancreatic Tumor Growth through T Cell Suppression and Maintenance of Key Gene Programs that Define the Squamous Subtype. Cel Rep. 2018. 23, 1448–1460.
76. 93. Ge L, Pan B, Song F, et al. Comparing the diagnostic accuracy of five common tumour biomarkers and CA19-9 for pancreatic cancer: a protocol for a network meta-analysis of diagnostic test accuracy. BMJ Open. 2017;7(12):e018175
77. Steele CW, Jamieson NB, Evans TR, et al. Exploiting inflammation for therapeutic gain in pancreatic cancer. Br J Cancer. 2013;108(5):997–1003.
78. Cicenas J, Kvederaviciute K, Meskinyte I, et al. KRAS, TP53, CDKN2A, SMAD4, BRCA1, and BRCA2 mutations in pancreatic cancer. Cancers. 2017; 9(5):42
79. Gemmel C, Eickhoff A, Helmstadter L, Riemann JF. Pancreatic cancer screening: state of the art. Expert Rev Gastroenterol Hepatol. 2009;3(1):89–96.
80. Kamisawa T, Wood LD, Itoi T, Takaori K. Pancreatic cancer. Lancet. 2016;388(10039):73–85.
81. Lee B, Gibbs P. Inflammation, biomarkers and immuno-oncology pathways in pancreatic cancer. J Pers Med. 2019;9(2): 20.
82. Daamen LA, Vincent PG, Hanne DH, et al. Systematic review on the role of serum tumor markers in the detection of recurrent pancreatic cancer. HPB (Oxford). 2018;20(4):297–304.
83. Shen L, Yun Q, Weigen W, et al. B7-H4 is a prognostic biomarker for poor survival in patients with pancreatic cancer. Hum Pathol. 2017;66:79–85.
84. Feng L, Qi Q, Peng W, et al. Serum levels of IL-6, IL-8, and IL-10 are indicators of prognosis in pancreatic cancer. J Int Med Res. 2018;46(12):5228–5236.

85. Hufnagl C, Leisch M, Weiss L, et al. Evaluation of circulating cell-free DNA as a molecular monitoring tool in patients with metastatic cancer. Oncol Lett. 2020;19(2):1551–1558.
86. He J, Page AJ, Weiss M, et al. Management of borderline and locally advanced pancreatic cancer: where do we stand? World J Gastroenterol. 2014;20(9):2255–2266.
87. Seufferlein T, Hammel P, Delpero JR, et al. Optimizing the management of locally advanced pancreatic cancer with a focus on induction chemotherapy: expert opinion based on a review of current evidence. Cancer Treat Rev. 2019;77:1–10.
88. Benakis C, Brea D, Caballero S, et al. Commensal microbiota affects ischemic stroke outcome by regulating intestinal gammadelta T cells. Nat Med. 2016;22(5):516–523.
89. Schulz MD, Atay Ç, Heringer J, et al. High-fat-diet-mediated dysbiosis promotes intestinal carcinogenesis independently of obesity. Nature. 2014;514(7523):508–512.
90. Kamisawa T, Wood LD, Itoi T, Takaori K. Pancreatic cancer. Lancet. 2016;388(10039):73–85.
91. Goodenough DA, Paul DL. Gap junctions. Cold Spring Harb Perspect Biol. 2009. 1: 1-19.
92. Lucas WJ, Yoo BC, Kragler F. RNAas a long-distance information macromolecule in plants. Nat. Rev. Mol. Cell Biol. 2001; 2: 849-857.
93. Levine SJ. Mechanisms of soluble cytokine re- ceptor generation. J Immunol. 2004. 173: 5343- 5348.
94. Albi E, Viola Magni MP. The role of intranuclear lipids. Biol Cell. 96: 657-667. 2004.
95. Taback B, Hoon DS. Circulating nucleic acids and proteomics of plasma/serum: clinical utility. Ann N Y Acad. Sci. 2004. 1022: 1-8.
96. R. Nieuwland and A. Sturk, 'Why do cells release vesicles?', Thrombosis Research, vol. 125, no. SUPPL. 1. Pergamon. 2010; S49–S51.
97. Turturici G, Tinnirello R, Sconzo G, Geraci F. Extracellular membrane vesicles as a mechanism of cell-to-cell communication: advantages and disadvantages. Am. Physiol Cell Physiol. 2014. 306: 621-633..
98. E. van der Pol, A. N. Böing, P. Harrison, A. Sturk, and R. Nieuwland, 'Classification, functions, and clinical relevance of extracellular vesicles', Pharmacol. Rev. 2012; vol. 64, no. 3, pp. 676–705.
99. B. Li, M. A. Antonyak, J. Zhang, and R. A. Cerione, 'RhoA triggers a specific signaling pathway that generates transforming microvesicles in cancer cells', Oncogene. 2012; vol. 31, no. 45, pp. 4740–4749.
100. L. Ma et al., 'Discovery of the migrasome, an organelle mediating release of cytoplasmic contents during cell migration', Cell Res. 2015; vol. 25, no. 1, pp. 24–38.
101. J. Kowal et al., 'Proteomic comparison defines novel markers to characterize heterogeneous populations of extracellular vesicle subtypes', Proc. Natl. Acad. Sci. U. S. A. 2016; vol. 113, no. 8, pp. E968–E977.
102. Cocucci E, Racchetti G, Meldolesi J. Shedding microvesicles: artefacts no more. Trends Cell Biol. 2009; 19: 43-51.
103. A. Piccin, W. G. Murphy, and O. P. Smith, 'Circulating microparticles: pathophysiology and clinical implications', Blood Rev. 2007; vol. 21, no. 3, pp. 157–171,
104. Baj-Krzyworzeka M, Szatanek R, Weglarczyk K, Baran J, Urbanowicz B, Brański P, Ratajczak MZ, Zembala M. Tumour-derived microvesicles carry several surface determinants and mRNA of tumour cells and transfer some of these determinants to monocytes. Cancer Immunol Immunother 2006; 55: 808-18.
105. Pilzer D, Gasser O, Moskovich O, Schifferli JA, Fishelson Z. Emission of membrane vesicles: roles in complement resistance, immunity and cancer. Springer Semin Immunopathol. 2005. 27: 375-387.
106. Sidhu SS, Mengistab AT, Tauscher AN, LaVail J, Basbaum C. The microvesicle as a vehicle for EMMPRIN in tumor-stromal interactions. Oncogene. 2004. 23: 956-963.
107. M. Colombo, G. Raposo, and C. Théry, 'Biogenesis, Secretion, and Intercellular Interactions

of Exosomes and Other Extracellular Vesicles', Annu. Rev. Cell Dev. Biol. 2014; vol. 30, pp. 255–289.
108. W. M. Henne, N. J. Buchkovich, and S. D. Emr, 'The ESCRT Pathway', Developmental Cell. 2011; vol. 21, no. 1. pp. 77–91.
109. D. J. Gill et al., 'Structural insight into the ESCRT-I/-II link and its role in MVB trafficking', EMBO J. 2007; vol. 26, no. 2, pp. 600–612.
110. S. Ghazi-Tabatabai et al., 'Structure and Disassembly of Filaments Formed by the ESCRT-III Subunit Vps24', Structure. 2008; vol. 16, no. 9, pp. 1345–1356.
111. M. F. Baietti et al., 'Syndecan-syntenin-ALIX regulates the biogenesis of exosomes', Nat. Cell Biol. 2012; vol. 14, no. 7, pp. 677–685.
112. S. Stuffers, C. Sem Wegner, H. Stenmark, and A. Brech, 'Multivesicular Endosome Biogenesis in the Absence of ESCRTs', Traffic. 2009; vol. 10, no. 7, pp. 925–937.
113. K. Trajkovic et al., 'Ceramide triggers budding of exosome vesicles into multivesicular endosomes', Science. 2008; vol. 319, no. 5867, pp. 1244–1247.
114. D. Perez-Hernandez et al., 'The intracellular interactome of tetraspanin-enriched microdomains reveals their function as sorting machineries toward exosomes', J. Biol. Chem. 2013; vol. 288, no. 17, pp. 11649–11661.
115. A. Chairoungdua, D. L. Smith, P. Pochard, M. Hull, and M. J. Caplan, 'Exosome release of β-catenin: A novel mechanism that antagonizes Wnt signaling', J. Cell Biol. 2010; vol. 190, no. 6, pp. 1079–1091.
116. S. Charrin, S. Jouannet, C. Boucheix, and E. Rubinstein, 'Tetraspanins at a glance', J. Cell Sci. 2014; vol. 127, no. 17, pp. 3641–3648.
117. R. E. McConnell, J. N. Higginbotham, D. A. Shifrin, D. L. Tabb, R. J. Coffey, and M. J. Tyska, 'The enterocyte microvillus is a vesicle-generating organelle', J. Cell Biol. 2009; vol. 185, no. 7, pp. 1285–1298.
118. M. Ostrowski et al., 'Rab27a and Rab27b control different steps of the exosome secretion pathway', Nat. Cell Biol. 2010; vol. 12, no. 1, pp. 19–30.
119. C. Hsu et al., 'Regulation of exosome secretion by Rab35 and its GTPase-activating proteins TBC1D10A-C', J. Cell Biol. 2010; vol. 189, no. 2, pp. 223–232.
120. A. Savina, M. Vidal, and M. I. Colombo, 'The exosome pathway in K562 cells is regulated by Rab11', J. Cell Sci. 2002; vol. 115, no. 12, pp. 2505–2515.
121. S. R. Pfeffer, 'Unsolved Mysteries in Membrane Traffic', Annu. Rev. Biochem. 2007; vol. 76, no. 1, pp. 629–645.
122. N. P. Hessvik and A. Llorente, 'Current knowledge on exosome biogenesis and release', Cellular and Molecular Life Sciences. 2018; vol. 75, no. 2. Birkhauser Verlag AG, pp. 193–208.
123. J.-M. Pasquet, J. Dachary-Prigent, and A. T. Nurden, 'Calcium Influx is a Determining Factor of Calpain Activation and Microparticle Formation in Platelets', Eur. J. Biochem. 1996; vol. 239, no. 3, pp. 647–654.
124. Z. Andreu and M. Yáñez-Mó, 'Tetraspanins in extracellular vesicle formation and function', Front. Immunol. 2014; vol. 5, no. SEP.
125. C. Théry et al., 'Proteomic Analysis of Dendritic Cell-Derived Exosomes: A Secreted Subcellular Compartment Distinct from Apoptotic Vesicles', J. Immunol., 2001; vol. 166, no. 12, pp. 7309–7318.
126. G. Palmisano et al., 'Characterization of membrane-shed microvesicles from cytokine-stimulated β-cells using proteomics strategies', Mol. Cell. Proteomics, 2012; vol. 11, no. 8, pp. 230–243.
127. A. Sinha, V. Ignatchenko, A. Ignatchenko, S. Mejia-Guerrero, and T. Kislinger, 'In-depth proteomic analyses of ovarian cancer cell line exosomes reveals differential enrichment of functional categories compared to the NCI 60 proteome', Biochem. Biophys. Res. Commun. 2014; vol. 445, no. 4, pp. 694–701.
128. M. Shimoda and R. Khokha, 'Proteolytic factors in exosomes', Proteomics. 2013; vol. 13,

no. 10–11, pp. 1624–1636, .
129. K. Laulagnier et al., ‘Mast cell- and dendritic cell-derived display a specific lipid composition and an unusual membrane organization’, Biochem. J., 2004; vol. 380, no. 1, pp. 161–171.
130. X. Huang et al., ‘Characterization of human plasma-derived exosomal RNAs by deep sequencing’, BMC Genomics, 2013; vol. 14, no. 1, p. 319.
131. M. Mittelbrunn et al., ‘Unidirectional transfer of microRNA-loaded exosomes from T cells to antigen-presenting cells’, Nat. Commun., 2011; vol. 2, no. 1, p. 282.
132. J. S. Redzic, L. Balaj, K. E. van der Vos, and X. O. Breakefield, ‘Extracellular RNA mediates and marks cancer progression’, Seminars in Cancer Biology. 2014; vol. 28. pp. 14–23, ,
133. B. K. Thakur et al., ‘Double-stranded DNA in exosomes: A novel biomarker in cancer detection’, Cell Research, 2014; vol. 24, no. 6. pp. 766–769.
134. A. Hoshino et al., ‘Tumour exosome integrins determine organotropic metastasis’, Nature, 2015; vol. 527, no. 7578, pp. 329–335.
135. H. Valadi, K. Ekström, A. Bossios, M. Sjöstrand, J. J. Lee, and J. O. Lötvall, ‘Exosome-mediated transfer of mRNAs and microRNAs is a novel mechanism of genetic exchange between cells’, Nat. Cell Biol., 2007; vol. 9, no. 6, pp. 654–659.
136. H. C. Christianson, K. J. Svensson, T. H. Van Kuppevelt, J. P. Li, and M. Belting, ‘Cancer cell exosomes depend on cell-surface heparan sulfate proteoglycans for their internalization and functional activity’, Proc. Natl. Acad. Sci. U. S. A. 2013; vol. 110, no. 43, pp. 17380–17385.
137. K. J. Svensson et al., ‘Exosome uptake depends on ERK1/2-heat shock protein 27 signaling and lipid raft-mediated endocytosis negatively regulated by caveolin-1’, J. Biol. Chem. 2013; vol. 288, no. 24, pp. 17713–17724.
138. S. Rana, S. Yue, D. Stadel, and M. Zöller, ‘Toward tailored exosomes: The exosomal tetraspanin web contributes to target cell selection’, Int. J. Biochem. Cell Biol. 2012; vol. 44, no. 9, pp. 1574–1584.
139. A. E. Morelli et al., ‘Endocytosis, intracellular sorting, and processing of exosomes by dendritic cells’, Blood, . 2004; vol. 104, no. 10, pp. 3257–3266.
140. I. Parolini et al., ‘Microenvironmental pH is a key factor for exosome traffic in tumor cells’, J. Biol. Chem. 2009; vol. 284, no. 49, pp. 34211–34222.
141. C. Escrevente, S. Keller, P. Altevogt, and J. Costa, ‘Interaction and uptake of exosomes by ovarian cancer cells’, BMC Cancer. 2011; vol. 11, p. 108.
142. A. Montecalvo et al., ‘Mechanism of transfer of functional microRNAs between mouse dendritic cells via exosomes’, Blood, 2012; vol. 119, no. 3, pp. 756–766.
143. D. Feng et al., ‘Cellular Internalization of Exosomes Occurs Through Phagocytosis’, Traffic, 2010; vol. 11, no. 5, pp. 675–687.
144. A. Nanbo, E. Kawanishi, R. Yoshida, and H. Yoshiyama, ‘Exosomes Derived from Epstein-Barr Virus-Infected Cells Are Internalized via Caveola-Dependent Endocytosis and Promote Phenotypic Modulation in Target Cells’, J. Virol. 2013; vol. 87, no. 18, pp. 10334–10347.
145. M. C. Kerr and R. D. Teasdale, ‘Defining Macropinocytosis’, Traffic 2009; vol. 10, no. 4, pp. 364–371.
146. D. Fitzner et al., ‘Selective transfer of exosomes from oligodendrocytes to microglia by macropinocytosis’, J. Cell Sci. 2011; vol. 124, no. 3, pp. 447–458.
147. N. Izquierdo-Useros et al., ‘Capture and transfer of HIV-1 particles by mature dendritic cells converges with the exosome-dissemination pathway’, Blood. 2009; vol. 113, no. 12, pp. 2732–2741.
148. R. B. Koumangoye, A. M. Sakwe, J. S. Goodwin, T. Patel, and J. Ochieng, ‘Detachment of breast tumor cells induces rapid secretion of exosomes which subsequently mediate cellular adhesion and spreading’, PLoS One, 2011; vol. 6, no. 9.
149. Nieuwland R, Sturk A. Why do cells release vesicles? Thromb Res. 2010.125: S49-51.
150. Sims PJ, Faioni EM, Wiedmer T, Shattil SJ. Complement proteins C5b-9 cause release of

membrane vesicles from the platelet surface that are enriched in the membrane 131 receptor for coagulation factor Va and express prothrombinase activity. J Biol Chem. 1988. 263: 18205–18212.
151. Dolo V, Ginestra A, Cassarà D, Violini S, Lucania G, Torrisi MR, Nagase H, Canevari S, Pavan A, Vittorelli ML. Selective localization of matrix metalloproteinase 9, beta1 integrins, and human lymphocyte antigen class I molecules on membrane vesicles shed by 8701-BC breast carcinoma cells. Cancer Res. 1998. 58: 4468-4474.
152. Ginestra A, La Placa MD, Saladino F, Cassarà D, Nagase H, Vittorelli ML. The amount and proteolytic content of vesicles shed by human cancer cell lines correlates with their in vitro invasiveness. Anticancer Res. 1998. 18: 3433-3437.
153. Ginestra A, Miceli D, Dolo V, Romano FM, Vittorelli ML. Membrane vesicles in ovarian cancer fluids: a new potential marker. Anticancer Res. 1999. 19: 3439-3445.
154. Angelucci A, D'Ascenzo S, Festuccia C, Gravina GL, Bologna M, Dolo V, Pavan A. Vesicle-associated urokinase plasminogen activator promotes invasion in prostate cancer cell lines. Clin Exp Metastasis. 2000. 18: 163-170.
155. Safaei R, Larson BJ, Cheng TC, Gibson MA, Otani S, Naerdemann W, Howell SB. Abnormal lysosomal trafficking and enhanced exosomal export of cisplatin in drugresistant human ovarian carcinoma cells. Mol Cancer Ther. 2005. 4: 1595-1604.
156. Shedden K, Xie XT, Chandaroy P, Chang YT, Rosania GR. Expulsion of small molecules in vesicles shed by cancer cells: association with gene expression and chemosensitivity profiles. Cancer Res. 2003. 63: 433–437.
157. Andreola G, Rivoltini L, Castelli C, Huber V, Perego P, Deho P, Squarcina P, Accornero P, Lozupone F, Lugini L, Stringaro A, Molinari A, Arancia G, Gentile M, Parmiani G, Fais S. Induction of lymphocyte apoptosis by tumor cell secretion of FasL-bearing microvesicles. J Exp Med. 2002. 195: 1303-1316.
158. Valenti R, Huber V, Filipazzi P, Pilla L, Sovena G, Villa A, Corbelli A, Fais S, Parmiani G, Rivoltini L. Human tumor-released microvesicles promote the differentiation of myeloid cells with transforming growth factor-beta-mediated suppressive activity on T lymphocytes. Cancer Res. 2006. 66: 9290-9298.
159. Jin, H.; Liu, P.; Wu, Y.; Meng, X.; Wu, M.; Han, J.; Tan, X. Exosomal zinc transporter ZIP4 promotes cancer growth and is a novel diagnostic biomarker for pancreatic cancer. Cancer Sci. 2018; 109, 2946–2956.
160. Wei, Q.; Wei, L.; Zhang, J.; Li, Z.; Feng, H.; Ren, L. EphA2-enriched exosomes promote cell migration and are a potential diagnostic serum marker in pancreatic cancer. Mol. Med. Rep. 2020, 22, 2941–2947.
161. Belvedere, R.; Bizzarro, V.; Popolo, A.; Piaz, F.D.; Vasaturo, M.; Picardi, P.; Parente, L.; Petrella, A. Role of intracellular and extracellular annexin A1 in migration and invasion of human pancreatic carcinoma cells. BMC Cancer 2014, 14, 961.
162. Belvedere, R.; Bizzarro, V.; Forte, G.; Piaz, F.D.; Parente, L.; Petrella, A. Annexin A1 contributes to pancreatic cancer cell phenotype, behaviour and metastatic potential independently of Formyl Peptide Receptor pathway. Sci. Rep. 2016, 6, 29660.
163. Pessolano, E.; Belvedere, R.; Bizzarro, V.; Franco, P.; De Marco, I.; Porta, A.; Tosco, A.; Parente, L.; Perretti, M.; Petrella, A. Annexin A1 May Induce Pancreatic Cancer Progression as a Key Player of Extracellular Vesicles Effects as Evidenced in the In Vitro MIA PaCa-2 Model System. Int. J. Mol. Sci. 2018, 19, 3878.
164. Costa-Silva B., Aiello N.M., Ocean A.J., Singh S., Zhang H., Thakur B.K., Becker A., Hoshino A., Mark M.T., Molina H., et al. Pancreatic cancer exosomes initiate pre-metastatic niche formation in the liver. Nat. Cell Biol. 2015;17:816–826.
165. Hoshino A, Costa-Silva B, Shen TL, Rodrigues G, Hashimoto A, Tesic Mark M, Molina H, Kohsaka S, Di Giannatale A, Ceder S, et al. Tumour exosome integrins determine organotropic metastasis. Nature. 2015;527:329 –35
166. Solito E, de Coupade C, Parente L, Flower RJ, Russo-Marie F. Human annexin 1 is highly

expressed during the differentiation of the epithelial cell line A 549: involvement of nuclear factor interleukin 6 in phorbol ester induction of annexin 1. Cell Growth Differ. 1998; 9(4):327-36.
167. Morgan RO & Fernández MP. Annexin gene structures and molecular evolutionary genetics. Cell Mol Life Sci. 1997; 53(6):508-15.
168. Morgan RO, Jenkins NA, Gilbert DJ, Copeland NG, Balsara BR, Testa JR, Fernandez MP. Novel human and mouse annexin A10 are linked to the genome duplications during early chordate evolution. Genomics. 1999: 60(1):40- 9.
169. Wallner BP, Mattaliano RJ, Hession C, Cate RL, Tizard R, Sinclair LK, Foeller C, Chow EP, Browing JL, Ramachandran KL, et al. Cloning and expression of human lipocortin, a phospholipase A2 inhibitor with potential anti-inflammatory activity. Nature. 1986; 320(6057):77-81.
170. Weng X, Luecke H, Song IS, Kang DS, Kim SH, Huber R. Crystal structure of human annexin I at 2.5 A resolution. Protein Sci. 1993; 2(3):448-58.
171. A. Rosengarth, V. Gerke, and H. Luecke, 'X-ray structure of full-length annexin 1 and implications for membrane aggregation', J. Mol. Biol., . 2001; vol. 306, no. 3, pp. 489–498.
172. Grewal T., Hoque M., Conway J.R.W., Reverter M., Wahba M., Beevi S.S., Timpson P., Enrich C., Rentero C. Annexin A6-A multifunctional scaffold in cell motility. Cell Adhes. Migr. 2017; 11:288–304.
173. Lim L.H., Pervaiz S. Annexin 1: The new face of an old molecule. FASEB J. 2007; 21:968–975.
174. V. Gerke and S. E. Moss. 'Annexins: From structure to function', Physiological Reviews. 2002; vol. 82, no. 2. American Physiological Society, pp. 331–371.
175. L. C. Alldridge and C. E. Bryant, 'Annexin 1 regulates cell proliferation by disruption of cell morphology and inhibition of cyclin D1 expression through sustained activation of the ERK1/2 MAPK signal', Exp. Cell Res. 2003; vol. 290, no. 1, pp. 93–107.
176. Han, G., Tian, Y., Duan, B., Sheng, H., Gao, H. and Huang, J. Association of nuclear annexin A1 with prognosis of patients with esophageal squamous cell carcinoma. Int. J. Clin. Exp. Pathol. 2014; 7, 751–759.
177. Zhu, F., Xu, C., Jiang, Z., Jin, M., Wang, L., Zeng, S., Teng, L. and Cao, J. Nuclear localization of annexin A1 correlates with advanced disease and peritoneal dissemination in patients with gastric carcinoma. Anat. Rec. (Hoboken). 2010; 293, 1310–1314.
178. Rhee, H. J., Kim, G.Y., Huh, J.W., Kim, S.W. and Na, D.S. Annexin I is a stress protein induced by heat, oxidative stress and a sulfhydryl-reactive agent. Eur. J. Biochem. 2000; 267, 3220–3225.
179. Kim, Y.S., Ko, J., Kim, I.S., Jang, S. W., Sung, H.J., Lee, H.J., Lee, S.Y., Kim, Y. and Na, D.S. PKCdelta-dependent cleavage and nuclear translocation of annexin A1 by phorbol 12-myristate 13-acetate. Eur. J. Biochem. 2003; 270, 4089–4094.
180. Hoque, M., Rentero, C., Cairns, R., Tebar, F., Enrich, C. and Grewal, T. Annexins - Scaffolds modulating PKC localization and signaling. Cell Signal. 2014; 26, 1213–1225.
181. Hirata, F., Thibodeau, L.M. and Hirata, A. Ubiquitination and SUMOylation of annexin A1 and helicase activity. Biochim. Biophys. Acta. 2010; 1800, 899–905.
182. Caron, D., Maaroufi, H., Michaud, S., Tanguay, R.M. and Faure, R.L. Annexin A1 is regulated by domains cross-talk through post-translational phosphorylation and SUMOYlation. Cell Signal. 2013; 25, 1962–1969.
183. Sakaguchi, M., Murata, H., Sonegawa, H., Sakaguchi, Y., Futami, J., Kitazoe, M., Yamada, H. and Huh, N.H. Truncation of annexin A1 is a regulatory lever for linking epidermal growth factor signaling with cytosolic phospholipase A2 in normal and malignant squamous epithelial cells. J. Biol. Chem. 2007; 282, 35679–35686.
184. F. D'Acquisto, M. Perretti, and R. J. Flower, 'Annexin-A1: A pivotal regulator of the innate and adaptive immune systems', British Journal of Pharmacology, vol. 155, no. 2. Br J Pharmacol, 2008; pp. 152–169.

185. U. Rescher and V. Gerke, ‘Annexins - Unique membrane binding proteins with diverse functions’, Journal of Cell Science, 2004; vol. 117, no. 13. J Cell Sci, pp. 2631–2639.
186. M. Perretti and E. Solito, ‘Annexin 1 and neutrophil apoptosis’, in Biochemical Society Transactions, Jun. 2004, vol. 32, no. 3, pp. 507–510.
187. C. D. John, H. C. Christian, J. F. Morris, R. J. Flower, E. Solito, and J. C. Buckingham, ‘Annexin 1 and the regulation of endocrine function’, Trends in Endocrinology and Metabolism. 2004; vol. 15, no. 3, pp. 103–109.
188. H. H. Gerdes, ‘Membrane traffic in the secretory pathway’, Cellular and Molecular Life Sciences, 2008; vol. 65, no. 18. pp. 2779–2780.
189. B. P. Wallner et al., ‘Cloning and expression of human lipocortin, a phospholipase A2 inhibitor with potential anti-inflammatory activity’, Nature, 1986; vol. 320, no. 6057, pp. 77–81.
190. P. Christman, J. Callaway, J. Fallon, J. Jones, and H. T. Haigler, ‘Selective secretion of annexin 1, a protein without a signal sequence, by the human prostate gland’, J. Biol. Chem. 1991; vol. 266, no. 4, pp. 2499–2507.
191. A. A. Aderem, K. A. Albert, M. M. Keum, J. K. T. Wang, P. Greengard, and Z. A. Cohn, ‘Stimulus-dependent myristoylation of a major substrate for protein kinase C’, Nature, 1988; vol. 332, no. 6162, pp. 362–364.
192. S. Omer, D. Meredith, J. F. Morris, and H. C. Christian, ‘Evidence for the role of adenosine 5′-triphosphate-binding cassette (ABC)-A1 in the externalization of annexin 1 from pituitary folliculostellate cells and ABCA1-transfected cell models’, Endocrinology, 2006; vol. 147, no. 7, pp. 3219–3227.
193. H. S. Euzger, R. J. Flower, N. J. Goulding, and M. Perretti, ‘Differential modulation of annexin I binding sites on monocytes and neutrophils’, Mediators Inflamm., 1999; vol. 8, no. 1, pp. 53–62.
194. J. Dalli, L. V. Norling, D. Renshaw, D. Cooper, K. Y. Leung, and M. Perretti, ‘Annexin 1 mediates the rapid anti-inflammatory effects of neutrophil-derived microparticles’, Blood, 2008; vol. 112, no. 6, pp. 2512–2519.
195. G. Raposo and W. Stoorvogel, ‘Extracellular vesicles: Exosomes, microvesicles, and friends’, Journal of Cell Biology, 2013; vol. 200, no. 4. J Cell Biol, pp. 373–383..
196. G. Leoni et al., ‘Annexin A1’containing extracellular vesicles and polymeric nanoparticles promote epithelial wound repair’, J. Clin. Invest. 2015; vol. 125, no. 3, pp. 1215–1227.
197. E. Pessolano et al., ‘Annexin A1 may induce pancreatic cancer progression as a key player of extracellular vesicles effects as evidenced in the in vitro MIA PaCa-2 model system’, Int. J. Mol. Sci. 2018; vol. 19, no. 12.
198. J. Skog et al., ‘Glioblastoma microvesicles transport RNA and proteins that promote tumour growth and provide diagnostic biomarkers’, Nat. Cell Biol. 2008; vol. 10, no. 12, pp. 1470–1476.
199. Boudhraa Z., Bouchon B., Viallard C., D’Incan M., Degoul F. Annexin A1 localization and its relevance to cancer. Clin. Sci. 2016;130:205–220.
200. Liu Y., Hu X., Han C., Wang L., Zhang X., He X., Lu X. Targeting tumor suppressor genes for cancer therapy. BioEssays. 2015;37:1277–1286.
201. Cao Y., Li Y., Edelweiss M., Arun B., Rosen D., Resetkova E., Wu Y., Liu J., Sahin A., Albarracin C.T. Loss of Annexin A1 expression in breast cancer progression. Appl. Immunohistochem. Mol. Morphol. 2008;16:530–534.
202. Hnisz D., Weintraub A.S., Day D.S., Valton A.L., Bak R.O., Li C.H., Goldmann J., Lajoie B.R., Fan Z.P., Sigova A.A., et al. Activation of proto-oncogenes by disruption of chromosome neighborhoods. Science. 2016;351:1454–1458.
203. Anderson M.W., Reynolds S.H., You M., Maronpot R.M. Role of proto-oncogene activation in carcinogenesis. Environ. Health Perspect. 1992;98:13–24.
204. Mussunoor S & Murray GI. The role of annexins in tumour development and progression. J Pathol. 2008; 216(2):131-40.

205. Foo S.L., Yap G., Cui J., Lim L.H.K. Annexin-A1—A Blessing or a Curse in Cancer? Trends Mol. Med. 2019;25:315–327.
206. Sobral-Leite M., Wesseling J., Smit V.T., Nevanlinna H., van Miltenburg M.H., Sanders J., Hofland I., Blows F.M., Coulson P., Patrycja G., et al. Annexin A1 expression in a pooled breast cancer series: Association with tumor subtypes and prognosis. BMC Med. 2015;13:156.
207. Vecchi L., Alves Pereira Zoia M., Goss Santos T., de Oliveira Beserra A., Colaco Ramos C.M., Franca Matias Colombo B., Paiva Maia Y.C., Piana de Andrade V., Teixeira Soares Mota S., Goncalves de Araujo T., et al. Inhibition of the AnxA1/FPR1 autocrine axis reduces MDA-MB-231 breast cancer cell growth and aggressiveness in vitro and in vivo. Biochim. Biophys. Acta Mol. Cell Res. 2018;1865:1368–1382.
208. Boudhraa Z., Rondepierre F., Ouchchane L., Kintossou R., Trzeciakiewicz A., Franck F., Kanitakis J., Labeille B., Joubert-Zakeyh J., Bouchon B., et al. Annexin A1 in primary tumors promotes melanoma dissemination. Clin. Exp. Metastasis. 2014;31:749–760
209. Lin Y., Lin G., Fang W., Zhu H., Chu K. Increased expression of Annexin A1 predicts poor prognosis in human hepatocellular carcinoma and enhances cell malignant phenotype. Med Oncol. 2014;31:327.
210. Bai X.F., Ni X.G., Zhao P., Liu S.M., Wang H.X., Guo B., Zhou L.P., Liu F., Zhang J.S., Wang K., et al. Overexpression of annexin 1 in pancreatic cancer and its clinical significance. World J. Gastroenterol. 2004;10:1466–1470.
211. Su N., Xu X.Y., Chen H., Gao W.C., Ruan C.P., Wang Q., Sun Y.P. Increased expression of Annexin A1 is correlated with K-ras mutation in colorectal cancer. Tohoku J. Exp. Med. 2010;222:243–250.
212. Zhu, F., Xu, C., Jiang, Z., Jin, M., Wang, L., Zeng, S., Teng, L. and Cao, J. Nuclear localization of annexin A1 correlates with advanced disease and peritoneal dissemination in patients with gastric carcinoma. Anat. Rec. (Hoboken). 2010; 293, 1310–1314
213. Cheng S.X., Tu Y., Zhang S. FoxM1 promotes glioma cells progression by up-regulating Anxa1 expression. PLoS ONE. 2013;8:e72376.
214. Liu Y.F., Zhang P.F., Li M.Y., Li Q.Q., Chen Z.C. Identification of Annexin A1 as a proinvasive and prognostic factor for lung adenocarcinoma. Clin. Exp. Metastasis. 2011;28:413–425.
215. Sato Y., Kumamoto K., Saito K., Okayama H., Hayase S., Kofunato Y., Miyamoto K., Nakamura I., Ohki S., Koyama Y., et al. Up-regulated Annexin A1 expression in gastrointestinal cancer is associated with cancer invasion and lymph node metastasis. Exp. Ther. Med. 2011;2:239–243.
216. Rodrigo J.P., Garcia-Pedrero J.M., Fernandez M.P., Morgan R.O., Suárez C., Herrero A. Annexin A1 expression in nasopharyngeal carcinoma correlates with squamous differentiation. Am. J. Rhinol. 2005;19:483–487.
217. Jin-Feng Zhu,1,2 Wei Huang,1 Hong-Mei Yi,1 Ta Xiao,1,3 Jiao-Yang Li,1 Juan Feng,1 Hong Yi,1 Shan-Shan Lu,1 Xin-Hui Li,1 Rou-Huang Lu,1 Qiu-Yan He,1,4 and Zhi-Qiang Xiao. Annexin A1-suppressed autophagy promotes nasopharyngeal carcinoma cell invasion and metastasis by PI3K/AKT signaling activation. Cell Death Dis. 2018; 9(12): 1154.
218. Gaohua Han, Ye Tian, Bensong Duan, Haihui Sheng,4 Hengjun Gao, Junxing Huang. Association of nuclear annexin A1 with prognosis of patients with esophageal squamous cell carcinoma. Int J Clin Exp Pathol. 2014; 7(2): 751–759.
219. Bizzarro V. et al.. Annexin A1 is involved in the acquisition and maintenance of a stem cell-like/aggressive phenotype in prostate cancer cells with acquired resistance to zoledronic acid. Oncotarget. 2015; 6, 25076–25092.
220. Petrella A., Festa M., Ercolino S.F., Zerilli M., Stassi G., Solito E., Parente L. Annexin-1 downregulation in thyroid cancer correlates to the degree of tumor differentiation. Cancer Biol. Ther. 2006; 5:643–647.

221. Garcia Pedrero J.M., Fernandez M.P., Morgan R.O., Herrero Zapatero A., Gonzalez M.V., Suarez Nieto C., Rodrigo J.P. Annexin A1 down-regulation in head and neck cancer is associated with epithelial differentiation status. Am. J. Pathol. 2004;164:73–79.
222. Shen D., Nooraie F., Elshimali Y., Lonsberry V., He J., Bose S., Chia D., Seligson D., Chang H.R., Goodglick L. Decreased expression of Annexin A1 is correlated with breast cancer development and progression as determined by a tissue microarray analysis. Hum. Pathol. 2006;37:1583–1591.
223. Shen D, Chang HR, Chen Z, He J, Lonsberry V, Elshimali Y, Chia D, Seligson D, Goodglick L, Nelson SF, Gornbein JA. Loss of annexin A1 expression in human breast cancer detected by multiple high-throughput analyses. Biochem Biophys Res Commun. 2005; 326(1):218-27.
224. Ou K, Yu K, Kesuma D, Hooi M, Huang N, Chen W, Lee SY, Goh XP, Tan LK, Liu J, Soon SY, Bin Abdul Rashid S, Putti TC, Jikuya H, Ichikawa T, Nishimura O, Salto-Tellez M, Tan P. Novel breast cancer biomarkers identified by integrative proteomic and gene expression mapping. J Proteome Res. 2008; 7(4):1518-28.
225. Ang EZ, Nguyen HT, Sim HL, Putti TC, Lim LH. Annexin-1 regulates growth arrest induced by high levels of estrogen in MCF-7 breast cancer cells. Mol Cancer Res. 2009; 7(2):266-74.
226. Khau T, Langenbach SY, Schuliga M, Harris T, Johnstone CN, Anderson RL, Stewart AG. 2011 Annexin-1 signals mitogen-stimulated breast tumor cell proliferation by activation of the formyl peptide receptors (FPRs) 1 and 2. FASEB J. 25(2):483-96.
227. Maschler S, Gebeshuber CA, Wiedemann EM, Alacakaptan M, Schreiber M, Custic I, Beug H. Annexin A1 attenuates EMT and metastatic potential in breast cancer. EMBO Mol Med. 2010; 2(10):401-14.
228. de Graauw M., van Miltenburg M.H., Schmidt M.K., Pont C., Lalai R., Kartopawiro J., Pardali E., Le Devedec S.E., Smit V.T., van der Wal A., et al. Annexin A1 regulates TGF-beta signaling and promotes metastasis formation of basal-like breast cancer cells. Proc. Natl. Acad. Sci. USA. 2010; 107:6340–6345.
229. Anbalagan D., Yap G., Yuan Y., Pandey V.K., Lau W.H., Arora S., Bist P., Wong J.S., Sethi G., Nissom P.M., et al. Annexin-A1 regulates microRNA-26b* and microRNA-562 to directly target NF-kappaB and angiogenesis in breast cancer cells. PLoS ONE. 2014;9:e114507.
230. Swa HL, Shaik AA, Lim LH, Gunaratne J. Mass spectrometry based quantitative proteomics and integrative network analysis accentuates modulating roles of annexin-1 in mammary tumorigenesis. Proteomics. 2015; 15(2- 3):408-18.
231. Paweletz CP, Ornstein DK, Roth MJ, Bichsel VE, Gillespie JW, Calvert VS, Vocke CD, Hewitt SM, Duray PH, Herring J, Wang QH, Hu N, Linehan WM, Taylor PR, Liotta LA, Emmert-Buck MR, Petricoin EF 3rd. Loss of annexin 1 correlates with early onset of tumorigenesis in esophageal and prostate carcinoma. Cancer Res. 2000; 60(22):6293-7.
232. Patton KT, Chen HM, Joseph L, Yang XJ. Decreased annexin I expression in prostatic adenocarcinoma and in high-grade prostatic intraepithelial neoplasia. Histopathology. 2005; 47(6):597-601.
233. Kang JS, Calvo BF, Maygarden SJ, Caskey LS, Mohler JL, Ornstein DK. Dysregulation of annexin I protein expression in high-grade prostatic intraepithelial neoplasia and prostate cancer. Clin Cancer Res. 2002; 8(1):117-23.
234. Hsiang CH, Tunoda T, Whang YE, Tyson DR, Ornstein DK. The impact of altered annexin I protein levels on apoptosis and signal transduction pathways in prostate cancer cells. Prostate. 2006; 66(13):1413-24.
235. Geary LA, Nash KA, Adisetiyo H, Liang M, Liao CP, Jeong JH, Zandi E, Roy-Burman P. CAF-secreted annexin A1 induces prostate cancer cells to gain stem cell-like features. Mol Cancer Res. 2014; 12(4):607-21
236. Guzmán-Aránguez A, Olmo N, Turnay J, Lecona E, Pérez-Ramos P, López de Silanes I,

Lizarbe MA. Differentiation of human colon adenocarcinoma cells alters the expression and intracellular localization of annexins A1, A2, and A5. J Cell Biochem. 2005; 94(1):178-93.
237. Duncan R, Carpenter B, Main LC, Telfer C, Murray GI. Characterisation and protein expression profiling of annexins in colorectal cancer. Br J Cancer. 2008; 98(2):426-33.
238. Liang L, Qu L, Ding Y. Protein and mRNA characterization in human colorectal carcinoma cell lines with different metastatic potentials. Cancer Invest. 2007; 25(6):427-34.
239. Su N, Xu XY, Chen H, Gao WC, Ruan CP, Wang Q, Sun YP. Increased expression of annexin A1 is correlated with K-ras mutation in colorectal cancer. Tohoku J Exp Med. 2010; 222(4):243-50.
240. Babbin BA, Lee WY, Parkos CA, Winfree LM, Akyildiz A, Perretti M, Nusrat A. Annexin I regulates SKCO-15 cell invasion by signaling through formyl peptide receptors. J Biol Chem. 2006; 281(28):19588-99.
241. Biaoxue R, Xiling J, Shuanying Y, Wei Z, Xiguang C, Jinsui W, Min Z. Upregulation of Hsp90-beta and annexin A1 correlates with poor survival and lymphatic metastasis in lung cancer patients. J Exp Clin Cancer Res. 2012; 31:70.
242. Liu YF, Zhang PF, Li MY, Li QQ, Chen ZC. Identification of annexin A1 as a proinvasive and prognostic factor for lung adenocarcinoma. Clin Exp Metastasis. 2011; 28(5):413-25.
243. Rong B, Zhao C, Liu H, Ming Z, Cai X, Gao W, Yang S. Elevated serum annexin A1 as potential diagnostic marker for lung cancer: a retrospective case-control study. Am J Transl Res. 2014; 6(5):558-69.
244. Wang C, Xiao Q, Li YW, Zhao C, Jia N, Li RL, Cao SS, Cui J, Wang L, Wu Y, Wen AD. Regulatory mechanisms of annexin-induced chemotherapy resistance in cisplatin resistant lung adenocarcinoma. Asian Pac J Cancer Prev. 2014; 15(7):3191-4
245. Rondepierre F, Bouchon B, Papon J, Bonnet-Duquennoy M, Kintossou R, Moins N, Maublant J, Madelmont JC, D'Incan M, Degoul F. Proteomic studies of B16 lines: involvement of annexin A1 in melanoma dissemination. Biochim Biophys Acta. 2009; 1794(1):61-9.
246. Boudhraa Z, Rondepierre F, Ouchchane L, Kintossou R, Trzeciakiewicz A, Franck F, Kanitakis J, Labeille B, Joubert-Zakeyh J, Bouchon B, Perrot JL, Mansard S, Papon J, Dechelotte P, Chezal JM, Miot-Noirault E, Bonnet M, D'Incan M, Degoul F. Annexin A1 in primary tumors promotes melanoma dissemination. Clin Exp Metastasis. 2014; 31(7):749-60.
247. Boudhraa Z, Merle C, Mazzocut D, Chezal JM, Chambon C, MiotNoirault E, Theisen M, Bouchon B, Degoul F. Characterization of proinvasive mechanisms and N-terminal cleavage of ANXA1 in melanoma. Arch Dermatol Res. 2014; 306(10):903-14.
248. 131. Movitz C., Sjolin C., Dahlgren C. Cleavage of Annexin I in human neutrophils is mediated by a membrane-localized metalloprotease. Biochim. Biophys. Acta. 1999;1416:101–108.
249. Zied Boudhraa 1, Bernadette Bouchon 2, Claire Viallard 2, Michel D'Incan 2, Françoise Degoul 2. Annexin A1 localization and its relevance to cancer. Clin Sci (Lond). 2016;130(4):205-20.
250. Yoshida K, Kuramitsu Y, Murakami K, Ryozawa S, Taba K, Kaino S, Zhang X, Sakaida I, Nakamura K. Proteomic differential display analysis for TS-1-resistant and -sensitive pancreatic cancer cells using twodimensional gel electrophoresis and mass spectrometry. Anticancer Res. 2011; 31(6):2103-8.
251. Chen CY, Shen JQ, Wang F, Wan R, Wang XP. Prognostic significance of annexin A1 expression in pancreatic ductal adenocarcinoma. Asian Pac J Cancer Prev. 2012; 13(9):4707-12
252. Bai XF, Ni XG, Zhao P, Liu SM, Wang HX, Guo B, Zhou LP, Liu F, Zhang JS, Wang K, Xie YQ, Shao YF, Zhao XH. Overexpression of annexin 1 in pancreatic cancer and its clinical significance. World J Gastroenterol. 2004; 10(10):1466-70.
253. Yu Z., Zhao S., Ren L., Wang L., Chen Z., Hoffman R.M., Zhou J. Pancreatic cancer-derived exosomes promote tumor metastasis and liver pre-metastatic niche formation. Oncotarget. 2017; 8:63461–63483.
254. Belvedere, R.; Saggese, P.; Pessolano, E.; Memoli, D.; Bizzarro, V.; Rizzo, F.; Parente, L.;

Weisz, A.; Petrella, A. miR-196a Is Able to Restore the Aggressive Phenotype of Annexin A1 Knock-Out in Pancreatic Cancer Cells by CRISPR/Cas9 Genome Editing. Int. J. Mol. Sci. 2018, 19, 1967.
255. Bernfield M., Götte M., Park P.W., Reizes O., Fitzgerald M.L., Lincecum J., Zako M. Functions of cell surface heparan sulfate proteoglycans. Annu. Rev. Biochem. 1999; 68:729–777.
256. Rudd T.R., Skidmore M.A., Guerrini M., Hricovini M., Powell A.K., Siligardi G., Yates E.A. The conformation and structure of GAGs: Recent progress and perspectives. Curr. Opin. Struct. Biol. 2010; 20:567–574.
257. Sarrazin S., Lamanna W.C., Esko J.D. Heparan sulfate proteoglycans. Cold Spring Harb. Perspect. Biol. 2011; 3.
258. Shriver Z., Capila I., Venkataraman G., Sasisekharan R. Heparin and heparan sulfate: Analyzing structure and microheterogeneity. In: Heparin-A century of ProgressLever R., Mulloy B., Page C.P., editors. Handbook Experimental Pharmacology. 2012; vol 207. pp. 159–176.
259. Gallangher J.T. Heparan sulfate: A heparin in miniature. In: Heparin-A century of ProgressLever R., Mulloy B., Page C.P., editors. Handbook Experimental Pharmacology. 2012; vol 207. pp. 347–360.
260. Li J.P., Kusche-Gullberg M. Heparan sulfate: Biosynthesis, structure, and function. Int. Rev. Cell. Mol. Biol. 2016; 325:215–273.
261. Mulloy B., Hogwood J., Gray E., Lever R., Page C.P. Pharmacology of heparin and related drugs. Pharmacol. Rev. 2016; 68:76–141.
262. Rudd T.R., Preston M.D., Yates E.A. The nature of the conserved basic amino acid sequences found among 437 heparin binding proteins determined by network analysis. Mol. Biosyst. 2017;13:852–865.
263. Meneghetti M.C., Hughes A.J., Rudd T.R., Nader H.B., Powell A.K., Yates E.A., Lima M.A. Heparan sulfate and heparin interactions with proteins. J. R. Soc. Interface. 2015;12
264. Lanzi C and Cassinelli G. Heparan Sulfate Mimetics in Cancer Therapy: The Challenge to Define Structural Determinants and the Relevance of Targets for Optimal Activity. Molecules. 2018 Nov; 23(11): 2915.
265. Theocharis A.D., Skandalis S.S., Tzanakakis G.N., Karamanos N.K. Proteoglycans in health and disease: Novel roles for proteoglycans in malignancy and their pharmacological targeting. FEBS J. 2010; 277:3904–3923.
266. Iozzo R.V., Sanderson R.D. Proteoglycans in cancer biology, tumour microenvironment and angiogenesis. J. Cell. Mol. Med. 2011; 15:1013–1031.
267. Knelson E.H., Nee J.C., Blobe G.C. Heparan sulfate signaling in cancer. Trends Biochem. Sci. 2014; 39:277–288.
268. Parish C.R. The role of heparan sulphate in inflammation. Nat. Rev. Immunol. 2006; 6:633–643.
269. Chiodelli P., Bugatti A., Urbinati C., Rusnati M. Heparin/Heparan sulfate proteoglycans glycomic interactome in angiogenesis: Biological implications and therapeutical use. Molecules. 2015; 20:6342–6388.
270. Couchman J.R., Multhaupt H., Sanderson R.D. Recent insights into cell surface heparan sulphate proteoglycans and cancer. F1000 Res. 2016;5
271. Nagarajan A., Malvi P., Wajapeyee N. Heparan sulfate and heparan sulfate proteoglycans in cancer initiation and progression. Front. Endocrinol. 2018; 9:483.
272. Bai, X.F.; Ni, X.G.; Zhao, P.; Liu, S.M.; Wang, H.X.; Guo, B.; Zhou, L.P.; Liu, F.; Zhang, J.S.; Wang, K.; Xie, Y.Q.; Shao, Y.F.; Zhao, X.H. Overexpression of annexin 1 in pancreatic cancer and its clinical significance. World J. Gastroenterol. 2004; 10:1466-1470.
273. Chen, C.Y.; Shen, J.Q.; Wang, F.; Wan, R.; Wang, X.P. Prognostic significance of annexin A1 expression in pancreatic ductal adenocarcinoma. Asian Pac. J. Cancer Prev. 2012; 13, 4707–4712.

274. Bizzarro, V.; Fontanella, B.; Carratù, A.; Belvedere, R.; Marfella, R.; Parente, L.; Petrella, A. Annexin A1 N-terminal derived peptide Ac2-26 stimulates fibroblast migration in high glucose conditions. PLoS One. 2012; 7:e45639.
275. Guo, C.; Liu, S.; Sun, M.Z. Potential role of Anxa1 in cancer. Future Oncol. 2013 9,1773–1793.
276. Barash U., Cohen-Kaplan V., Dowek I., Sanderson R.D., Ilan N., Vlodavsky I. Proteoglycans in health and disease: New concepts for heparanase function in tumor progression and metastasis. FEBS J. 2010; 277:3890–3903.
277. Levy-Adam F., Ilan N., Vlodavsky I. Tumorigenic and adhesive properties of heparanase. Semin. Cancer Biol. 2010; 20:153–160.
278. Erik H Knelson , Jasmine C Nee , Gerard C Blobe. Heparan sulfate signaling in cancer. Trends Biochem Sci. 2014; 39(6):277-88.
279. T. Horlacher, C. Noti, J.L. de Paz, P. Bindschadler, M.-L. Hecht, D.F. Smith, M. N. Fukuda, P.H. Seeberger, Characterization of annexin A1 glycan binding reveals binding to highly sulfated glycans with preference for highly sulfated heparan sulfate and heparin, Biochemistry. 2011; 2650–2659.
280. Belvedere, R.; Bizzarro, V.; Parente, L.; Petrella, F.; Petrella, A. Effects of Prisma® Skin dermal regeneration device containing glycosaminoglycans on human keratinocytes and fibroblasts. Cell Adhes. Migr. 2018; 12,168–183.
281. E.H. Knelson, J.C. Nee, G.C. Blobe. Heparan sulfate signaling in cancer. Trends Biochem Sci. 2014; 39:277–288.
282. Mulloy B., Hogwood J., Gray E., Lever R., Page C.P. Pharmacology of heparin and related drugs. Pharmacol. Rev. 2016; 68:76–141.
283. Chiodelli P., Bugatti A., Urbinati C., Rusnati M. Heparin/Heparan sulfate proteoglycans glycomic interactome in angiogenesis: Biological implications and therapeutical use. Molecules. 2015; 20:6342–6388.
284. Cassinelli G., Naggi A. Old and new applications of non-anticoagulant heparin. Int. J. Cardiol. 2016; 212:S14–S21.
285. Lima M., Rudd T., Yates E.A. New applications of heparin and other glycosaminoglycans. Molecules. 2017;22.
286. Smorenburg S.M., Hettiarachchi R.J., Vink R., Büller H.R. The effects of unfractionated heparin on survival in patients with malignancy—A systematic review. Thromb. Haemost. 1999; 82:1600–1604.
287. Couchman J.R., Multhaupt H., Sanderson R.D. Recent insights into cell surface heparan sulphate proteoglycans and cancer. F1000 Res. 2016; 5.
288. Hammond E., Khurana A., Shridhar V., Dredge K. The role of heparanase and sulfatases in the modification of heparan sulfate proteoglycans within the tumor microenvironment and opportunities for novel cancer therapeutics. Front. Oncol. 2014; 4:195.
289. Lanzi C., Zaffaroni N., Cassinelli G. Targeting heparan sulfate proteoglycans and their modifying enzymes to enhance anticancer chemotherapy efficacy and overcome drug resistance. Curr. Med. Chem. 2017; 24:2860–2886.
290. Vivès R.R., Seffouh A., Lortat-Jacob H. Post-Synthetic Regulation of HS Structure: The Yin and Yang of the Sulfs in cancer. Front. Oncol. 2014; 3:331.
291. Smorenburg S.M., Hettiarachchi R.J., Vink R., Büller H.R. The effects of unfractionated heparin on survival in patients with malignancy—A systematic review. Thromb. Haemost. 1999; 82:1600–1604.
292. Kakkar A.K. Thrombosis and cancer. Hematol. J. 2004; 5:S20–S23.
293. Kuderer N.M., Ortel T.L., Francis C.W. Impact of venous thromboembolism and anticoagulation on cancer and cancer survival. J. Clin. Oncol. 2009; 27:4902–4911.
294. Lyman G.H., Bohlke K., Khorana A.A., Kuderer N.M., Lee A.Y., Arcelus J.I., Balaban E.P., Clarke J.M., Flowers C.R., Francis C.W., et al. American Society of Clinical Oncology. Venous

thromboembolism prophylaxis and treatment in patients with cancer: American Society of clinical oncology clinical practice guideline update 2014. J. Clin. Oncol. 2015; 33:654–656.
295. García-Escobar I., Beato-Zambrano C., Muñoz Langa J., Brozos Vázquez E., Obispo Portero B., Gutiérrez-Abad D., Muñoz Martín A.J. Cancer and Thrombosis Working Group of the Spanish Society of Medical Oncology (SEOM). Pleiotropic effects of heparins: Does anticoagulant treatment increase survival in cancer patients? Clin. Transl. Oncol. 2018; 20:1097–1108.
296. Läubli H., Varki A., Borsig L. Antimetastatic properties of low molecular weight heparin. J. Clin. Oncol. 2016; 34:2560–2561.
297. Barash U., Cohen-Kaplan V., Dowek I., Sanderson R.D., Ilan N., Vlodavsky I. Proteoglycans in health and disease: New concepts for heparanase function in tumor progression and metastasis. FEBS J. 2010; 277:3890–3903.
298. Levy-Adam F., Ilan N., Vlodavsky I. Tumorigenic and adhesive properties of heparanase. Semin. Cancer Biol. 2010; 20:153–160.
299. Vlodavsky I., Elkin M., Ilan N. Impact of heparanase and the tumor microenvironment on cancer metastasis and angiogenesis: Basic aspects and clinical applications. Rambam. Maimonides Med. J. 2011; 2:e0019.
300. Vlodavsky I., Beckhove P., Lerner I., Pisano C., Meirovitz A., Ilan N., Elkin M. Significance of heparanase in cancer and inflammation. Cancer Microenviron. 2012;5:115–132.
301. Vlodavsky I., Singh P., Boyango I., Gutter-Kapon L., Elkin M., Sanderson R.D., Ilan N. Heparanase: From basic research to therapeutic applications in cancer and inflammation. Drug Resist. Updat. 2016; 29:54–75.
302. Hammond E., Khurana A., Shridhar V., Dredge K. The role of heparanase and sulfatases in the modification of heparan sulfate proteoglycans within the tumor microenvironment and opportunities for novel cancer therapeutics. Front. Oncol. 2014; 4:195.
303. Pisano C., Vlodavsky I., Ilan N., Zunino F. The potential of heparanase as a therapeutic target in cancer. Biochem. Pharmacol. 2014; 89:12–19.
304. Cassinelli G., Zaffaroni N., Lanzi C. The heparanase/heparan sulfate proteoglycan axis: A potential new therapeutic target in sarcomas. Cancer Lett. 2016; 382:245–254.
305. Rivara S., Milazzo F.M., Giannini G. Heparanase: A rainbow pharmacological target associated to multiple pathologies including rare diseases. Future Med. Chem. 2016; 8:647–680.
306. Lanzi C., Zaffaroni N., Cassinelli G. Targeting heparan sulfate proteoglycans and their modifying enzymes to enhance anticancer chemotherapy efficacy and overcome drug resistance. Curr. Med. Chem. 2017; 24:2860–2886.
307. Jia L., Ma S. Recent advances in the discovery of heparanase inhibitors as anti-cancer agents. Eur. J. Med. Chem. 2016;121:209–220.
308. Parish C.R., Freeman C., Brown K.J., Francis D.J., Cowden W.B. Identification of sulfated oligosaccharide-based inhibitors of tumor growth and metastasis using novel in vitro assays for angiogenesis and heparanase activity. Cancer Res. 1999; 59:3433–3441.
309. Khachigian L.M., Parish C.R. Phosphomannopentaose sulfate (PI-88): Heparan sulfate mimetic with clinical potential in multiple vascular pathologies. Cardiovasc. Drug Rev. 2004; 22:1–6.
310. Ferro V., Dredge K., Liu L., Hammond E., Bytheway I., Li C., Johnstone K., Karoli T., Davis K., Copeman E., et al. PI-88 and novel heparan sulfate mimetics inhibit angiogenesis. Semin. Thromb. Hemost. 2007; 33:557–568.
311. Dredge K., Hammond E., Davis K., Li C.P., Liu L., Johnstone K., Handley P., Wimmer N., Gonda T.J., Gautam A., et al. The PG500 series: Novel heparan sulfate mimetics as potent angiogenesis and heparanase inhibitors for cancer therapy. Investig. New Drugs. 2010; 28:276–283.
312. Yamada KM, Cukierman E. Modeling tissue morphogenesis andcancer in 3D. Cell 2007; 130:601-610.
313. Pampaloni F, Reynaud EG, Stelzer EH. The third dimension bridges the gap between cell culture and live tissue. Nat Rev Mol Cell Biol 2007; 8:839-845.

314. Kim JB. Three-dimensional tissue culture models in cancer biology. Semin Cancer Biol 2005; 15:365-377.
315. Sutherland RM, Inch WR, McCredie JA, Kruuv J.A multi-component radiation survival curve using an in vitro tumour model. Int J Radiat Biol Relat Stud Phys Chem Med 1970; 18:491-495.
316. Yuhas JM, Li AP, Martinez AO, Ladman AJ. A simplified method for production and growth of multicellular tumor spheroids. Cancer Res 1977; 37:3639-3643.
317. Acker H, Carlsson J, Mueller-Klieser W, Sutherland RM. Comparative pO2 measurements in cell spheroids cultured with different techniques. Br J Cancer 1987; 56:325-327
318. Kelm JM, Timmins NE, Brown CJ, Fussenegger M, Nielsen LK. Method for generation of homogeneous multicellular tumor spheroids applicable to a wide variety of cell types. Biotechnol Bioeng 2003; 20; 83:173-180.
319. Sutherland RM. Cell and environment interactions in tumor microregions: the multicell spheroid model. Science 1988; 240:177-184.
320. Ivascu A, Kubbies M. Rapid generation of single-tumor spheroids for high-throughput cell function and toxicity analysis. J Biomol Screen 2006; 11:922-932.
321. Yeon SE, No da Y, Lee SH, Nam SW, Oh IH, Lee J, et al. Application of concave microwells to pancreatic tumor spheroids enabling anticancer drug evaluation in a clinically relevant drug resistance model. PLoS One. 2013; 8(9):e73345.
322. Linde N, Gutschalk CM, Hoffmann C, Yilmaz D, Mueller MM. Integrating Macrophages into Organotypic Co-Cultures: A 3D In Vitro Model to Study Tumor-Associated Macrophages. PLoS One. 2012; 7(7).
323. Hardelauf H, Frimat JP, Stewart JD, Schormann W, Chiang YY, Lampen P, Franzke J, Hengstler JG, Cadenas C, Kunz-Schughart LA, West J. Microarrays for the scalable production of metabolically relevant tumour spheroids: a tool for modulating chemosensitivity traits. Lab Chip 2011; 11:419-428.
324. Burdett E, Kasper FK, Mikos AG, Ludwig JA. Engineering tumors: a tissue engineering perspective in cancer biology. Tissue Eng Part B Rev 2010; 16:351-359.
325. Friedrich J, Seidel C, Ebner R, Kunz-Schughart LA. Spheroid-based drug screen: considerations andpractical approach. Nat Protoc 2009; 4:309-324.
326. Timmins NE, Harding FJ, Smart C, Brown MA, Nielsen LK. Method for the generation and cultivation of functional three-dimensional mammary constructs without exogenous extracellular matrix. Cell Tissue Res 2005; 320:207-210.
327. Kurosawa H. Methods for inducing embryoid body formation: in vitro differentiation system of embryonic stem cells. J Biosci Bioeng 2007; 103:389-398
328. Leca J, Martinez S, Lac S, Nigri J, Secq V, Rubis M, Bressy C, Serge A, Lavaut MN, Dusetti N, et al. Cancer-associated fibroblast-derived annexin A6+ extracellular vesicles support pancreatic cancer aggressiveness. J Clin Invest. 2016; 126:4140–4156
329. Théry, C.; Amigorena, S.; Raposo, G.; Clayton, A. Isolation and Characterization of Exosomes from Cell Culture Supernatants and Biological Fluids. Curr. Protoc. Cell Biol. 2006; 30, 3.22.1–3.22.29.
330. Belvedere, R.; Pessolano, E.; Porta, A.; Tosco, A.; Parente, L.; Petrella, F.; Perretti, M.; Petrella, A. Mesoglycan induces the secretion of microvesicles by keratinocytes able to activate human fibroblasts and endothelial cells: A novel mechanism in skin wound healing. Eur. J. Pharmacol. 2020; 869, 172894.
331. Rossi, F.W.; Napolitano, F.; Pesapane, A.; Mascolo, M.; Staibano, S.; Matucci-Cerinic, M.; Guiducci, S.; Ragno, P.; di Spigna, G.; Postiglione, L.; Marone, G.; Montuori, N.; de Paulis, A. Upregulation of the N-formyl Peptide receptors in scleroderma fibroblasts fosters the switch to myofibroblasts. J Immunol. 2015; 194:5161-73.

332. Yu-Ting Chang, Hsuan-Yu Peng, Chun-Mei Hu, Shih-Chia Huang, Sui-Chi Tien, Yung-Ming Jeng. Pancreatic cancer-derived small extracellular vesical Ezrin regulates macrophage polarization and promotes metastasis. Am J Cancer Res. 2020; 10(1): 12–37.
333. Thaize Quiroga Chometon, Mariana da Silva Siqueira, Julie Carmo Sant Anna, Matheus Rogério Almeida, Mariana Gandini, Ana Cristina Martins de Almeida Nogueira, Paulo Renato Zuquim Antas. A protocol for rapid monocyte isolation and generation of singular human monocyte-derived dendritic cells. PLoS One. 2020;15(4):e0231132.
334. Rosowski, K.A.; Boltyanskiy, R.; Xiang, Y.; Van den Dries, K.; Schwartz, M.A.; Dufresne, E.R. Vinculin and the mechanical response of adherent fibroblasts to matrix deformation. Sci Rep. 2018; 8:17967.
335. Lee, H.T.; Sharek, L.; O'Brien, E.T.; Urbina, F.L.; Gupton, S.L.; Superfine, R.; Burridge, K.; Campbell, S.L. Vinculin and metavinculin exhibit distinct effects on focal adhesion properties, cell migration, and mechanotransduction. PLoS One. 2019; 14:e0221962.
336. Ren, B.; Cui, M.; Yang, G.; Wang, H.; Feng, M.; You, L.; Zhao, Y. Tumor microenvironment participates in metastasis of pancreatic cancer. Mol Cancer. 2018 17:108.
337. Papageorgis, P.; Stylianopoulos, T. Role of TGFβ in regulation of the tumor microenvironment and drug delivery (review). Int J Oncol. 2015; 46:933-43.
338. Lu Gao, Wei Zhang, Wen-Qun Zhong, Zhuo-Jue Liu, Hui-Min Li, Zi-Li Yu, Yi-Fang Zhao. Tumor associated macrophages induce epithelial to mesenchymal transition via the EGFR/ERK1/2 pathway in head and neck squamous cell carcinoma. Oncol Rep. 2018; 40(5):2558-2572.
339. Luga V., Zhang L., Viloria-Petit A.M., Ogunjimi A.A., Inanlou M.R., Chiu E., Buchanan M., Hosein A.N., Basik M., Wrana J.L. Exosomes Mediate Stromal Mobilization of Autocrine Wnt-PCP Signaling in Breast Cancer Cell Migration. Cell. 2012; 151:1542–1556.
340. Yu Z., Zhao S., Ren L., Wang L., Chen Z., Hoffman R.M., Zhou J. Pancreatic cancer-derived exosomes promote tumor metastasis and liver pre-metastatic niche formation. Oncotarget. 2017; 8:63461–63483.
341. A. Rosengarth, H. Luecke, A calcium-driven conformational switch of the N terminal and core domains of annexin A1, J. Mol. Biol. 2003; 326:1317–1325.
342. A. Walther, K. Riehemann, V. Gerke, A novel ligand of the formyl peptide receptor: Annexin I regulates neutrophil extravasation by interacting with the FPR, Mol Cell. 2005; 5 831–840.
343. M.P. Marmorato, A.D. Gimenes, F.E.C. Andrade, S.M. Oliani, C.D. Gil, Involvement of the annexin A1-Fpr anti-inflammatory system in the ocular allergy, Eur. J. Pharmacol. 2019; 842 298–305.
344. T. Santana Gastardelo, B. Rodrigues Cunha, L.S. Raposo, J.V. Maniglia, P. Maluf Cury, F.C. Rodrigues Lisoni, E.H. Tajara, S.M. Oliani. Inflammation and Cancer: Role of Annexin A1 and FPR2/ALX in Proliferation and Metastasis in Human Laryngeal Squamous Cell Carcinoma. PLoS One. 2014; 9:e111317.
345. U. Fahrioglu, ˇ Y. Dodurga, L. Elmas, M. Seçme, Ferulic acid decreases cell viability and colony formation while inhibiting migration of MIA PaCa-2 human pancreatic cancer cells in vitro, Gene 2015; 576 476–482.
346. Y. Shichi, N. Sasaki, M. Michishita, F. Hasegawa, Y. Matsuda, T. Arai, F. Gomi, J. Aida, K. Takubo, M. Toyoda, H. Yoshimura, K. Takahashi, T. Ishiwata. Enhanced morphological and functional differences of pancreatic cancer with epithelial or mesenchymal characteristics in 3D culture. Sci Rep. 2019; 9:10871.
347. J.E. Schnitzer, Impaired tumor growth, metastasis, angiogenesis and wound healing in annexinnA1-null mice, Proc. Natl. Acad. Sci. USA. 2009; 106 17886–17891.
348. J.Z. Lacerda, C.C. Drewes, K.K.O. Mimura, C.F. Zanon, T. Ansari, C.D. Gil, K.V. Greco, S.H.P. Farsky, S.M. Oliani. Annexin A12-26 Treatment Improves Skin Heterologous Transplantation by Modulating Inflammation and Angiogenesis Processes. Front. Pharmacol. 2018; 9:1015.

349. V. Bizzarro, R. Belvedere, F. Dal Piaz, L. Parente, A. Petrella, Annexin A1 induces skeletal muscle cell migration acting through formyl peptide receptors, PLoS One. 2012; 7 e48246.
350. Chronopoulos, A.; Robinson, B.; Sarper, M.; Cortes, E.; Auernheimer, V.; Lachowski, D.; Attwood, S.; Garcia, R.; Ghassemi, S.; Fabry, B.; Del Rio, H.A. ATRA mechanically reprograms pancreatic stellate cells to suppress matrix remodelling and inhibit cancer cell invasion. Nat Commun. 2016; 7:12630.
351. Hood, J.L.; San, R.S.; Wickline, S.A. Exosomes released by melanoma cells prepare sentinel lymph nodes for tumor metastasis. Cancer Res. 2011; 71:3792-3801.
352. Luga, V.; Zhang, L.; Viloria-Petit, A.M.; Ogunjimi, A.A.; Inanlou, M.R.; Chiu, E.; Buchanan, M.; Hosein, A.N.; Basik, M.; Wrana, J.L. Exosomes mediate stromal mobilization of autocrine Wnt-PCP signaling in breast cancer cell migration. Cell. 2012; 151:1542-1556.
353. Beuran, M.; Negoi, I.; Paun, S.; Ion, A.D.; Bleotu, C.; Negoi, R.I.; Hostiuc, S. The epithelial to mesenchymal transition in pancreatic cancer: A systematic review. Pancreatology. 2015; 15, 217–225.
354. Hwang, R.F.; Moore, T.; Arumugam, T.; Ramachandran, V.; Amos, K.D.; Rivera, A.; Ji, B.; Evans, D.B.; Logsdon, C.D. Cancer-associated stromal fibroblasts promote pancreatic tumor progression. Cancer Res. 2008; 68:918-26.
355. Olive, K.P.; Jacobetz, M.A.; Davidson, C.J.; Gopinathan, A.; McIntyre, D.; Honess, D.; et al. Inhibition of Hedgehog signaling enhances delivery of chemotherapy in a mouse model of pancreatic cancer. Science. 2009; 324:1457-1461.
356. Erdogan, B.; Webb, D.J. Cancer-associated fibroblasts modulate growth factor signaling and extracellular matrix remodeling to regulate tumor metastasis. Biochem Soc Trans. 2017; 45: 229–236.
357. Richards, K.E.; Zeleniak, A.E.; Fishel, M.L.; Wu, J.; Littlepage, L.E.; Hill, R. Cancer-associated fibroblast exosomes regulate survival and proliferation of pancreatic cancer cells. Oncogene. 2017; 36:1770-1778.
358. Quail, D.F.; Joyce, J.A. Microenvironmental regulation of tumor progression and metastasis. Nat Med. 2013; 19:1423-1437.
359. Todorova, D.; Simoncini, S.; Lacroix, R.; Sabatier, F.; Dignat-George, F. Extracellular Vesicles in Angiogenesis. Circ Res. 2017; 120:1658-1673
360. Chiba, M.; Kubota, S.; Sato, K.; Monzen, S. Exosomes released from pancreatic cancer cells enhance angiogenic activities via dynamin-dependent endocytosis in endothelial cells in vitro. Sci. Rep. 2018; 8, 11972.
361. Campos-Silva. C.; Suárez, H.; Jara-Acevedo, R.; Linares-Espinós, E.; Martinez-Piñeiro, L.; Yáñez-Mó, M.; Valés-Gómez, M. High sensitivity detection of extracellular vesicles immune-captured from urine by conventional flow cytometry. Sci Rep. 2019 9:2042.
362. Kikuchi, S.; Yoshioka, Y.; Prieto-Vila, M.; Ochiya T. Involvement of Extracellular Vesicles in Vascular-Related Functions in Cancer Progression and Metastasis. Int J Mol Sci. 2019; 20: 2584.
363. Yeon, J.H.; Jeong, H.E.; Seo, H.; Cho, S.; Kim, K.; Na, D.; Chung, S.; Park, J.; Choi, N.; Kang, J.Y. Cancer-derived exosomes trigger endothelial to mesenchymal transition followed by the induction of cancer-associated fibroblasts. Acta Biomater. 2018 76:146-153.
364. Walther, A.; Riehemann, K.; Gerke, V. A novel ligand of the formyl peptide receptor: Annexin I regulates neutrophil extravasation by interacting with the FPR. Mol. Cell 2000; 5, 831–840.
365. Ilseon Hwang; Jeong Won Kim; Kris Ylaya; Eun Joo Chung; Haruhisa Kitano; Candice Perry; Jun Hanaoka; Junya Fukuoka; Joon Yong Chung; Stephen M. Hewitt. Tumor-associated macrophage, angiogenesis and lymphangiogenesis markers predict prognosis of non-small cell lung cancer patients. J Transl Med. 2020; 18:443.
366. Cho, H.; Seo, Y.; Loke, K.M.; Kim, S-W.;. Oh, S-M; Kim, J-H.; Soh, J.; Kim, H. S.; Lee, H.; Kim, J.; Min, J-J.; Jung, D-W.; Williams, D. R. Cancer-Stimulated CAFs Enhance Monocyte

Differentiation and Protumoral TAM Activation via IL6 and GM-CSF Secretion. Clin Cancer Res. 2018; 24(21):5407-5421.
367. Kelly, T.; Huang, Y.; Simms, A.E.; Mazur, A. Fibroblast activation protein-α: a key modulator of the microenvironment in multiple pathologies. Int Rev Cell Mol Biol. 2012; 297:83-116.
368. Timmins NE, Harding FJ, Smart C, Brown MA, Nielsen LK. Method for the generation and cultivation of functional three-dimensional mammary constructs without exogenous extracellular matrix. Cell Tissue Res 2005; 320:207-210
369. Sheikh, M.; Solito, E. Annexin A1: Uncovering the Many Talents of an Old Protein. Int J Mol Sci. 2018; 19:1045.
370. Rong, B.; Zhao, C.; Liu, H.; Ming, Z.; Cai, X.; Gao, W.; Yang, S. Elevated serum annexin A1 as potential diagnostic marker for lung cancer: a retrospective case-control study. Am J Transl Res. 2014; 6: 558–569.
371. J. Gao, Y. Li, H. Yan, NMR solution structure of domain 1 of human annexin I shows an autonomous folding unit, J. Biol. Chem. 1999; 274 2971–2977.
372. A. MacDonald, M. Priess, J. Curran, J. Guess, V. Farutin, I. Oosterom, C.L. Chu, E. Cochran, L. Zhang, K. Getchel, M. Lolkema, B.C. Schultes, S. Krause. Necuparanib, a multitargeting heparan sulfate mimetic, targets tumor and stromal compartments in pancreatic cancer, Mol. Cancer Ther. 2019; 18 245–256.
373. N. Veraldi, N. Zouggari, A. de Agostini The Challenge of Modulating Heparan Sulfate Turnover by Multitarget Heparin Derivatives. Molecules. 2020; 25:390.
374. A.E. Frampton, M. Mato Prado, E. Lopez-Jim ´ ´enez, A.B. Fajardo-Puerta, Z.A.R. Jawad, P. Lawton, E. Giovannetti, N.A. Habib, L. Castellano, J. Stebbing, J. Krell, L. R. Jiao. Glypican-1 is enriched in circulating-exosomes in pancreatic cancer and correlates with tumor burden. Oncotarget. 2018; 9:19006-19013.
375. S.A. Melo, L.B. Luecke, C. Kahlert, A.F. Fernandez, S.T. Gammon, J. Kaye, V. S. LeBleu, E.A. Mittendorf, J. Weitz, N. Rahbari, C. Reissfelder, C. Pilarsky, M. F. Fraga, D. Piwnica-Worms, R. Kalluri, Glypican-1 identifies cancer exosomes and detects early pancreatic cancer, Nature. 2015; 523 177–182.
376. W. Yao, J.L. Rose, W. Wang, S. Seth, H. Jiang, A. Taguchi, J. Liu, L. Yan, A. Kapoor, P. Hou, Z. Chen, Q. Wang, L. Nezi, Z. Xu, J. Yao, B. Hu, P.F. Pettazzoni, I.L. Ho, N. Feng, V. Ramamoorthy, S. Jiang, P. Deng, G.J. Ma, P. Den, Z. Tan, S.X. Zhang, H. Wang, Y.A. Wang, A.K. Deem, J.B. Fleming, A. Carugo, T.P. Heffernan, A. Maitra, A. Viale, H. Ying, S. Hanash, R.A. DePinho, G.F. Draetta, Syndecan 1 is a critical mediator of macropinocytosis in pancreatic cancer, Nature. 2019; 568 410–414.
377. R. Sasisekharan, Z. Shriver, G. Venkataraman, U. Narayanasami, Roles of heparansulphate glycosaminoglycans in cancer, Nat. Rev. Cancer. 2 (2002) 521–528.
378. N. Turner, R. Grose, Fibroblast growth factor signalling: From development to cancer, Nat. Rev. Cancer 2010; 10 116–129.
379. E. Migliorini, D. Thakar, J. Kühnle, R. Sadir, D.P. Dyer, Y. Li, C. Sun, B.F. Volkman, T.M. Handel, L. Coche-Guerente, D.G. Fernig, H. Lortat-Jacob, R.P. Richter. Cytokines and growth factors cross-link heparan sulfate. Open Biol. 5(2015): 150046.
380. M.M. Fuster, L. Wang, Endothelial heparan sulfate in angiogenesis, Prog. Mol. Biol. Transl. Sci. 2010; 93 179–212.
381. B.E. Stopschinski, B.B. Holmes, G.M. Miller, V.A. Manon, J. Vaquer-Alicea, W. L. Prueitt, L.C. Hsieh-Wilson, M.I. Diamond, Specific glycosaminoglycan chain length and sulfation patterns are required for cell uptake of tau versus α-synuclein and β-amyloid aggregates, J. Biol. Chem. 2018; 293 10826–10840.
382. A. Meirovitz, E. Hermano, I. Lerner, E. Zcharia, C. Pisano, T. Peretz, M. Elkin, Role of heparanase in radiation-enhanced invasiveness of pancreatic carcinoma, Cancer Res. 2011; 71 2772–2780.

383. V. Masola, G. Zaza, G. Gambaro, M. Franchi, M. Onisto, Role of heparanase in tumor progression: Molecular aspects and therapeutic options, Semin. Cancer Biol. 2020; 62 86–98.
384. K.T. Ostapoff, N. Awasthi, B.K. Cenik, S. Hinz, K. Dredge, R.E. Schwarz, R. A. Brekken, PG545, an angiogenesis and heparanase inhibitor, reduces primary tumor growth and metastasis in experimental pancreatic cancer, Mol. Cancer Ther. 2013; 12 1190–1201.
385. O'Reilly E.M., Roach J., Miller P., Yu K.H., Tjan C., Rosano M., Krause S., Avery W., Wolf J., Flaherty K., et al. Safety, Pharmacokinetics, Pharmacodynamics, and Antitumor Activity of Necuparanib Combined with Nab-Paclitaxel and Gemcitabine in Patients with Metastatic Pancreatic Cancer: Phase I Results. Oncologist. 2017; 22:1429.
386. O'Reilly E.M., Barone D., Mahalingam D., Bekaii-Saab T., Shao S.H., Wolf J., Rosano M., Krause S., Richards D.A., Yu K.H., et al. Randomised phase II trial of gemcitabine and nab-paclitaxel with necuparanib or placebo in untreated metastatic pancreas ductal adenocarcinoma. Eur. J. Cancer. 2020; 132:112–121.